Experimental Investigation on Flow Structures behind Tandem Bluff Bodies

Arian Bahrami

Submitted to the
Institute of Graduate Studies and Research
in partial fulfillment of the requirements for the degree of

Doctor of Philosophy
in
Mechanical Engineering

Eastern Mediterranean University
July 2019
Gazimağusa, North Cyprus

Approval of the Institute of Graduate Studies and Research

Prof. Dr. Ali Hakan Ulusoy
Acting Director

I certify that this thesis satisfies the requirements as a thesis for the degree of Doctor of Philosophy in Mechanical Engineering.

Assoc. Prof. Dr. Hasan Hacışevki
Chair, Department of Mechanical Engineering

We certify that we have read this thesis and that in our opinion it is fully adequate in scope and quality as a thesis for the degree of Doctor of Philosophy in Mechanical Engineering.

Assoc. Prof. Dr. Hasan Hacışevki
Supervisor

Examining Committee

1. Prof. Dr. Şenol Başkaya

2. Prof. Dr. Beşir Şahin

3. Assoc. Prof. Dr. Hüseyin Çamur

4. Assoc. Prof. Dr. Hasan Hacışevki

5. Asst. Prof. Dr. Devrim Aydın

ABSTRACT

The vortex shedding phenomenon in the wake region behind bluff bodies is the most significant feature of flow around these bodies. One consideration regarding this phenomenon is the induced unsteady loading on the structure which can lead to possible structural damages. Therefore, to prevent any damages, the engineers are required to consider this phenomenon during design stages of industrial systems.

In this study, vortex shedding in the wake region of single and dual bluff bodies have been investigated in detail. Firstly, the effects of entrainment of fluid through the hollow space in square and triangular cylinders have been studied experimentally. The flow structures have been investigated in terms of velocity components, turbulent kinetic energy and similarities and dissimilarities in coherent and incoherent structures have been addressed in detail. It was found that the wake region behind the U shape cylinder exhibits a delay in the wake recovery in comparison to the square cylinder. It was observed that the coherent turbulent kinetic energy (TKE) peak of U shape cylinder is about 25 % lower than the coherent TKE peak of square cylinder in the near wake region while on average it is about 15 % higher in the far wake region. Similarly, it was also observed that the wake region behind the L shape cylinder exhibits a delay in the wake recovery in comparison to the triangular cylinder. It was seen that the coherent TKE peak of L shape cylinder is about 22 % lower than the coherent TKE peak of the triangular cylinder in the near wake region while on average it is about 20 % higher in the far wake region.

Moreover, interacting wakes of two inclined flat plates in tandem arrangement have been studied experimentally. The effects of gap ratio (g/D) between the plates and the angle of attack (α) on the flow structure in the wake region have been investigated. Different set of experiments have been conducted for gap ratios 0.5 and 1.0 between the plates. In addition, various angles of attack (70-90 degrees) have been considered to probe the effects of inclination on the wake region in terms of the shedding frequency and the Strouhal number variation. The results revealed that both the coherent TKE peak production and the Strouhal number decrease as the angle of attack increases. Moreover, it was observed that for a given angle of attack $\boldsymbol{\alpha}$, the Strouhal number increases as the gap ratio g/D increases. Furthermore, the coherent TKE peak production decreases as the gap ratio g/D increases in cases of the angle of attack of 70 and 80 degrees while in case of the angle of attack of 90 degree, the coherent TKE peak production increases as the gap ratio g/D increases.

Keywords: Vortex shedding, Incoherent and coherent flow structure, Triangular cylinder, Inclined flat plate, Interacting wake, Tandem arrangement

ÖZ

Cisimlerin arkasındaki dalga alanındakı girdap oluşumu cisimleri etrafındakı akışın en belirgin özelliklerden biridir. Bu oluşum yapılar üzerinde buna bağlı oluşan karasız yüklemelere sebebiyet verir ki bunlar da yıkıma sebebiyet verebilirler. Bu yüzden mühendisler endüstriyel yapıları tasarlarken oluşabilecek zararları önlemek için bu konuyu dikkate almaktadırlar.

Bu çalışmada tek ve çift gövdelerin dalga alanında oluşan girdapları detaylı bir şekilde incelenmiştir. Öncelikle akışkanın kare ve üçgen silindirler arasına nüfuz etmesinin etkileri deneysel olarak araştırılmıştır. Akış yapıları hız komponenti, türbülans kinetik enerjisi, koherent ve inkoherent yapılardaki benzerlikler ve farklılıklar araştırılmıştır. U kesitli silindir kare şeklindeki silindire göre dalga düzenlemelerinde gecikme göstermektedir. Ayrıca koherent türbülans kinetik enerjisinin U kesitli silindirde kare silindire göre dalga yakın bölgelerinde % 25 az olduğu ve uzak dalga bölgelerinde ise % 15 fazla olduğu gözlemlenmiştir. Ayni şekilde L kesitli silindirin dalga düzenlemesinin üçgen silindire göre daha geç oluştuğu gözlemlenmiştir. Koherent türbülans kinetik enerjisinin L kesitli silindirede üçgen silindire göre yakın dalga bölgesinde % 22 az olduğu ve uzak dalga bölgesinde ise % 20 yüksek olduğu gözlemlendi. Bunun yanında arka arkaya yerleştirilmiş iki eğimli düz plakanın dalga etkileşimleri deneysel olarak incelenmiştir.

Anahtar Kelimeler: Vorteks oluşumu, Inkoherent ve koherent akış yapıları, Üçgen silindir, Eğimli dik plaka, Etkileşimli dalga, Tandem düzen

DEDICATED TO

My Family,

Mahroo, Davood, and Arash

ACKNOWLEDGMENT

I would like to thank my supervisor Assoc. Prof. Dr. Hasan Hacışevki, not only for his scientific oversight of my research but also for the friendly manner in which he would resolve all my problems. He has inspired me to become an independent researcher and helped me to realize the power of critical reasoning.

My family, Mahroo, Davood, and Arash receive my deepest love for their dedication and many years of unconditional support. You have been a source of inspiration throughout the years for me, and you show me the path toward success. I am indebted to you forever.

TABLE OF CONTENTS

LIST OF TABLES

LIST OF FIGURES

LIST OF SYMBOLS AND ABBREVIATIONS

D	Square cylinder/ Flat plate width [mm]
g	Gap between two plates in tandem arrangement [mm]
R_e	Reynolds number (uD/ν)
R_w	Wire resistance [Ohm]
S_t	Strouhal number (fD/U_∞)
S_t'	Modified Strouhal number (fD'/U_∞)
u	Streamwise direction velocity [m/s]
$\bar{u}$	Time mean velocity component [m/s]
u'	Incoherent velocity component [m/s]
$\widetilde{u}$	Coherent velocity component [m/s]
v	Transverse direction velocity [m/s]
x	Streamwise direction
y	Transverse direction
α	Angle of Attack
f	Vortex shedding frequency [Hz]
ν	Kinematic viscosity [m^2 / s]
< >	Phase averaging
CCA	Constant Current Anemometer
CTA	Constant Temperature Anemometer
FFT	Fast Fourier Transform
HWA	Hot Wire Anemometer
LSC	L Shape Cylinder
MSE	Mean Square Error

SC	Square Cylinder
SN	Single Normal Probe
TC	Triangular Cylinder
USC	U Shape Cylinder

Chapter 1

INTRODUCTION

1.1 Vortex Shedding Phenomenon

Development of Vortex shedding phenomenon in the wake region behind bluff bodies is the most significant features of flow around these bodies. This phenomenon has been widely investigated by many researchers for decades. One reason for such attention is due to numerous application of bluff bodies in engineering and industry. These applications range from various engineering disciplines; from civil engineering to wind engineering or aeronautical engineering. Cooling towers, bridges and skyscraper are among many examples illuminating the importance of vortex shedding in the wake region of bluff bodies.

In literature, geometries such as flat plate, rectangular or circular cylinders are referred as bluff bodies. Fluid flow is disturbed as it passes over such geometries and as a result vortices are being formed in the wake region. The frequency of shedding as the key property of this phenomenon is influenced by the geometry, orientation of the body, and velocity of the fluid.

The separation point can be used as a parameter to categorize bluff bodies. In the case of bluff bodies with sharp edges, the separation point is fixed such as flat plate for instance. On the other hand, bluff bodies with rounded edges exhibit a flexible separation point to be adjusted with flow structures.

One consideration regarding this phenomenon is the induced unsteady loading on the structure which can lead to possible structural damages. Therefore, to prevent any damages, the engineers are required to consider this phenomenon during the design stages of industrial systems.

Therefore, researchers have investigated different geometries to improve our understanding of such unsteady phenomenon. These geometries have been investigated in various arrangements namely tandem, staggered or several other arrangements which resemble applications in civil or wind engineering.

In the present study, vortex shedding phenomenon behind various bluff bodies have been studied experimentally. The considered geometries in this study are not chosen because of their simple geometries but rather due to their complex wake structures and application in the industry. Coherent and incoherent flow structures in the wake region behind the bluff bodies have been investigated. Turbulent Kinetic Energy (TKE) and time averaged properties are probed to identify any similarity between different geometries.

1.2 Literature Review on Vortex Shedding from Bluff Bodies

Vortex shedding phenomenon from bluff bodies has attracted many researchers due to its vast industrial application in the engineering world. Therefore, this phenomenon has been studied for different bluff bodies either as a single or different arrangement such as staggered or tandem. For instance, a single circular cylinder can resemble the mast of a wind turbine and the circular cylinders in tandem or staggered arrangement can resemble a wind farm. Hence significance of such a phenomenon in the engineering world such as civil engineering, wind engineering and the aerospace

engineering is apparent. Vortex shedding is an unsteady phenomenon by nature and incurs an unsteady loading on the structures which requires great consideration during design stages of industrial systems. Vortex-induced vibration as a result of this fluctuating forces in the wake region causes several examples of disastrous structural failures.

Ferrybridge Cooling Towers in West Yorkshire, England is one of the examples of such destructive phenomena as shown in Figure 1.1. On November 1965, three of the cooling towers collapsed due to vibrations caused by 85 mph wind speeds. Although the towers had been built to withstand high wind speeds, the vortex causing from the grouped mounted of the cooling towers had not been considered in the design stage. As a result, three out of the original eight cooling towers were destroyed and the remaining five were severely damaged.

Figure 1.1. Ferrybridge Cooling Towers (UK)

1.2.1 Vortex Shedding from Square Cylinder

The geometry of square cylinder has been investigated by numerous researchers such as Bearman and Trueman (1972), Okajima (1982), Sakamoto and Arie (1983), Lyn et al. (1995), Saha et al. (2000), Kurtulus et al. (2007), Yen and Yang (2011). These studies focused on features of vortex shedding behind a single square cylinder by investigating the wake region in terms of flow structure, variation of the Strouhal number (St) and aerodynamic forces.

Fluid flows around rectangular cylinders were investigated by Bearman and Trueman (1972). They studied the base pressure, drag coefficient and Strouhal numbers. They found that $C_D = 2.8$ when the D/h is just over 0.6.

Okajima (1982) conducted an extended research on the vortex shedding from rectangular cylinders with various aspect ratios and Reynolds numbers. He reported that at specific range of Reynolds numbers and for aspect ratios of 2 and 3, there are sudden changes in the Strouhal number.

Sakamoto and Arie (1983) investigated the vortex shedding from rectangular and circular cylinders placed vertically in a turbulent boundary layer for different aspect ratios (L/H). They found that depending on the aspect ratio, the type of vortices forming behind each cylinder changes. The type of vortex shedding changes from arch type vortex to the Karman type as the aspect ratio increases for the circular cylinder above 2.5 and for the rectangular prism above 2.0.

Lyn et al. (1995) investigated the turbulent near-wake flow around a square cylinder at the Reynolds number of 21,400 by means of two-component Laser-Doppler

measurements. The observation was at the near wake where the shed vortices are mature and apparent whereas in the base region, vortices grow to maturity and then the vortices are shed. The result of the study is in general agreement with other investigations of flow around a circular cylinder regarding flow features in the near wake. Also, some features such as the possibility of high Reynolds shear stresses in regions of peak vorticity, or asymmetries near the streamline saddle were apparent from the observations.

Saha et al. (2000) investigated the wake of a square cylinder by employing a hot-wire anemometer. The experiment conducted at Reynolds numbers of 8,700 and 17,625. The presented results show good agreement with the available results from the literature. However, the turbulence fluctuations in the experiments were lower than other works (Lyn et al., 1995). It was suggested that the difference was due to the factors such as the aspect ratio, blockage ratio and upstream turbulence. At higher Reynolds numbers, the experimental data reveal anticipated trends in terms of wake recovery and turbulence decay. It was observed that the streamwise normal stresses were correlated with the vortex centers. In addition, a similar profile of the turbulence kinetic energy and the turbulence shear stress were observed. Furthermore, the spectral analysis of the velocity in the near wake region behind the square cylinder was conducted, and energy transfer from the mean flow to the streamwise velocity fluctuation was demonstrated in the near wake.

Kurtulus et al. (2007) employed time-resolved PIV to investigate the unsteady aerodynamic forces acting on a square cylinder at the Reynolds number of 4,900. These aerodynamic forces were computed by the control volume approach. From the obtained results, a periodic pattern in phase with the vortex shedding (Strouhal number

of 0.128) with amplitude of 0.9 was observed for lift coefficient. On the other hand, the drag coefficient did not show a clear periodical pattern.

On the other hand, there are several numerical studies regarding the square cylinder wake to predict the flow structure with the improved turbulent models. But yet these numerical studies face some difficulties to validate their results with experimental studies. Wang and Wu (2004); Yoon et al. (2010a), Raisee et al. (2010), Maiti and Bhatt (2014), Saha (2013), Saha and Shrivastava (2015), and Yagmur et al. (2017) are among those who devoted a great effort in the quest for an improved turbulent model.

1.2.1.1 Vortex Shedding from Modified Square Cylinder

Beside these enormous and extensive investigations on flow structures in the wake region of square cylinder, several studies focused on features of the flow behind modified square cylinder. Tamura and Miyagi (1999), Tamura et al. (1998), Carassale et al. (2014), and Miran and Sohn (2015) have investigated the vortex shedding from square cylinders with rounded corners. The results demonstrate that rounding the corners of square cylinders is an effective approach to reduce the drag and lift forces. It was demonstrated that in the wake region of square cylinder, the alternate vortices are deflecting away from the centerline. On the contrary, in the wake region of rounded corner square, such a phenomenon has not been observed. As a result, the drag and lift coefficients decrease by reducing the wake width. In addition, it was reported that as the corner radius ratio, R/D, increases, the Strouhal number also increases.

While it is essential to investigate the features of modified square cylinder due to their applications in industry, identifying the similarities and dissimilarities between different geometries will be also valuable. In this context, flow similarity between different geometries such as circular and rectangular cylinder (Ozgoren, 2006;

Sarioglu and Yavuz, 2000) and two tandem plates and square cylinder (Hacışevki and Teimourian, 2015) have been investigated in detail. In case of comparison between rectangular and circular cylinder, it was reported that the square cylinder at zero angle of rotation with equal hydraulic diameter to the circular cylinder, exhibits lower Strouhal number. In addition, a larger length scale for the square cylinder was observed in both streamwise and transverse directions. On the other hand, in the wake region of both square and circular cylinders, a linear increment of Strouhal number on logarithmic scale was observed as the Reynolds number increased. As two identical tandem plates resemble a rectangular body without the top and bottom boundaries, Hacışevki and Teimourian (2015) investigated these geometries in terms of flow structure, turbulent kinetic energy and Strouhal numbers. It was reported that the wake region behind square cylinder, exhibits lower Strouhal numbers than two plates in tandem.

1.2.2 Vortex Shedding from Single Normal Flat Plate

In the context of single flat plate, previous studies such as Bearman (1971), Kiya and Matsumura (1988), Ingham et al. (1990), Nakamura et al. (1991), Sung et al. (1994), Najjar and Vanka (1995), Dennis et al. (1993), Balachandar et al. (1997), Mazharoğlu and Hacışevki (1999), Saha (2007), Narasimhamurthy and Andersson (2009), and recently Afgan et al. (2013) investigated flow structure past a normal flat plate. Despite the simplicity of such a geometry, they observed complex flow structures in the wake region.

An experimental study was conducted by Bearman (1971) on forces acting on the flat plates. He stated that there is a strong correlation between the fluctuating drag and velocity fluctuations in the approaching flow. He found that the base pressure was independent of the Reynolds number over the investigated range in the turbulent flow.

Kiya and Matsumura (1988) investigated coherent and incoherent flow structures behind a normal flat plate in near wake for x/D=8. They used triple decomposition techniques and found that the incoherent fluctuations were contributed to the components of frequencies around half of the main shedding frequency.

Ingham et al. (1990) investigated the flow through row of normal flat plates for the range of Reynolds Numbers $0 \leq Re \leq 500$ numerically and experimentally. They compared the numerical and experimental results and found good agreement for both flow streamlines and eddy lengths.

Vortex shedding from flat plates with square leading and trailing edges at the Reynolds number of Re=1-3 x 10^3 were investigated by Nakamura et al. (1991). To meet two-dimensionality condition, span to chord ratios ranging from 6.7 to 33.3 was used. They also performed flow visualization techniques by using liquid paraffin smoke. The velocities were measured by using hot wire anemometer and they observed that up to a chord thickness ratio of c/t= 15, it is possible to observe dominant frequencies where at c/t = 16, the spectra were broadened without dominant peaks. They found that for c/t =3-5, the Strouhal number is around 0.6 where with further increase in the c/t ratio up to 15, the Strouhal number shows a stepwise increase with the integral multiples of 0.6.

Dennis et al. (1993), experimentally and numerically investigated the viscous flow normal to flat plate at moderate Reynolds numbers. They claimed that the experimental and numerical results were quite satisfactory.

Sung et al. (1994) presented numerical studies for pulsating flow behind normal flat

plates. They used Discrete Vortex Simulation method and identified three characteristic flow modes. They claimed that the results showed similar characteristics with the results of other circular cylinders studies.

Najjar and Vanka (1995) have numerically investigated unsteady separated flow behind a normal flat plate. They used fifth order upwind scheme for convective terms and eigen value decomposition for pressure term for low Reynolds numbers successively. They compared their results with the previous experimental and numerical studies.

Turbulent concentration flow field in the wake of a normal flat plate was experimentally investigated by Balachandar et al. (1997). They used phase averaging techniques and found that the maximum values of concentration are between two to four times larger than the mean values occurring in the core region of vortices. Also, the widths of the wakes in the near wake are 1.5 to 2.5 times wider than the widths of the corresponding velocity profiles.

1.2.2.1 Vortex Shedding from Inclined and Tandem Flat Plates

Beside these enormous and extensive investigations on flow structure in the wake region of normal flat plate, several studies focused on the features of flow behind inclined flat plates or normal flat plates in tandem arrangements. Researchers such as Lam (1996), Lam and Leung (2005), Lam and Wei (2010) and Chen and Fang (1996) and Yang et al. (2012) studied single inclined flat plate.

Lam (1996), Lam and Leung (2005), and Lam and Wei (2010) have devoted a great deal of time to investigate the asymmetrical vortex shedding and flow structure in the wake region of single plate at incident. These studies reported different vortex

formation mechanisms for the leading and the trailing edges. Unlike the trailing edge vortex which is rolled up and shed directly from the trailing edge, the formation and detachment of the clockwise rotating vortex from the leading edge involves a more complex mechanism. Yang et al. (2012) also investigated this phenomenon numerically by employing Direct Numerical Simulation. In contrast to Lam and Leung (2005), they observed the Strouhal number independent of the angle of inclination. Moreover, the simulation revealed that the vortices which shed from the trailing edge contain higher vorticity level than those shed from the leading edge. In comparison while normal plates demonstrate a symmetrical flow structure, inclined flat plates exhibit asymmetrical structure with different vorticity strength.

In the context of normal flat plates in tandem, Hacışevki and Teimourian (2015), Hacışevki and Teimourian (2016), Auteri et al. (2009), Auteri et al. (2008), and Nakamura (1996) investigated the flow structures, vortex shedding and Strouhal number variation. Auteri et al. (2008) studied flow past two normal flat plates in tandem experimentally by means of smoke visualizations and CTA. They observed a double peak in FFT analysis spectrum of gap ratio g/D=0.9 which is an indication of existence of two distinct flow regimes in the neighborhood of that interval.

Nakamura (1996) smoke visualization demonstrated that at the gap ratio g/D=0.5, vortices shed behind the aft plate only and thus such an arrangement sheds vortices as a single body mode. However, at the gap ratio of g/D=2.0, the vortices also roll up inside the gap between the plates and dual body mode of vortex shedding occurs. Similarly, Auteri et al. (2008) smoke visualization demonstrated these two shedding modes at the gap ratios of 0.7 and 1.15, respectively.

1.2.3 Vortex Shedding from Triangular Cylinder

Vortex shedding behind bluff bodies is a widely investigated phenomenon by many researchers. Such interest on this phenomenon is due to numerous applications of bluff bodies in engineering and industry. The vortex shedding phenomenon inducing an unsteady loading on the structure with possible structural damages. Therefore, to prevent such destruction, it is required to consider this phenomenon during design stages of industrial systems.

Despite the fact that vortex shedding phenomenon in the wake region of bluff bodies is a common research field in fluid mechanics, limited studies investigated the flow structure in the wake of the triangular cross-sectional cylinder (Agarwal and Dhiman, 2014, 2015; Iungo and Buresti, 2009; Srigrarom and Koh, 2008; Tu et al., 2014; Wang et al., 2011; Yagmur et al., 2017). A triangular prism is a common cross-sectional cylinder to generate vortex shedding in a vortex flowmeter. A prismatic cross-sectional cylinder has superiority over a circular cylinder to generate better vortex shedding due to sharp corners. Previous studies reported that the Strouhal number was independent of the Reynolds number and a value of 0.22 was reported for an equilateral triangular cylinder (Yagmur et al., 2017).

On the other hand, several studies focused on the features of flow behind square cylinder at incident which resemble two attached triangular prisms (Chen and Liu, 1999; Huang and Lin, 2011; Huang et al., 2010; McClean and Sumner, 2014; Miran and Sohn, 2016; Sarioglu, 2017; Sheard, 2011; Sohankar et al., 2018; Sohankar and Najafi, 2018; Oudheusden et al., 2005; Yoon et al., 2010b). It was observed that the angle of incidence is the key parameters influencing the flow structure behind square cylinder. The angle of incidence causes a shift of the separation point location which

also affects the flow structure around the square cylinder (Yoon et al., 2010b). It was demonstrated that such a shift in the separation point affects the flow structure significantly which results in the variation of the Strouhal number, drag, and lift forces on the cylinder (Igarashi, 1984). The flow structure behind square cylinder at incident is classified into three distinct categories in terms of topological point of view namely main separation, vortex merging and steady. It was also observed that the flow structure in the wake region of square cylinder is symmetric only when theta=0° and 45° (Yoon et al., 2010b). The investigations on aerodynamics characteristics of square cylinder at incidence revealed that while the minimum drag coefficient occurs at the incident angle of 12 degrees, the minimum lift coefficient occurs at the angle of 13 degrees. It was also reported that the square cylinder normal to flow with zero angle of incidence demonstrates the minimum projected Strouhal-number (St) whereas the maximum St occurs at the incident angle of 15 degrees (Yen and Yang, 2011).

1.2.4 Vortex Shedding from Similar Geometries

While the purpose of the discussed studies is focused on a better understanding of vortex shedding phenomenon behind these bluff bodies, identifying the similarities and dissimilarities between different geometries will be also interesting (Hacışevki and Teimourian, 2015; Knauss et al., 1976; Ozgoren, 2006; Ozgoren et al., 2011; Sarioglu and Yavuz, 2000). For instance, Ozgoren (2006) investigated the flow structure in the wake of circular and square cylinders at incident angle of 45 degrees. It was reported that the square cylinder at zero angle of rotation with equal hydraulic diameter to the circular cylinder, exhibits lower Strouhal number. In addition, a larger length scale for the square cylinder was observed in both streamwise and transverse directions. On the other hand, in the wake region of both square and circular cylinders, a linear increment of Strouhal number on logarithmic scale was observed as the Reynolds number

increased. Strouhal numbers were observed to be in the ranges of St=0.204–0.212, St=0.12–0.134, and St=0.165–0.174 for the circular, square, and the square cylinder at incidence, respectively.

The vortex shedding frequency in the wake region of elliptical and square cylinders was studied by Knauss et al. (1976). It was reported that the Strouhal number is almost independent of the Reynolds number while it is dependent on the geometrical shape of the bluff body.

In addition, Ozgoren et al. (2011) and Provansal et al. (2004) investigated the flow characteristics in the wake region behind circular cylinder and sphere. These studies demonstrated that the wake flow of the sphere is more complex than the wake flow of the circular cylinder because of the 3-D flow. Furthermore, sphere exhibits higher vortex shedding frequency, while circular cylinder demonstrates higher power spectral density (PSD). It was also reported that turbulence kinetic energy peak in the wake of circular cylinder is 3 times higher than the peak values in the wake of sphere.

As two identical tandem plates resemble a rectangular body without definite top and bottom boundaries, Hacışevki and Teimourian (2015) investigated these geometries in terms of flow structure, turbulent kinetic energy and Strouhal number. It was reported that the wake region behind square cylinder, exhibits lower Strouhal number than two plates in tandem arrangement.

1.3 Scope of This Work

To sum up, the literature survey revealed that despite many efforts for better understanding of vortex shedding phenomenon, there are still gaps in the literature. In this work, each chapter addresses one gap in the literature.

Although numerous studies investigated the flow structure around square cylinders, there is a limited number of studies regarding the effect of shape modification such as rounded corners or perforation on the vortex shedding. In fact, the literature survey shows that there is no available study on effects of modifying a square cylinder to a U shape cylinder. Therefore, one objective of this study is to investigate the effects of such shape modification on the flow structures and vortex shedding phenomenon. The wake regions of a square and a U shape cylinder have been compared in terms of flow structures and other aerodynamic characteristics. Hence, coherent and incoherent flow structures of the wake regions are presented in detail for a square cylinder and a U shape cylinder to demonstrate the possible dissimilarities in flow structures.

In addition, the flow structure and downstream wake behind a triangular prism and an L shape cylinder as a hollow triangular prism have been studied experimentally. The previous studies revealed a complex flow structure behind triangular cylinders. However, no previous study has investigated the effect of such an L shape modification on the flow structures and vortex shedding phenomenon.

As the final remark, the previous investigations on the vortex shedding mechanism from dual bodies configuration, described the mechanism for various geometries. One particular study is the vortex shedding from flat plates in tandem arrangement. Although there is limited literature on this regard, the previous studies only tackled the

problem of normal flat plates in tandem. For that reason, in this study, two inclined flat plates in tandem arrangement are studied to investigate the effects of gap ratio and angle of attack on the flow structures.

In chapter 1, historical review and previous works on vortex shedding phenomenon from bluff bodies have been presented. In chapter 2, some theoretical methods such as triple decomposition and phase averaging have been defined and modified Navier-Stokes equations have been presented. In chapter 3, experimental setup, the subsonic wind tunnel and Hot-wire anemometry have been described. The flow structures in the wake region of a square cylinder and a U shape cylinder have been studied in chapter 4. In chapter 5, the flow structures in the wake region of a triangular cylinder and an L shape cylinder have been studied in detail. In chapter 6, interacting wakes of two inclined flat plates in tandem arrangement have been investigated in terms of flow structure, coherent and incoherent structures. Finally, some suggestion and future works to improve our understanding of vortex shedding phenomenon have been proposed.

Chapter 2

THEORETICAL DERIVATIONS

2.1 Introduction

In this study, the triple decomposition and ensemble averaging technique as proposed by Hussain (1986), Reynolds and Hussain (1972), Cantwell and Coles (1983), Kiya and Matsumura (1988), Perry and Steiner (1987), and Steiner and Perry (1987) are utilized to investigate the vortex shedding phenomenon and wake flow structures behind bluff bodies. Thus, the turbulent flow (incoherent turbulent fluctuations) and vortex shedding (coherent structure) could be identified and distinguished and resulted in a better understanding of this phenomenon.

Since vortex shedding phenomenon is a classical periodic flow in nature, therefore it is more appropriate to analyze such signal by employing the phase averaging technique. Hence only data acquired at the same phase of the signal is analyzed for all periods. In this chapter triple decomposition, ensemble and the phase averaging technique have been applied on the momentum equation and modified Navier-Stokes equation have been derived accordingly. As a result of such approach additional stress terms due to coherent structure and incoherent fluctuation can be studied as well. Properties such as coherent and incoherent stresses, turbulent kinetic energy (TKE) and other terms which are explained in this chapter are examined in detail for different bluff body arrangements.

2.2 Triple Decomposition Technique

As stated previously, triple decomposition was employed to analyze flow properties such as instantaneous velocity. This technique provides an improved clarification of coherent structure and incoherent turbulent fluctuations by decomposing instantaneous streamwise velocity u as follows:

$$u(\vec{x},t) = \bar{u}(\vec{x}) + \tilde{u}(\vec{x},t) + u'(\vec{x},t) \quad (2.1)$$

Where $\bar{u}$ the time-mean is averaged component, $\tilde{u}$ is the periodic coherent structure and $u'$is the random fluctuation incoherent structure. This definition can be applied for any other velocity components i.e. transverse velocity or product of velocity components such as Reynold normal or shear stresses.

Figure 2.1 illustrates an instantaneous velocity for a periodic signal superimposed with coherent and incoherent random fluctuations.

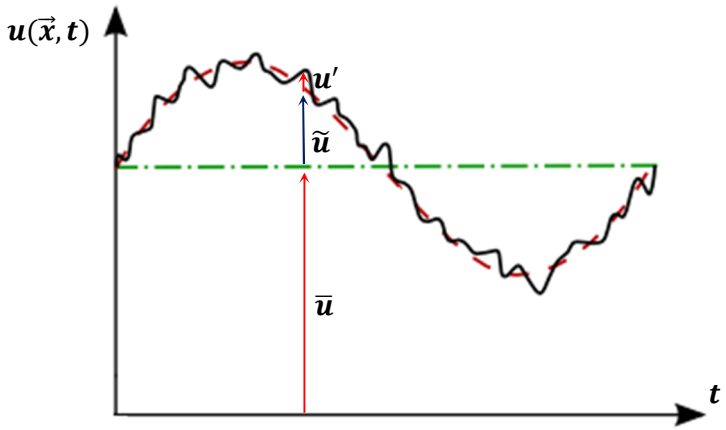

Figure 2.1. Mean, coherent and turbulent velocity components of periodic instantaneous velocity

2.3 Time Averaging and Rules

The time mean of incoherent fluctuations u' *and* v' are zero due to their random nature and as a result $\overline{u'} = 0$ and $\overline{v'} = 0$. Moreover, the time mean of coherent structure of a periodic vortex shedding is also zero, for instance $\overline{\tilde{u}} = 0, \quad \overline{\tilde{v}} = 0$. Moreover, the readers are referred to (Reynolds & Hussain, 1972) for additional averaging rules applied to derive the modified Navier-Stokes equation. Therefore, Time mean average of any flow property such as velocity is defined mathematically as (Bradshaw, 2013):

$$\overline{u} = \frac{1}{T}\int_0^T u(x,t)dt \tag{2.2}$$

In this study due to periodic nature of shedding phenomenon, $\overline{u}$ is not a function of time.

2.4 Phase Averaging

In order to employ triple decomposition we have to introduce the concept of phase averaging. This is an averaging operation over successive terms taken at exactly same phase during each period. Therefore, the phase average can be defined as follows:

$$<u(x,y,t)>=\lim_{N\to\infty}\frac{1}{N}\sum_{n=1}^{N}u(x,y,t+nT) \tag{2.3}$$

where N is the number of cycles used for phase averaging and u is the instantaneous velocity. The phase averaging is the average over large ensemble points having the same phase with respect to the specified wave. Therefore,

$$\tilde{u} = \langle u \rangle - \overline{u} \tag{2.4}$$

That is the phase averaging filters only the coherent oscillations from the instantaneous turbulent motion.

2.5 Derivation of Modified Navier-Stokes Equation

The Navier-Stokes momentum equation given in the following equation is formed by four terms

$$\underset{\text{(I)}}{\frac{\partial u_i}{\partial t}} + \underset{\text{(II)}}{u_j \frac{\partial u_i}{\partial x_j}} = \underset{\text{(III)}}{-\frac{1}{\rho}\frac{\partial P}{\partial x_j}} + \underset{\text{(IV)}}{\nu \frac{\partial^2 u_i}{\partial x_j \partial x_j}} \tag{2.5}$$

Applying phase averaging on each term will result in

Term (I):

$$\frac{\partial\langle \overline{u}_i + \widetilde{u}_i + u_i' \rangle}{\partial t} = \frac{\partial\langle \overline{u}_i \rangle}{\partial t} + \frac{\partial\langle \widetilde{u}_i \rangle}{\partial t} + \cancel{\frac{\partial\langle u_i' \rangle}{\partial t}} = \frac{\partial \overline{u}_i}{\partial t} + \frac{\partial\langle \widetilde{u}_i \rangle}{\partial t} \tag{2.6}$$

Term (II) from continuity can be written as $\dfrac{\partial(u_j u_i)}{\partial x_j}$

$$\therefore \quad \frac{\partial(u_j u_i)}{\partial x_j} = \frac{\partial}{\partial x_j}\left\langle (\overline{u}_j + \widetilde{u}_j + u_j')(\overline{u}_i + \widetilde{u}_i + u_i') \right\rangle$$

$$= \frac{\partial}{\partial x_j}\left\langle (\overline{u}_j\overline{u}_i + \overline{u}_j\widetilde{u}_i + \cancel{\overline{u}_j u_i'} + \widetilde{u}_j\overline{u}_i + \widetilde{u}_j\widetilde{u}_i + \cancel{\widetilde{u}_j u_i'} + \cancel{u_j'\overline{u}_i} + \cancel{u_j'\widetilde{u}_i} + u_j'u_i' \right\rangle$$

$$= \frac{\partial}{\partial x_j}\left(\overline{u}_i\overline{u}_j + \overline{u}_j\langle\widetilde{u}_i\rangle + \overline{u}_i\langle\widetilde{u}_j\rangle + \langle\widetilde{u}_i\widetilde{u}_j\rangle + \langle u_i'u_j'\rangle\right) \tag{2.7}$$

Term (III): $$-\frac{1}{\rho}\frac{\partial\langle \overline{P} + \widetilde{P} + P' \rangle}{\partial x_j} = -\frac{1}{\rho}\frac{\partial\langle \overline{P}\rangle}{\partial x_j} - \frac{1}{\rho}\frac{\partial\langle \widetilde{P}\rangle}{\partial x_j} - \frac{1}{\rho}\cancel{\frac{\partial\langle P'\rangle}{\partial x_j}}$$

$$= -\frac{1}{\rho}\frac{\partial\langle \overline{P}\rangle}{\partial x_j} - \frac{1}{\rho}\frac{\partial\langle \widetilde{P}\rangle}{\partial x_j} \tag{2.8}$$

and Term (IV):

$$\nu\frac{\partial^2\langle(\overline{u}_i + \widetilde{u}_i + u_i')\rangle}{\partial x_j \partial x_j} = \nu\frac{\partial^2\langle \overline{u}_i\rangle}{\partial x_j \partial x_j} + \nu\frac{\partial^2\langle \widetilde{u}_i\rangle}{\partial x_j \partial x_j} + \nu\cancel{\frac{\partial^2\langle u_i'\rangle}{\partial x_j \partial x_j}}$$

$$= \nu\frac{\partial^2\langle \overline{u}\rangle}{\partial x_j \partial x_j} + \nu\frac{\partial^2\langle \widetilde{u}\rangle}{\partial x_j \partial x_j} \tag{2.9}$$

Hence after applying phase averages of each part, the momentum equation can be re-arranged as follows:

$$\rho\frac{\partial\overline{u_i}}{\partial t}+\rho\frac{\partial\overline{u_i}\,\overline{u_j}}{\partial x_j}+\frac{\partial\bar{p}}{\partial x_j}-\frac{\partial}{\partial x_j}\left(\mu\frac{\partial\overline{u_i}}{\partial x_j}-\rho(\langle\tilde{u}_i\tilde{u}_j\rangle+\langle u'_i u'_j\rangle)-\rho\left(\overline{u_i}\langle\tilde{u}_j\rangle+\overline{u_j}\langle\tilde{u}_i\rangle\right)+\langle\tilde{p}\rangle\right)=0 \tag{2.10}$$

Finally, applying time–average rules on the obtained equation will result in the modified Navier-Stokes equation as follows:

$$\rho\overline{\frac{D\overline{u_i}}{Dt}}=-\overline{\frac{\partial\overline{P}}{\partial x_i}}+\frac{\partial}{\partial x_j}\left(\mu\frac{\partial\overline{u_i}}{\partial x_j}-\rho\left(\langle\overline{\tilde{u}_i\tilde{u}_j}\rangle+\langle\overline{u'_i u'_j}\rangle\right)\right)+\frac{\partial}{\partial x_j}\left(\rho\left(\cancel{\overline{\overline{u_i}\langle\tilde{u}_j\rangle}}+\cancel{\overline{\overline{u_j}\langle\tilde{u}_i\rangle}}\right)+\cancel{\langle\overline{\tilde{P}}\rangle}\right) \tag{2.11}$$

Hence

$$\rho\frac{D\overline{u}}{Dt}=-\frac{\partial\overline{P}}{\partial x_j}+\frac{\partial}{\partial x_j}\left(\mu\frac{\partial\overline{u_i}}{\partial x_j}-\rho(\overline{\tilde{u}_i\tilde{u}_j}+\overline{u'_i u'_j})\right) \tag{2.12}$$

Therefore, in the modified Navier-Stokes equation derived by triple decomposition for periodic flow, in addition to the Reynolds stress term $u'v'$, there is an additional term $\overline{\tilde{u}_i\tilde{u}_j}$ in the Reynolds stress term due to the coherent fluctuation.

Moreover, the Turbulence Kinetic Energy (TKE) can be defined in a similar manner as following equation:

$$\bar{k}=\frac{1}{2}\overline{u'_i u'_i}=\frac{1}{2}(\overline{u'_1u'_1+u'_2u'_2+u'_3u'_3})=\frac{1}{2}(\overline{u'u'+v'v'+w'w'}) \tag{2.13}$$

In this experimental study downstream wake behind the different bluff bodies has been measured quantitatively by employing Hotwire anemometry as described in chapter 3.

Chapter 3

EXPERIMENTAL FACILITY AND DATA ANALYSIS

In this chapter, the experimental facilities and set up, measurements techniques and data analysis are described. HWA measurements has been employed to acquire the velocity and fluctuating components in the region of interest in the wake of bluff bodies. HWA working principles, calibration procedure and instrumentation have been also described. Moreover, the traverse mechanism which have been employed to traverse the cross Hotwire probe in the wind tunnel's test section is described as well. The investigated bluff body models and arrangements throughout the experiments are given at corresponding chapters.

3.1 The EMU Subsonic Wind Tunnel

The experiments have been performed at the open type subsonic wind tunnel available in Aerodynamics laboratory of the Mechanical Engineering Department, EMU. The wind tunnel test section dimension is 0.5 x.0.5m and 1.4m long with contraction ratio of 10:1. The tunnel free stream turbulence level is less than 0.8 % at the maximum speed of 30 m/s. The wind tunnel is a suction driven type and the speed is controlled with a 12 kW Danfoss electronic frequency control unit (0 –50Hz). Figure 3.1 illustrated the schematic diagram of the wind tunnel, traverse mechanism and hotwire anemometry.

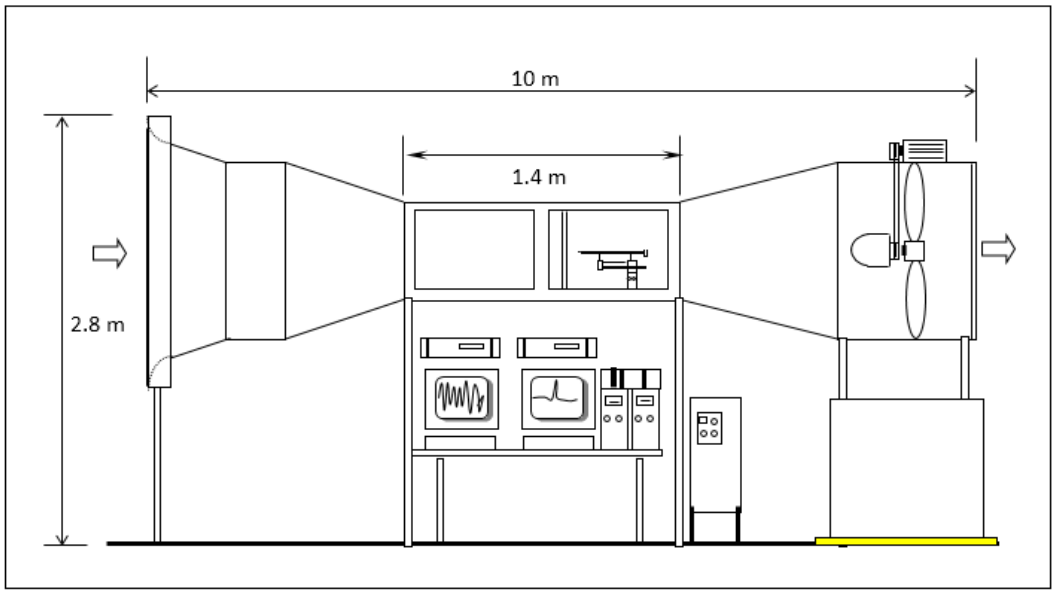

Figure 3.1. Schematic Side view of the Subsonic Wind Tunnel

3.2 Hot-Wire Anemometry

Hot wire anemometer (HWA) is one of the widely used technique in turbulent flow measurements which provide a high temporal resolution comparing to other techniques. The temporal resolution which is up to 400 kHz, provide capability of a real time analysis of the flow. Hot wire anemometer is also more affordable compared to other flow measurement systems such as PIV or LDA. Hot wire anemometer measurement principle is based on convective heat transfer from a heated sensing wire or film. For velocity measurement the electrically heated sensor will be exposed to the flow and the sensor maintains at constant temperature with the aid an electronic control unit. Consequently, based on the changes in heat transfer from the sensor, the anemometer measures the corresponding flow velocity.

The technology achievement in the late 1950's leads to development of an accurate technique in flow measurements. This newly developed technique was superior in accuracy and flexibility comparing with other available flow measurements technique

such as Pitot tube measurements (Bruun, 1996). It can be employed where fast response to the flow changes (high frequency response) are required. However, there are some limitation and drawbacks associated with hot wire anemometer. This method is an intrusive technique since the probe must be placed in the flow with adverse effects. In addition, the sensors are fragile and very susceptible to flows contaminants and requires calibration before and after each experiment for accurate measurements.

There are two types of hot wire anemometer based on their operating methods; Constant Current Anemometer (CCA) mode and Constant Temperature Anemometer (CTA). “Constant current” system operates in a manner to keep the current through the sensing element constant. However, for “constant temperature” operation the element temperature is kept constant by using an electronic control unit to change the electrical current accordingly. As a result the two mentioned methods significantly different in their circuit. In both anemometer systems electronic noises caused by amplifier circuit, resistors in the anemometer bridge and the sensors require special consideration (Brunn, 1995). CTA requires more complex circuit and more expensive comparing CCA, but it is easier to use with low noise problem. Nevertheless, “constant temperature anemometer” (CTA) is satisfying the modern requirements and accepted as standard with more popularity (Bradshaw, 1996). The probe requires frequent calibration due to the sensitivity of the sensor to temperature changes together with the effects of available dirt in flow.

3.2.1 Hot Wire Probe

Hot-wire and hot-film are the most common probe which are being employed in hot wire anemometer. These sensors facilitate turbulent flow studies and to provide accurate measurements of turbulent flow, it is recommended that dimension of the sensor should be chosen by considering the Kolmogorov length scale of the smallest eddies (Bradshaw, 1996).

The hot wire sensor is made of electrically conductive material and Tungsten, platinum and platinum alloys are among the common material for hot wire production. The hot wire is 5 μm in diameter and 1 mm in length welded to the single and cross probe prongs as illustrated in figure 3.2 and 3.3, respectively.

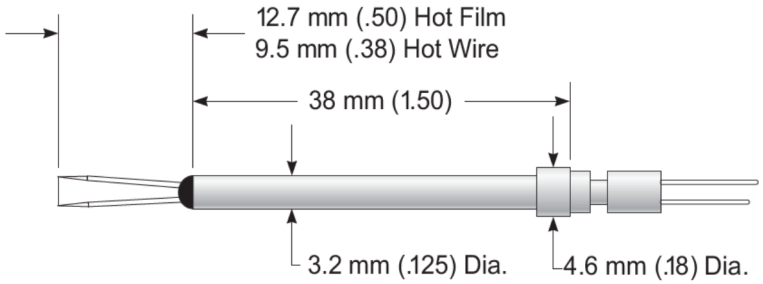

Figure 3.2. Single Hotwire probe Model 1210

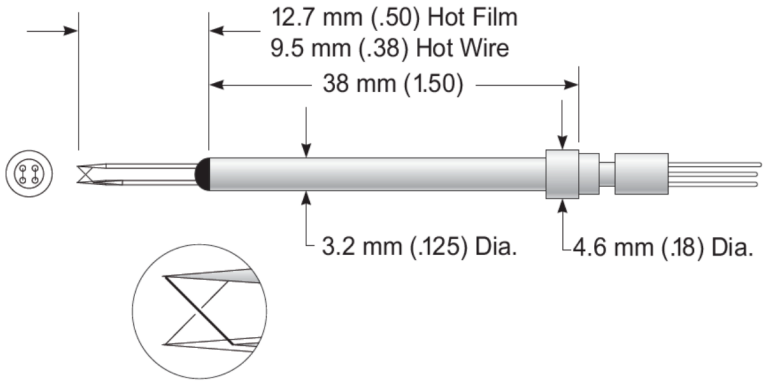

Figure 3.3. Cross Hotwire probe Model 1241

These fragile and highly sensitive wires will be installed on the probe prongs by spot welding or soldering techniques. The length of these prongs are critical and may affect the hot wire system. For instance, long prongs in periodic flows such as vortex shedding may vibrate and may introduce error into the measurements by the HWA. Hot-wire probes facilitate flow field measurements in gas and liquid with high accuracy and response.

3.2.2 HWA Principle

As mentioned before, the electrical current flows through the wire to maintain the wire temperature. Therefore the dissipated electrical energy from the sensor in form of heat is given by equation 3.1.

$$W_{elec} = I^2 R_w \tag{3.1}$$

Where I is the electrical current through the wire, and R_w is the sensor electrical resistance.

Therefore, an equilibrium between the generated thermal energy heat losses to the surrounding is required to keep the wire temperature constant. However the convective heat transfer will varies as the flow velocity changes and leads to a new equilibrium. As stated, the HWA output is correspondent the flow velocity and King's Law is an empirical law describing the non-linear relation between the measure voltage across the wire (E) and flow velocity (V) as follows:

$$E^2 = A + BV^n \tag{3.2}$$

where A, B, and n are the coefficient which obtained from calibration procedure. Therefore a 4^{th} order polynomial curve fit is to be used, which approximates the inverse of the King's law accurately and the output is directly proportional to the effective velocity.

$$V_{eff} = K + A \times N + B \times N^2 + C \times N^3 + D \times N^4 \quad (3.3)$$

Where V_{eff} is the effective velocity, N is the normalized bridge voltage and A, B, C, D and K are constant numbers which have to be determined by its calibration procedure. The normalized voltage N is obtained from the following equation:

$$N = \frac{E - E_{min}}{E_{max} - E_{min}} \quad (3.4)$$

Where, E is the Bridge voltage.

To generate a look up table which can be used for flow measurements, the fourth order polynomial curve fit have been applied for the normalized voltage to compute velocities. The calibration curve fit for a single probe SN 961171 is shown in figure 3.4. As it can be seen the calibration curve is non-linear, and the calibration have been performed for a velocity range of 0-20 m/s for 20 sample data points. The calibration at low velocities, where requires maximum sensitivity treatment, performed with higher sampling density comparing to high velocities.

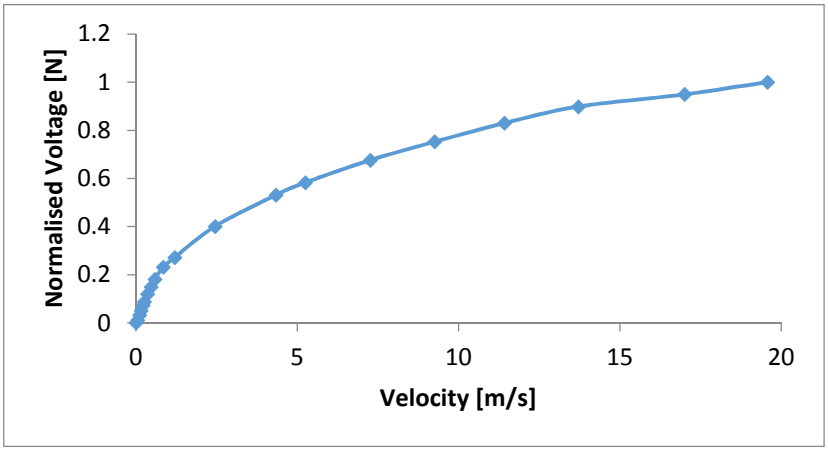

Figure 3.4. Calibration Curve Plot for single probe SN 961171

The look-up table is generated for each probe sensor for the specified flow velocity range which is used for the calibration. The curve fit and mean square error (MSE) can be employed to evaluate the accuracy of the calibration. If the MSE is higher than 0.01-0.02 %, the calibration procedure must be repeated to obtain an accurate calibration with proper curve fit and MSE. It should be stated that exceeding the MSE above this range would affect the data acquisition since some other parameter such as positioning effect, soldering and contact resistance have already affected the calibration.

3.2.3 Hot Wire Instrumentation

In this study, the employed HWA is a constant temperature anemometer and consists of a hot-wire probe connected to a Wheatstone bridge (TSI FlowPoint 1500 velocity transducer, CTA bridge) as illustrated in figure 3.5. A DAS-1402 data acquisition card transfer the velocity transducers output to FlowPoint velocity measuring system software.

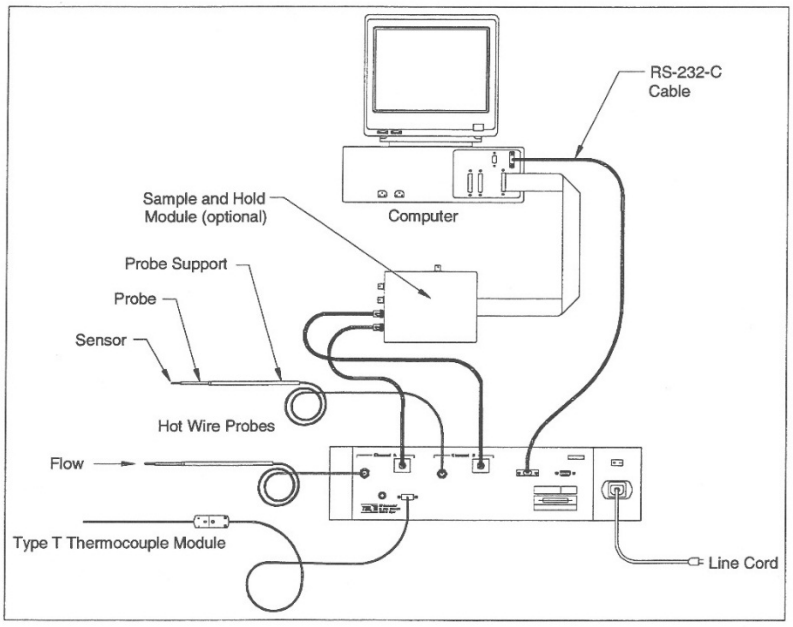

Figure 3.5. Hot wire anemometry system configuration (Figure taken from TSI FlowPoint 1500 Instruction Manual)

The TSI FlowPoint 1500 velocity transducer is the control circuit for the CTA hot-wire anemometry. The special bridges and amplifiers (figure 3.6) with filter circuits of the transducers ensure minimal noise during the data acquisition.

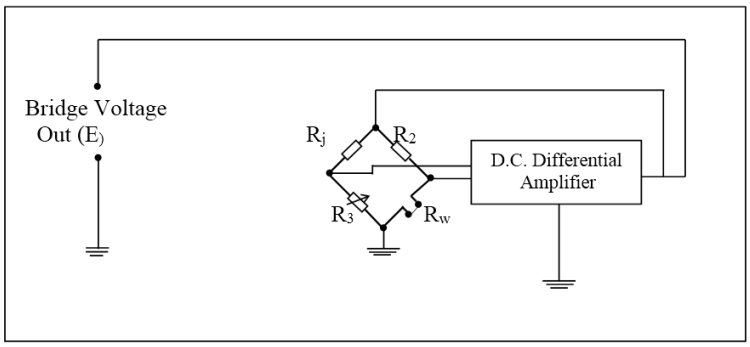

Figure 3.6. Schematic diagram of a thermal anemometer system (Wheatstone bridge)

For this work TSI model 1210-T1.5 type single normal (SN) probes and TSI 1241-T1.5 type x-wire probe have been employed. The sensors were made of tungsten and 3.8 μm in diameter.

3.2.4 Hot Wire Calibration

The HWA system requires to be calibrated before each experimental flow measurements. Therefore the voltage-velocity governing relation will be determined by calibration procedure as explained in previous section.

The hot wire probes have been calibrated by employing TSI Model 1125 calibrator which has provided the turbulence intensity less than 0.5% to eliminate any error in the calibration constants. The velocity range of the calibrator is between 0.01 and 300 m/s for this model. The calibrator equipped with three chambers for very low velocities (0.001 - 1 m/s), mid-range velocities (0.63 - 15 m/s) and higher velocities (2.5 - 300 m/s) called D3, D2 and D1, respectively.

In order to employ the CTA Hotwire system for data acquisition in the experiment, a calibration against known flow velocities are required. Therefore, the output voltage would be obtained as a function of the flow velocity.

Due to atmospheric pressure and temperature variation and their effects on the result, for all calibration procedures and data acquisitions, the ambient pressure and temperature have been considered for velocity calculations.

The TSI hot wire probes require an ambient condition correction throughout the calibration procedure with considering the temperature (Bearman, 1971) and pressure effects. Therefore, nominal velocities are modified by a correction factor K_{VCF} (TSI Manual):

$$K_{VCF} = \sqrt{\left(\frac{293}{273+T}\right)\left(\frac{P}{760}\right)} \tag{3.5}$$

where T = Atmospheric temperature (C)

P = atmospheric pressure (mm Hg)

In addition to ambient condition correction, it is also required to employ a directional sensitivity correction factor for the calibration with considering the direction of the flow as studied by (Jorgensen, 1971). End flow condition requires that the flow direction and the sensor axis to be in the same direction, whereas for cross flow condition the sensor axis is normal to flow direction. The Hot wire probe response to end flow and cross flow conditions are different. As a result of such directional sensitivity, a cross flow calibrated probe will produce error in measurement if exposed to end flow condition. Therefore, TSI probe were corrected for pitch response by employing correction factor K_{SF} as supplied by the manufacturer.

3.2.5 Hot Wire System Settings

As discussed in previous section, the HWA requires to be calibrated in order to compute a relation between velocity and voltage. The HWA setting such as probe type, probe-cable resistance, sensor resistance, gain, offset can be set within the FolwPoint software. The probe-cable resistance has been determined by employing a short-cut device and additional system's setting are provided by the manufacturer as given in table 3.1.

Table 3.1. Hot wire sensors settings

	Probe resistance	Wire resistance	Operating resistance	Operational temperature
1210-T.15	5.96 Ω	0.28 Ω	11.66 Ω	250 °C
1210-T.15	5.70 Ω	0.24 Ω	11.33 Ω	250 °C
1241-T.15	5.57 Ω	0.19 Ω	1082 Ω	250 °C

3.3 Hot Wire Probe Traverse Mechanism

The X probe has been mounted on a three-axis traverse mechanism to traverse in the domain of interest during data acquisition as illustrated in figure 3.7. The accuracy of mechanism is ±0.25 mm for traversing in all directions. All the measurements were acquired at the midpoint of the test section in the z-direction and the probe have been traversed in x-y for a domain of 1.0D to 6.0D in the downstream wake region.

Traverse Mechanism Specification:

- 250 x 250 [mm] operation domain in XY plane
- 250 [mm] operation in Z axis
- Accuracy Max. 1600 steps per revolution

The cross Hotwire sensor was mounted on model 1155 probe support 457 mm upstream of the traverse mechanism and the blockage ratio of the mechanism is calculated to be 6 %. Under these circumstances it is accepted that the effect of mechanism on the data measurement system is negligible.

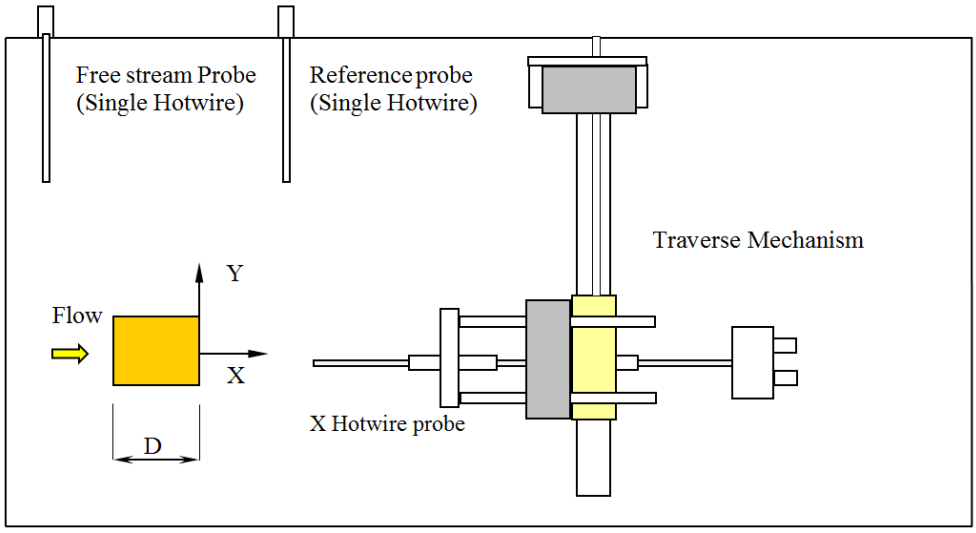

Figure 3.7. Schematic of Hotwire probe traverse mechanism

3.4 Data Analysis Program Code

In this study, the acquired velocity data have been analyzed by employing in house FORTRAN codes together with MATLAB/SIMULNIK software. Velocity data have been acquired by employing three velocity transducers. Two individual transducers were dedicated to acquiring free stream velocity and reference velocity signal separately. The last velocity transducer was employed to acquire u and v velocity components from x hotwire probe. Due to noise and distortion of the acquired velocity signal, it is required to clean up/filter the velocity signal.

Therefore, first the acquired velocity data have been converted to a matrix form to perform filtering operation within Matlab/Simulink on the acquired data. FORTRAN

program Convertor1.for has been employed for such reorganizing operation. Then, the velocity signal data have been cleaned up within MATLAB/SIMULINK (figure 3.8) for high and low frequency noises for cut-off value above 0.25 and below 0.40, respectively. After each filtering operation a delay with respect to the original signal have been observed. Therefore, after each filtering operation the delay value have been substituted into the circuit to correct the time shift. Figure 3.9 illustrated a typical filtered and unfiltered velocity signal.

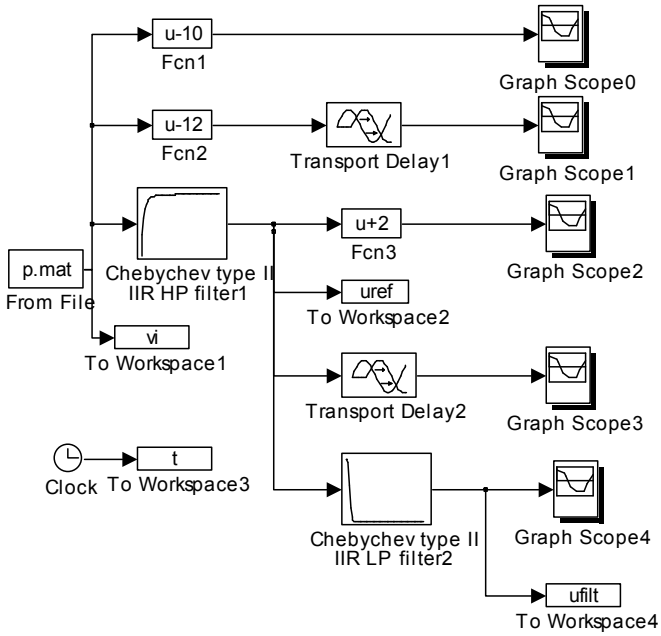

Figure 3.8. Simulink diagram of filtering program

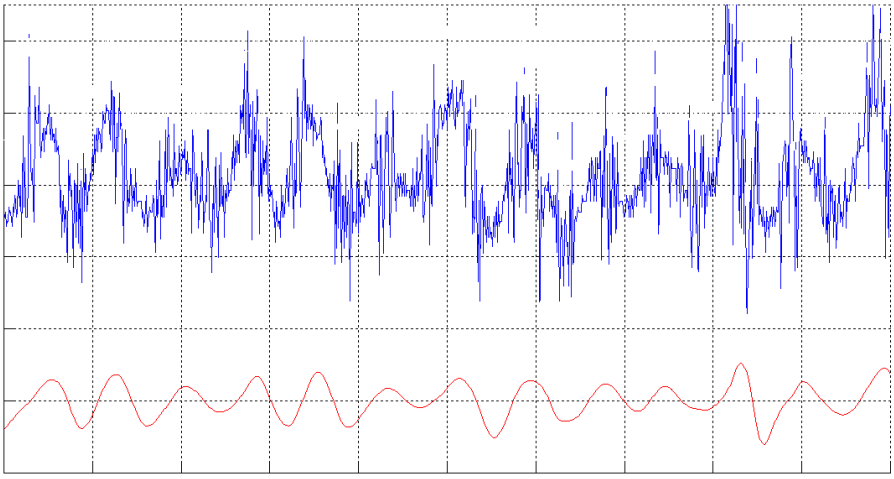

Figure 3.9. Acquired unfiltered and filtered velocity signal

Then, the original velocity signal and the filtered velocity data have been blended by using the FORTRAN program Convertor2.for to obtain the zero crossing point from reference signal analysis. Finally the velocity data have been analyzed and velocity properties have been computed by employing ensemble.for program. The phase averaging technique, ensemble averaging and triple decomposition technique have been applied on Navier-Stock equation and ensemble.for program code have been developed based on the modified Navier-Stock equations.

The velocity data have been acquired at sampling rate of 5 kHz for sampling time of 2.048 second with a sampling size of 10 kpts/ch (kilopoints/channel). In this work the flow properties have been analyzed by employing triple decomposition and ensemble averaging techniques as stated in previous chapter. Therefore, after decomposing the instantaneous velocity into three components and applying aforementioned techniques on the Navier-Stokes equation, the modified Navier-Stokes equation derived as:

$$\frac{D\overline{u}_i}{Dt} = -\frac{1}{\rho}\frac{\partial \overline{p}}{\partial x_j} + \nu\frac{\partial^2 \overline{u}_i}{\partial x_j \partial x_j} + \frac{\partial}{\partial x_j}\left(-\langle\overline{\tilde{u}_i \tilde{u}_j}\rangle - \langle\overline{u_i' u_j'}\rangle\right) \tag{3.6}$$

As a result $\langle\overline{\tilde{u}_i\tilde{u}_j}\rangle$ is an extra term contributes to Reynolds stress due to phase averaged product of coherent. Similar to incoherent Reynolds stress term, this coherent Reynolds stress term is a flow dependent property and required extra effort for periodic flow such as vortex shedding phenomenon.

In this study, it is required to obtain the dependence of the triple components of the velocity on time (normalized with respect to total period T) during one complete cycle of events. The periodic vortex shedding velocity fluctuation have been selected as reference signal. Therefore, corresponding to the same t/T of consecutive reference

cycles, the acquired streamwise and transverse velocity components at the same instant are summed and averaged. This averaging process is repeated for different normalized times during one cycle to construct the variation of different properties $\langle \widetilde{u} \rangle$ and $\langle \overline{\widetilde{u}} \rangle$ or $\langle \overline{\widetilde{v}} \rangle$, $\langle \widetilde{u}\widetilde{v} \rangle$ and $\langle \overline{\widetilde{u}\widetilde{v}} \rangle$ etc. The time averaging and phase averaging techniques are applied as defined in sections 2.3 and 2.4 and can be applied for all velocity components or products of velocity components.

Moreover, as mentioned earlier the reference signal required to obtain the corresponding phases of each velocity component. Therefore, placing the reference probe at proper location is very essential since improper location of the reference probe will affect the data analysis.

The final consideration is to determine the lowest acceptable number of cycles to perform phase averaging such that the properties were cycle independent. For such purpose a preliminary experiment was performed with number of cycles taken up to 400 cycles. It was observed that for convergence of properties such as normal and shear stress, steady values required at least 150 cycles. Therefore in this study, number of cycles to perform phase averaging was set as 300- 400 cycles.

Chapter 4

COMPARISON OF FLOW STRUCTURES IN THE WAKE REGION OF A SQUARE CYLINDER AND A U SHAPE CYLINDER

4.1 Introduction

In this chapter, the effect of shape modification on the flow structure and vortex shedding phenomena have been studied experimentally. For this purpose, a square cylinder (SC) has been modified to a U shape cylinder (USC) and the wake regions downstream of both cylinders have been compared in terms of flow structure and other aerodynamic characteristics. Hence, coherent and incoherent flow structures of the wake region have been presented in detail for a square cylinder and a U shape cylinder to demonstrate the possible dissimilarities in flow structures.

The experiment was conducted at free stream velocity U_∞=11.2 ± 2% m/s with measured turbulence intensity of 0.6% at this speed. A U shape cylinder and a square cylinder with a cross section of 25 mm x 25 mm were investigated in this study. Note that the thickness of the U shape cylinder profile is 2 mm. With the end plates employed, the aspect ratio (AR) of the cylinders were 14 and the corresponding blockage ratio of cylinders were 5%.

The experimental setup and schematic of the square and U shape cylinders have been illustrated in figures 4.1 (a) and 4.1 (b), respectively. The corresponding Reynolds

number in the domain of investigation between 1.0 D and 6.0 D in the wake region of cylinders (1.0 ≤x/D≤ 6.0) was Re= 18,100 (Re=ρUD/μ based on cylinder width D) resulted in turbulent vortex shedding behind the both cylinders.

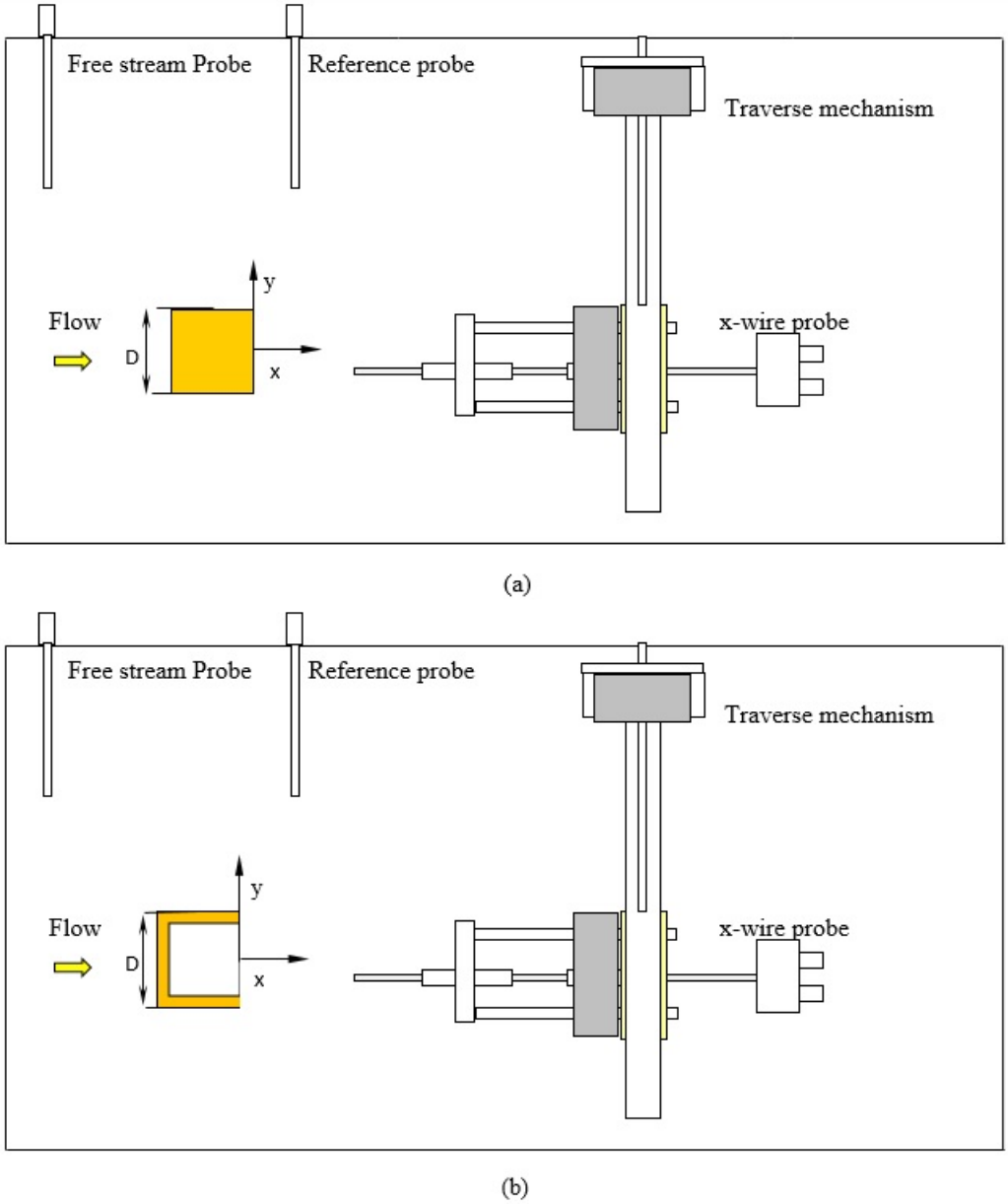

Figure 4.1. Experimental setup and coordinates (Top view) (a) Square cylinder. (b) U shape cylinder

4.2 Spectral Analysis

In order to identify the vortex shedding frequency and quantitative comparison between square and U shape cylinder, Fast Fourier Transform (FFT) has been implemented on the acquired velocity data. Therefore, the dominant shedding frequency (f) can be observed as a single peak corresponding to the Strouhal number in the wake behind cylinders. The instantaneous velocity acquired at various x/D locations downstream in the wake and various transverse directions have been used for frequency spectra determination. The dominant shedding frequency has been found as $f = 48.8\ Hz$ corresponding to the Strouhal number of s_t =0.109 which is identical for both cylinders.

4.3 Phase Averaged Properties

The objective of this study is to investigate the formation of vortex shedding phenomenon in the wake region behind square and U shape cylinders. For that reason, the development of vortex street in the wake region behind both cylinders, have been demonstrated in figures 4.2 to 4.5.

Figures 4.2 and 4.3 illustrate the phase averaged streamwise velocity components acquired at various x/D locations in the downstream wake region of the SC case and the USC case, respectively. From these figures, it is apparent that the flow structures behind the USC have been affected by the employed modification. It can be observed from the figures that the development of wake region downstream of the USC exhibit a delay comparing to the SC case. In other words, the dominant status of the vortex shedding phenomena occur at a higher x/D ratio for the USC in comparison to the SC.

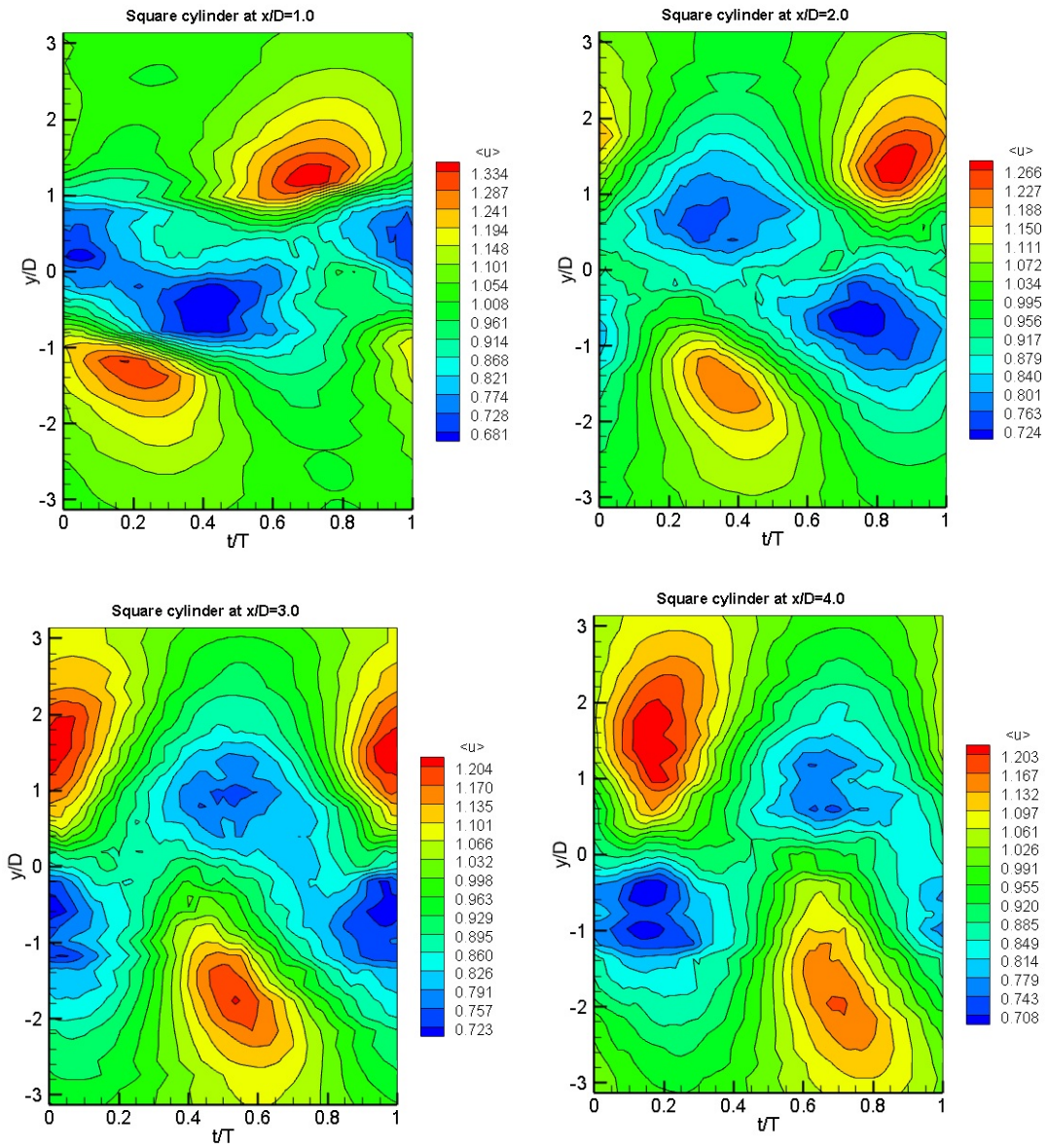

Figure 4.2. Streamwise velocity measured at various x/D locations downstream of the square cylinder

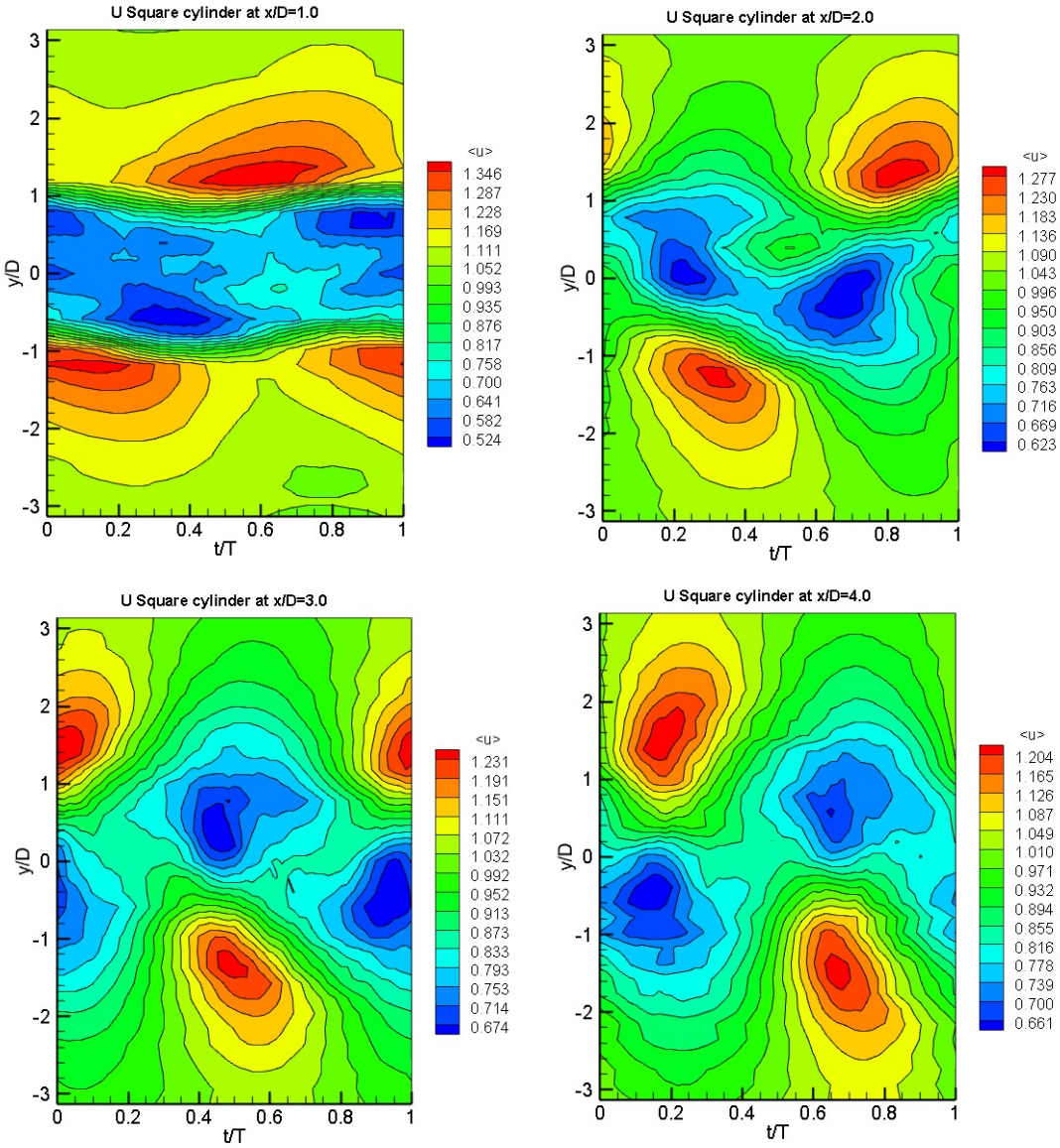

Figure 4.3. Streamwise velocity measured at various x/D locations downstream of the U shape cylinder

Figures 4.4 and 4.5 demonstrate the phase averaged transverse velocity components acquired at various x/D locations in the downstream wake regions of SC and USC, respectively. From these figures, it is also apparent that the flow structures behind the USC have been affected by the employed modification. It can be observed from the figures that the development of wake region downstream of the USC exhibit a delay comparing to the SC case. In other words, the dominant status of the vortex shedding phenomena occur at a higher x/D ratio for the USC in comparison to the SC.

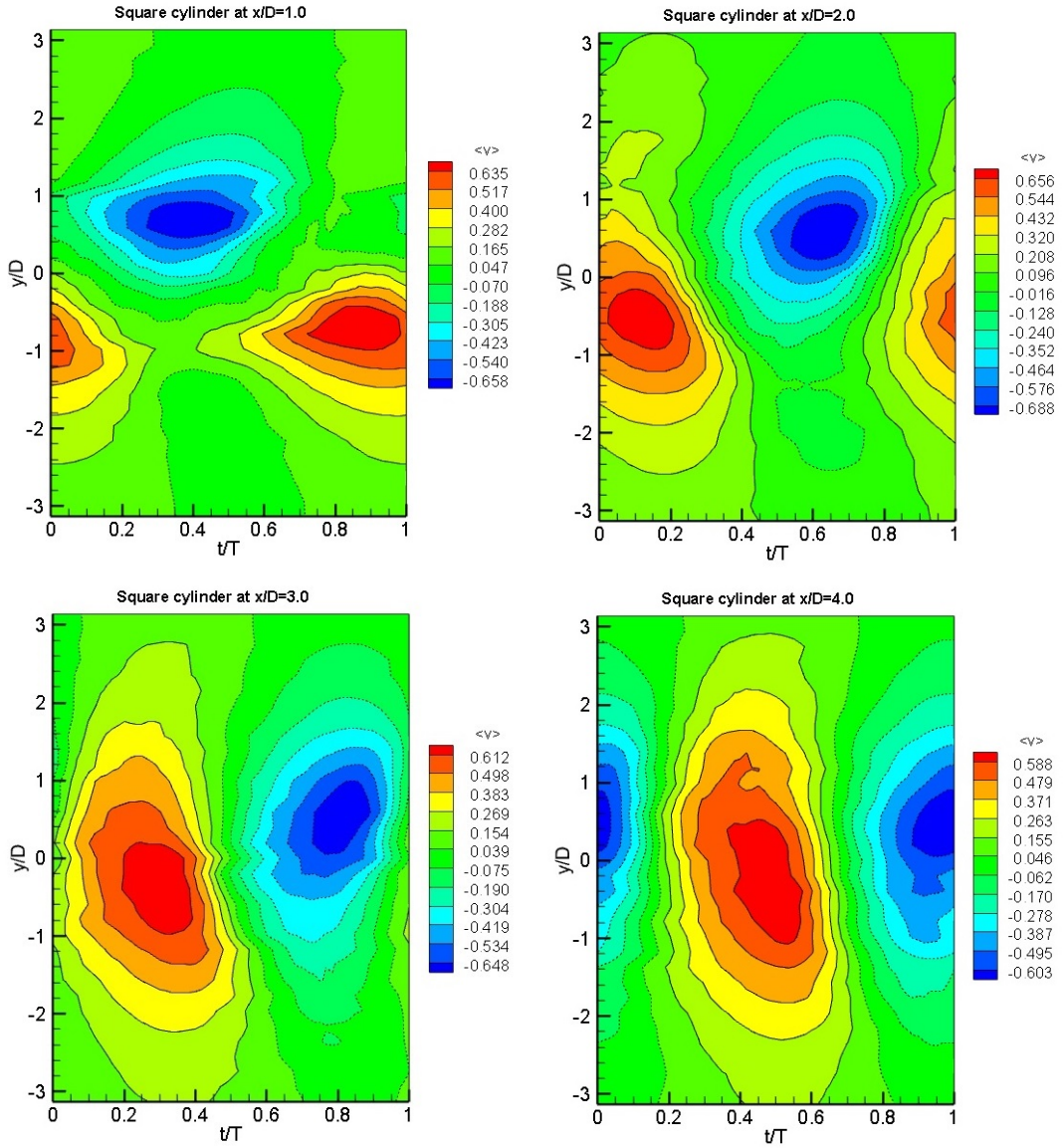

Figure 4.4. Transverse velocity measured at various x/D locations downstream of the square cylinder

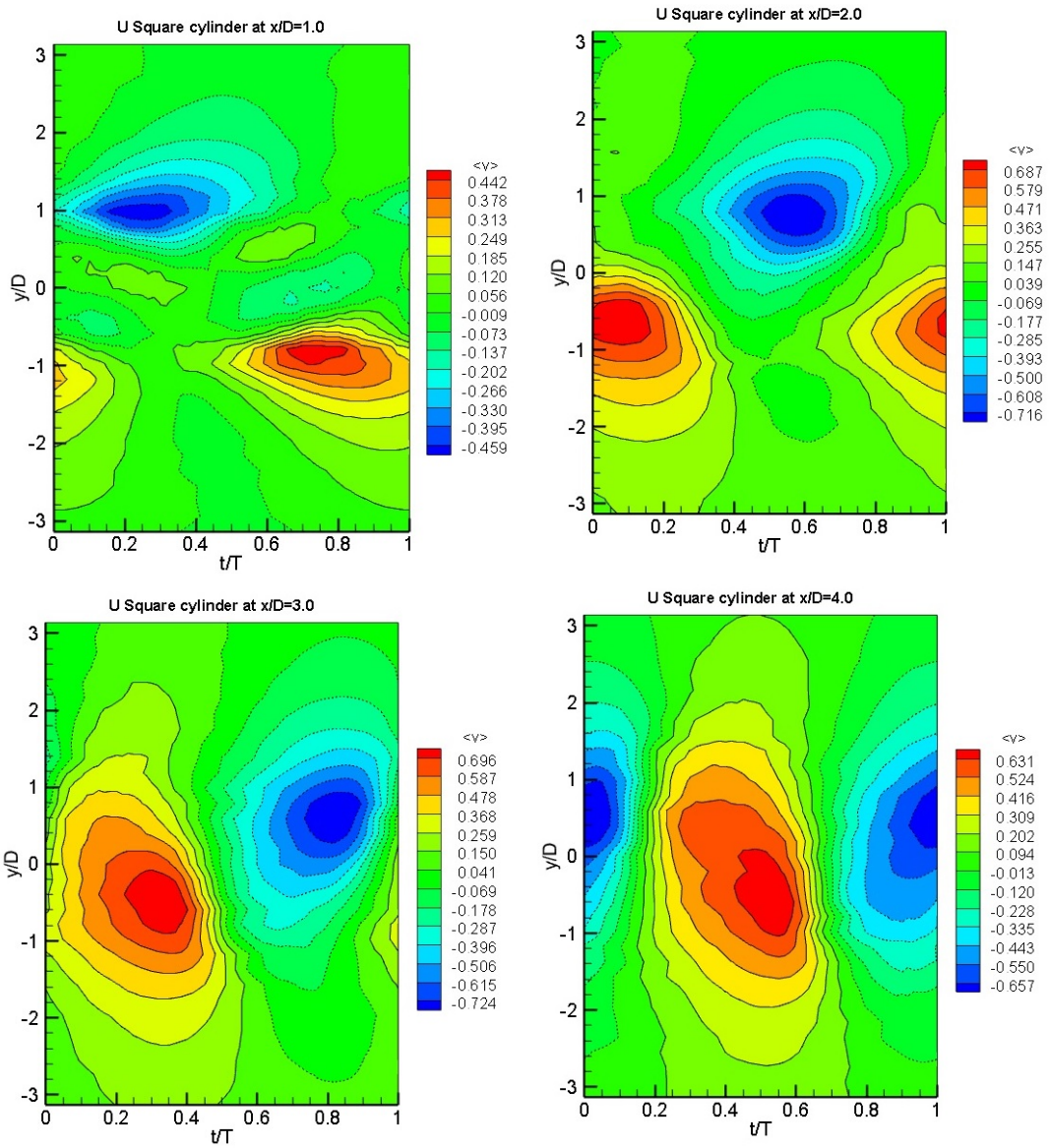

Figure 4.5. Transverse velocity measured at various x/D locations downstream of the U shape cylinder

4.4 Coherent Structure

The variation of phased averaged coherent velocities $\langle\tilde{u}\rangle$ and $\langle\tilde{v}\rangle$ are illustrated in figures 4.6-4.9. Figures 4.6 and 4.7 illustrate the phase averaged coherent streamwise velocity components acquired at various x/D locations in the downstream wake region of SC and USC, respectively. From these figures, it is apparent that the flow structures behind the USC have been affected by the employed modification. It can be concluded from the figure that the USC modification resulted in an alteration of coherent

structure in the wake region very close to the cylinder base (i.e. x/D=1.0) and a narrower coherent flow structure has been observed. However, further downstream in the wake region, the effect of the USC diminishes and flow exhibit similar structure to a SC. Development of the coherent structures is clearly apparent as the vortices being convected downstream through the wake region.

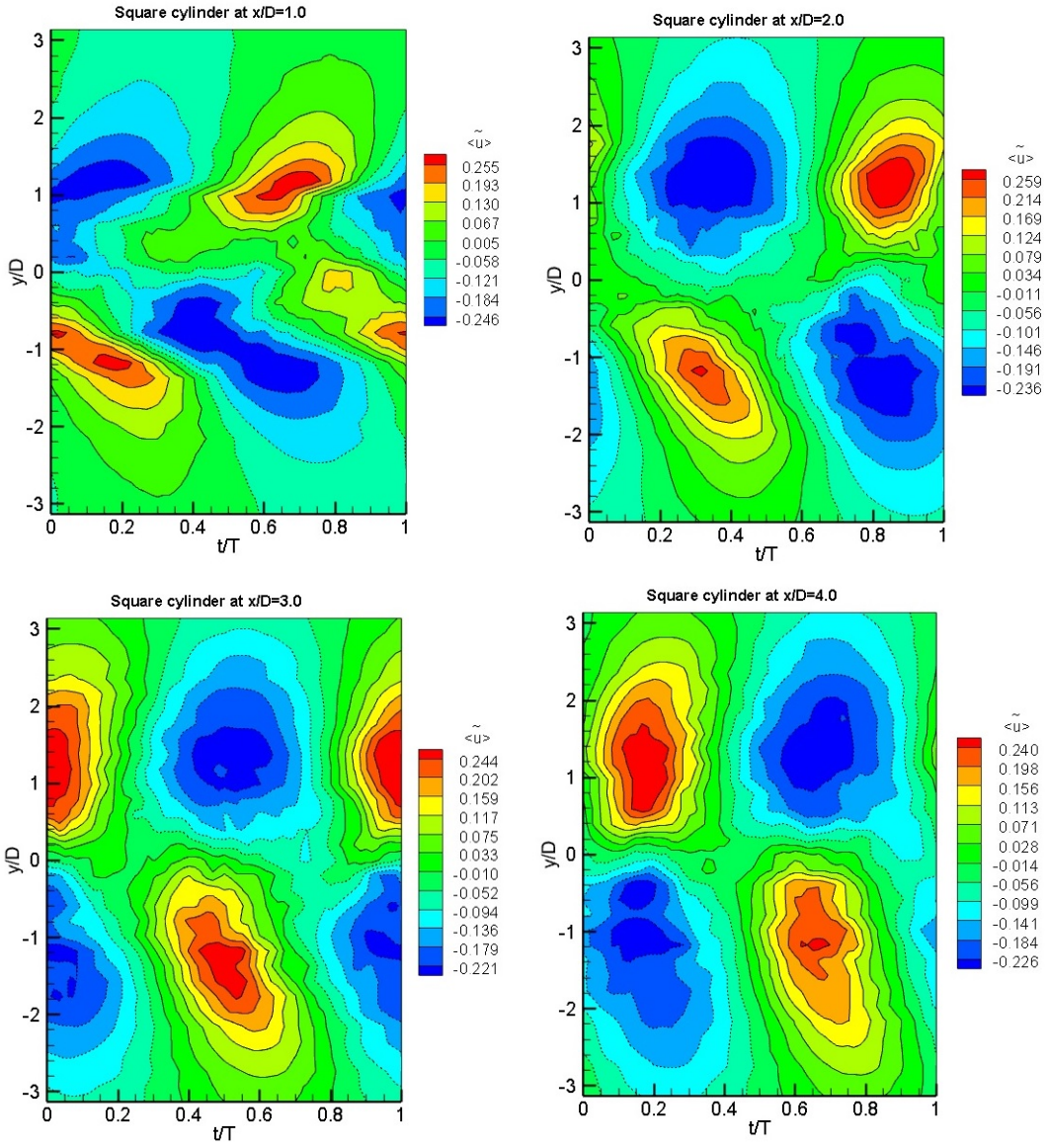

Figure 4.6. Coherent streamwise velocity measured downstream of the square cylinder

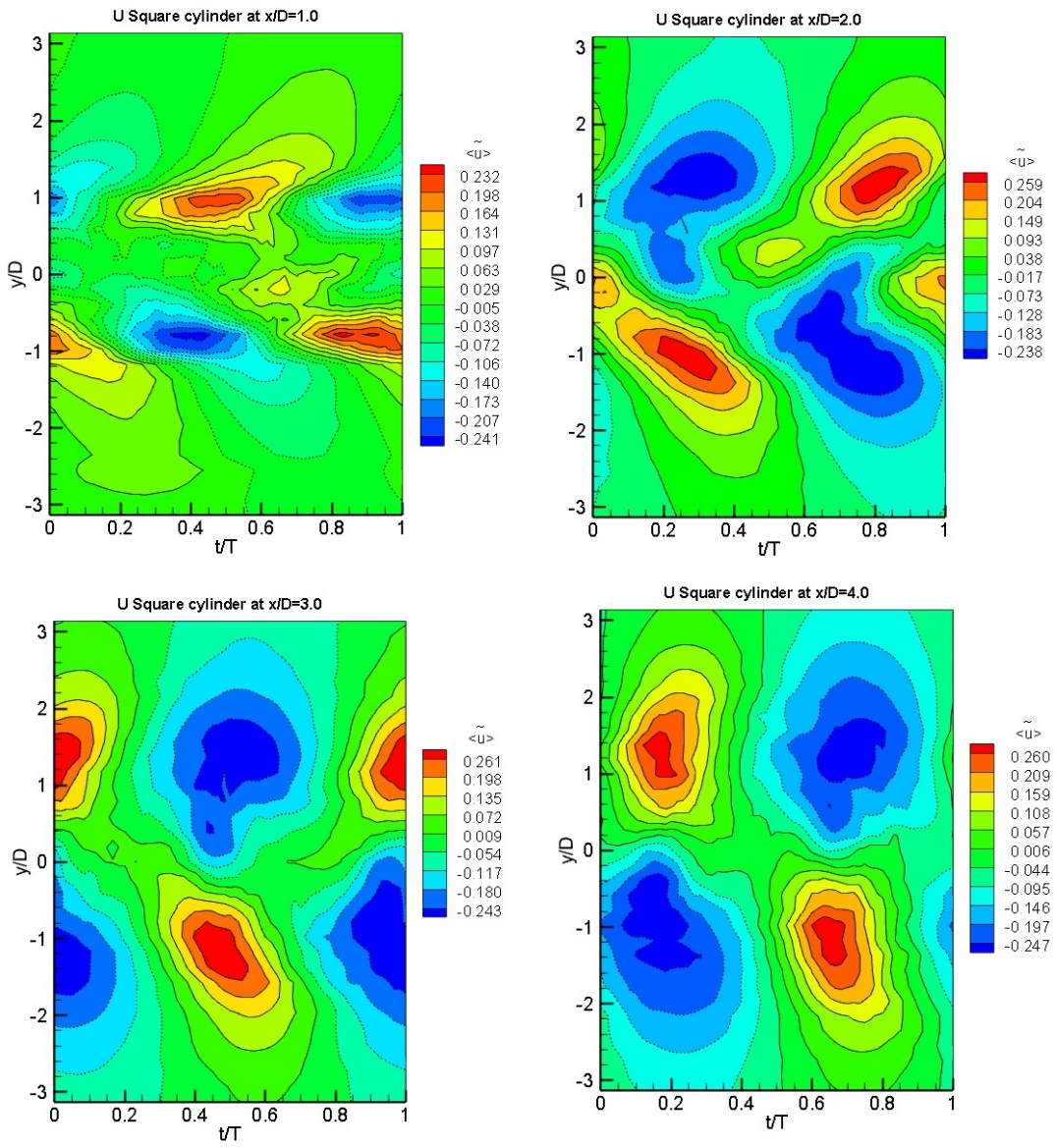

Figure 4.7. Coherent streamwise velocity measured downstream of the U shape cylinder

Figures 4.8 and 4.9 show the phase averaged coherent transverse velocity components acquired at various x/D locations in the downstream wake region of the SC and USC, respectively. From comparison between the $\langle u \rangle$ peak value and $\langle \tilde{u} \rangle$ peak value, on average, it was observed that the coherent structure peak is around 20% of the phase averaged values for both cases of USC and SC. On the other hand, for the case of transverse velocity, on average, the coherent structure peak is around 77 % and 70 %

of the SC and USC phase averaged values, respectively which was caused by a significant lateral momentum during the shedding process.

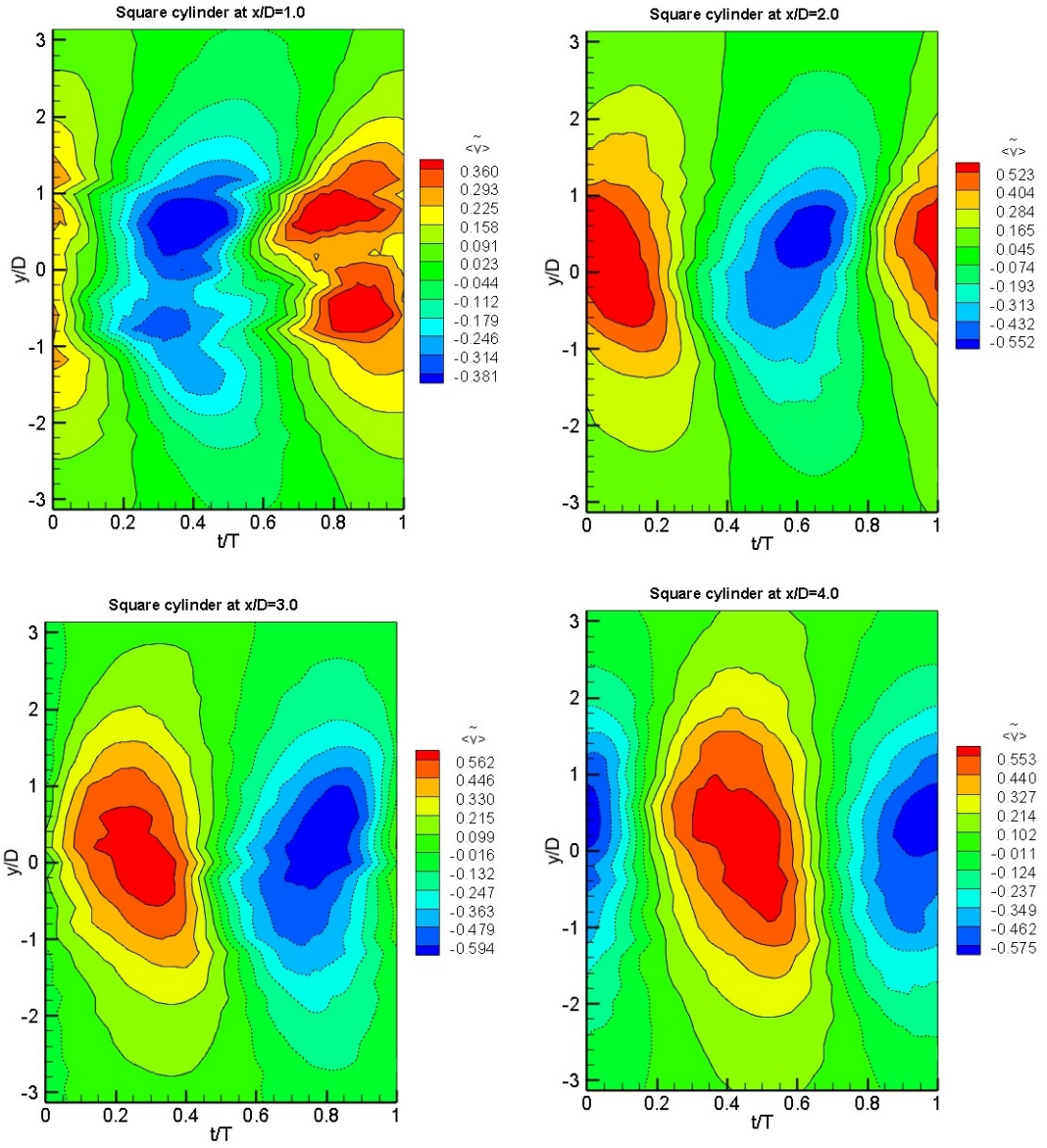

Figure 4.8. Coherent transverse velocity measured downstream of the square cylinder

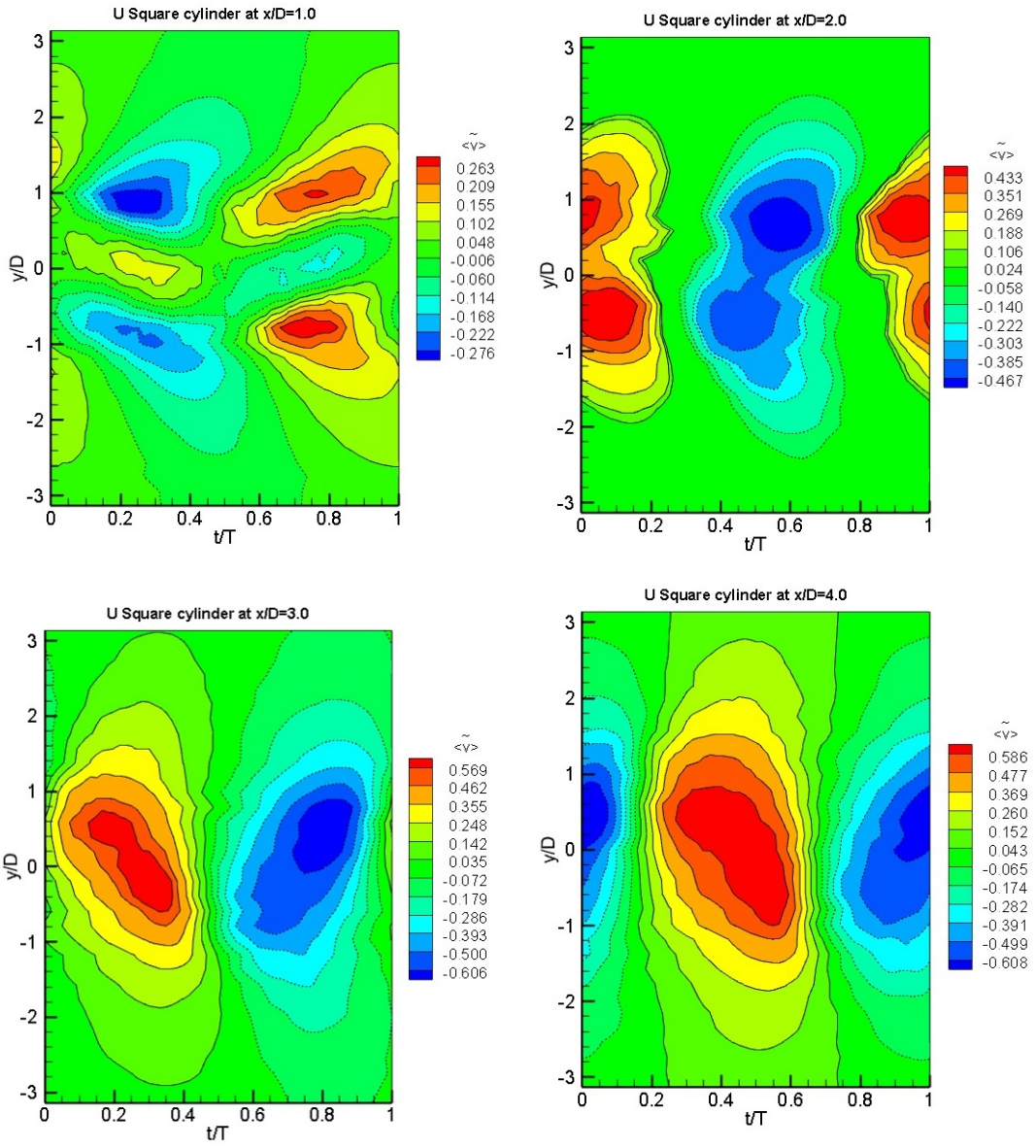

Figure 4.9. Coherent transverse velocity measured downstream of the U shape cylinder

As discussed previously, triple decomposition would provide a better illustration of vortex shedding phenomenon. Therefore, to investigate the development of coherent structure of shedding phenomenon, coherent Turbulent Kinetic Energy (TKE) production in the wake region behind square and U shape cylinders have been depicted in figures 4.10 and 4.11, respectively.

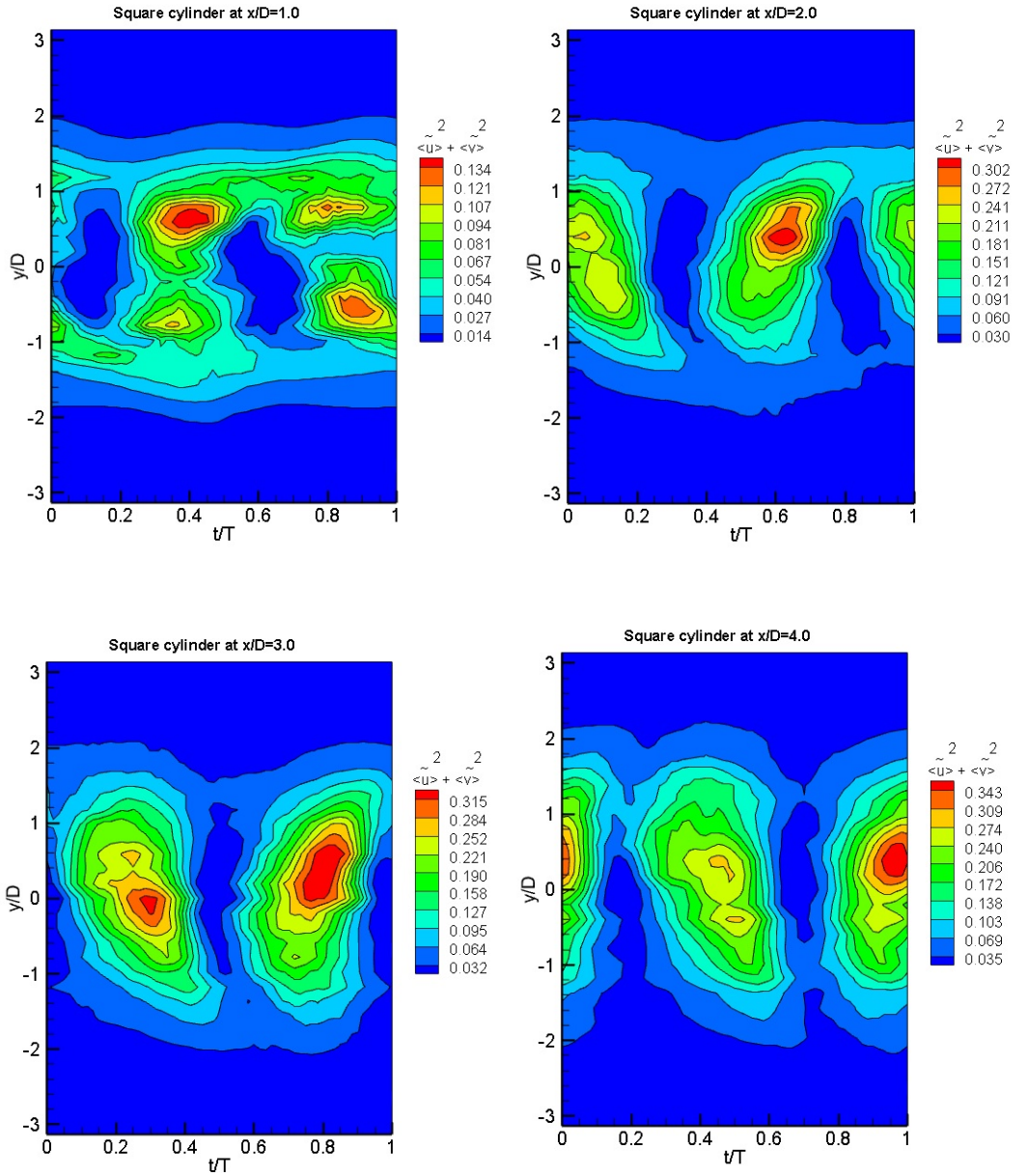

Figure 4.10. Coherent Turbulent Kinetic Energy production in the wake region of the square cylinder

Figures 4.10 and 4.11 demonstrate the coherent turbulent kinetic energy production acquired at various x/D locations in the downstream wake regions of SC and USC, respectively. A comparison between USC and SC shows a similar development of TKE in the wake region. At near wake (i.e. x/D=1.0), coherent turbulent kinetic energy peaks are observed along the edges. As the probe moves downstream in the wake region namely x/D= 3.0, these peaks are developed toward the centreline. However,

from a comparison between USC and SC it can be concluded that the U modification causes a delay in the development of such flow structures.

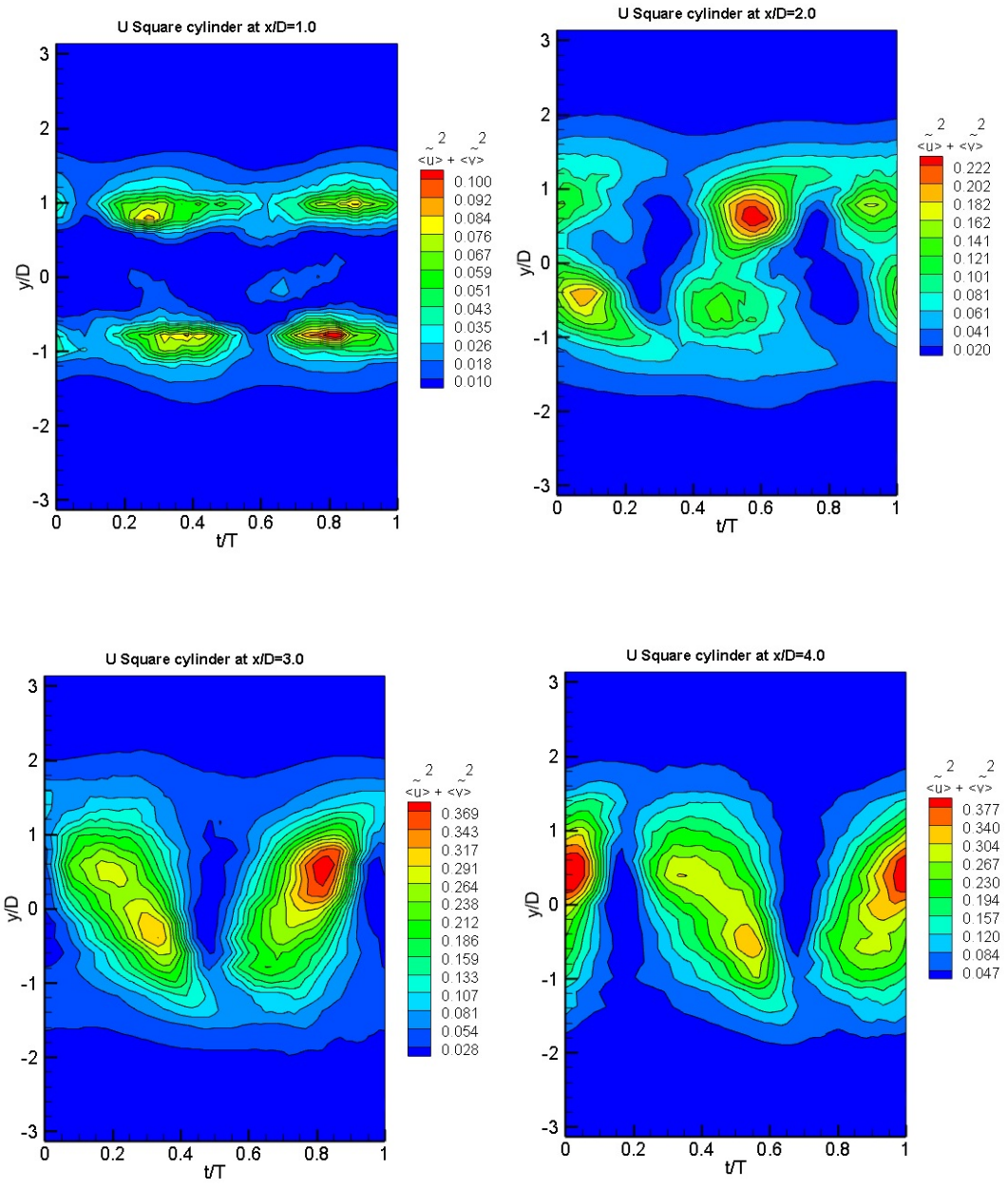

Figure 4.11. Coherent Turbulent Kinetic Energy production in the wake region of the U shape cylinder

It can be concluded from the figures that at wake region close to the base, the wake behind SC exhibit higher coherent TKE peak. On the contrary, further downstream the wake region, USC demonstrate higher peak level for coherent TKE. In other words,

the USC delays the development of alternate vortices at the near base. Hence, the wake region demonstrates lower coherent TKE as apparent in the figures. However, further downstream in the wake region behind USC, flow possess higher coherent TKE which implies that entrainment of fluid into USC gap eventually causes development of stronger vortices.

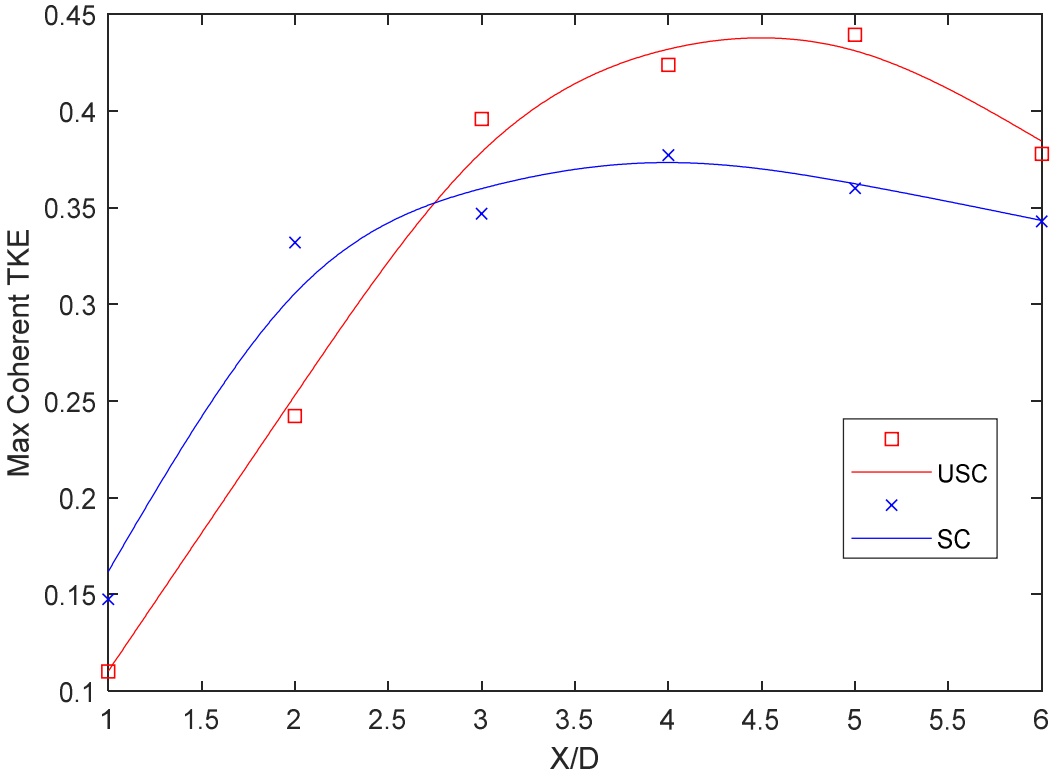

Figure 4.12. Maximum coherent TKE vs x/D location for SC and USC

Figure 4.12 shows the detected peak value of SC and USC coherent TKE for various x/D locations, respectively. It is seen from figure 4.12 that the coherent TKE peak of USC is lower than the coherent TKE peak of SC in the near wake region. The detected reductions in USC coherent TKE peak at x/D=1 and x/D=2 are about 26 % and 27 %, respectively. The situation is different in the far wake region. The coherent TKE peak of USC is higher than the coherent TKE peak of SC in the far wake region. The

detected increases in USC coherent TKE peak at x/D=3, x/D=4, x/D=5, and x/D=6 are about 15 %, 13 %, 22 %, and 11 % respectively. It is apparent from the figure that the maximum coherent TKE peak of USC occurs at a larger x/D which can be concluded as an indication of a location delay in the wake region in comparison to the SC case.

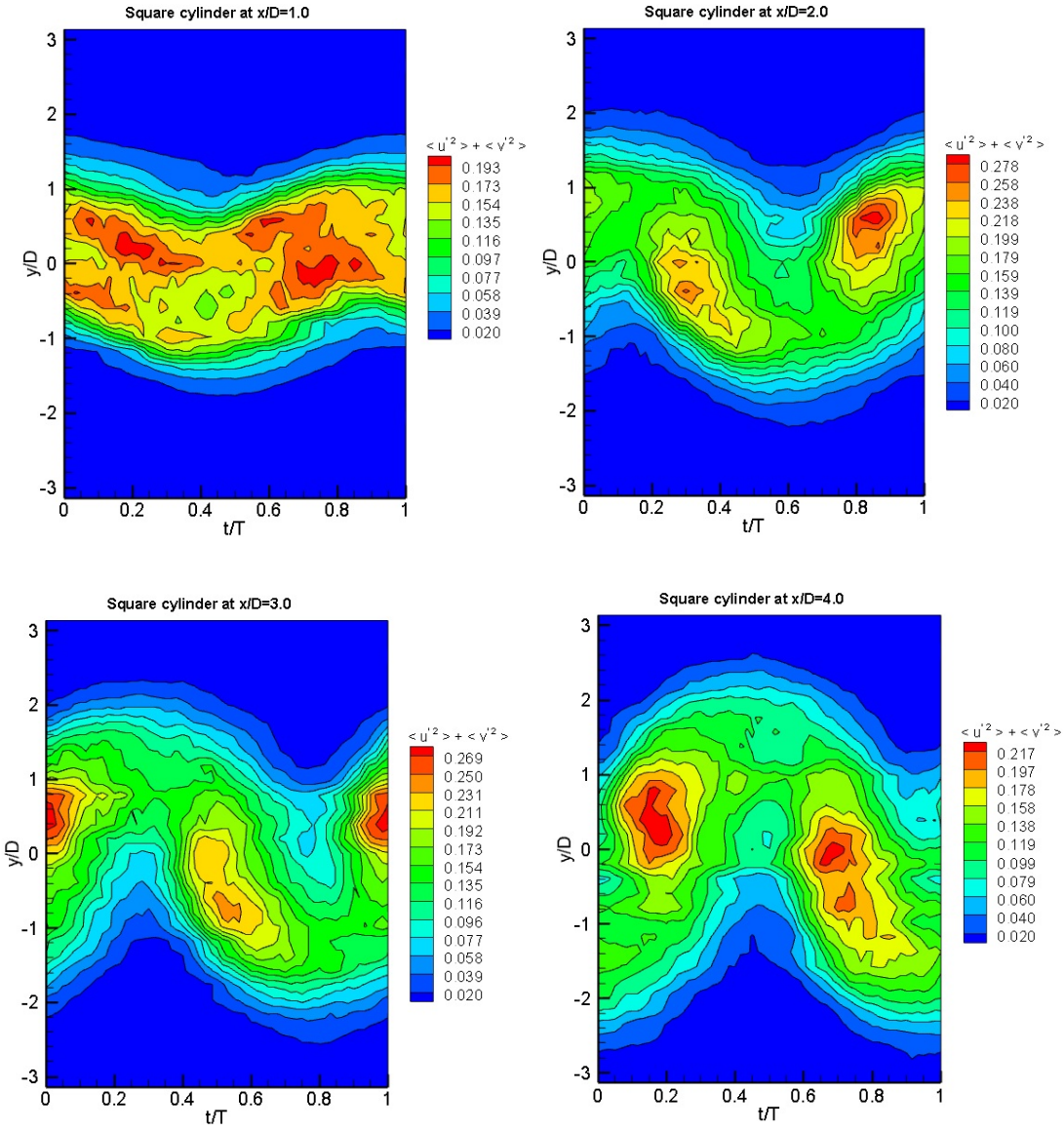

Figure 4.13. Incoherent Turbulent Kinetic Energy production in the wake region of the square cylinder

4.5 Turbulent Kinetic Energy

As discussed triple decomposition distinguishes between coherent structure or vortex shedding phenomenon and incoherent structure of turbulent flow fluctuations. Therefore, it is possible to put the periodic vortex shedding phenomenon a side and perform a detailed investigation on incoherent fluctuations.

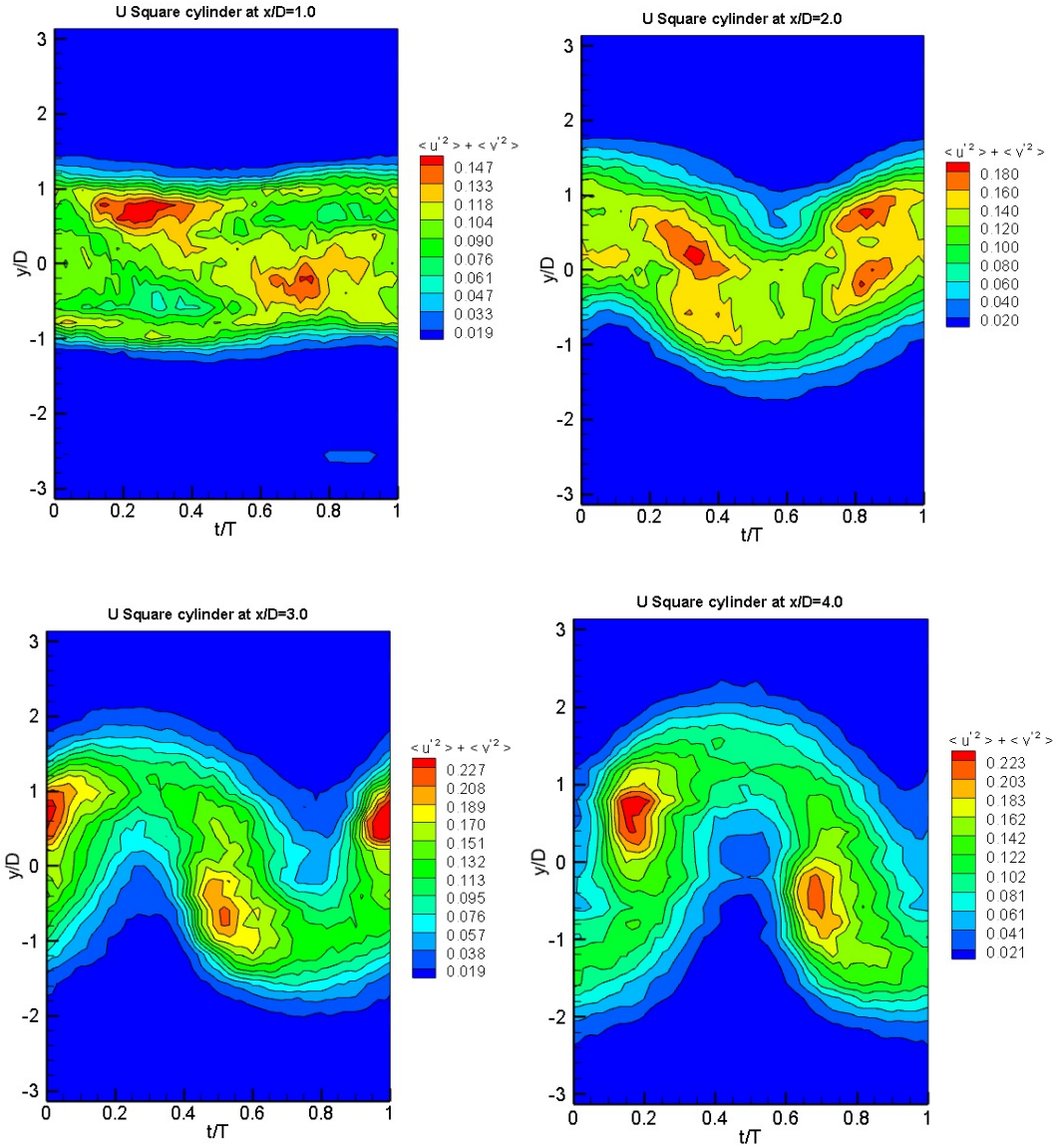

Figure 4.14. Incoherent Turbulent Kinetic Energy production in the wake region of the U shape cylinder

Figures 4.13 and 4.14 demonstrate the incoherent turbulent kinetic energy production acquired at various x/D locations in the wake region downstream of SC and USC, respectively. It can be observed from figures that higher incoherent TKE peaks in the wake behind square cylinder for all acquired x/D locations have been observed. Such reduction in incoherent TKE caused by flow entraining into the gap/space inside USC.

Figure 4.15 shows the detected peak value of SC and USC incoherent TKE for various x/D locations, respectively. It can be observed from the figure that the incoherent TKE peak of USC is lower than the incoherent TKE peak of SC. On average, the detected reduction in USC incoherent TKE peak is about 17 %. It is noticeable that the detected reduction in USC incoherent TKE peak is higher in the near wake region. It is also apparent from the figure that the maximum incoherent TKE peak of USC occurs at a larger x/D ratio in comparison to the SC case.

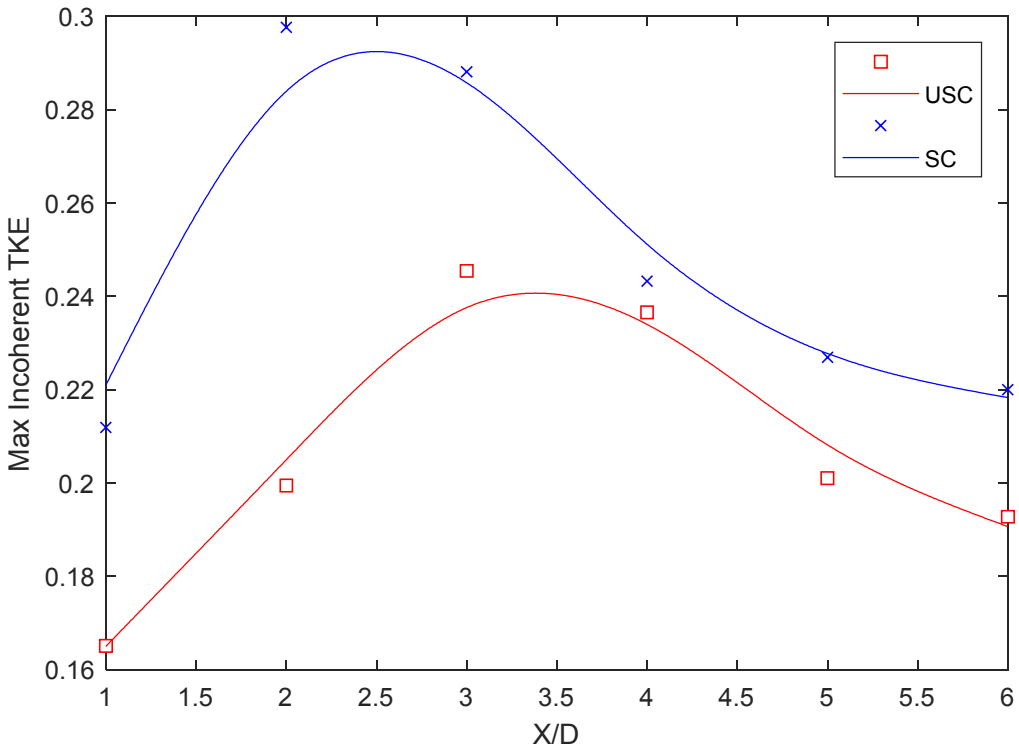

Figure 4.15. Maximum incoherent TKE vs x/D location for SC and USC

4.6 Time Averaged Properties

Better understanding of the flow structure also requires to quantify development and decay of flow properties such as streamwise velocity, transverse velocity and turbulent stresses in the downstream wake region. In this section quantitative comparison of time averaged streamwise, time averaged transverse velocity measured at various x/D locations in the wake region have been presented. The time averaged properties such as streamwise and transverse velocity are normalized with free stream velocity (U_∞). The time averaged streamwise $\langle \overline{u} \rangle$ and transverse velocity profiles $\langle \overline{v} \rangle$ are depicted in figures 4.16 and 4.17, respectively acquired at various x/D locations in the downstream wake of the cylinders. As it was anticipated, the wake region downstream of the USC demonstrate a symmetrical streamwise and transverse velocity profiles similar to SC as depicted in the figures. It can be observed from the figures that the wake region behind the USC exhibit a delay in wake recovery in comparison to the SC. Measurements revealed that in the near wake region (i.e. x/D=1.0) of the USC, the streamwise velocity is in order of 60% of free stream velocity. On the other hand, for the case of SC it was observed that the wake recovers to $0.8U_\infty$. As the probe moves downstream in the wake, the streamwise velocity component recovers to $0.8U_\infty$ and $0.9U_\infty$ for USC and SC, respectively. Such discrepancy caused by entrainment of fluid into the hollow space of USC and therefore the wake recovery is delayed. The transverse velocity profile decaying downstream in the wake region is also apparent from the figure. However, it can be seen from the figure that the wake region downstream of the USC exhibits higher momentum transfer towards the centerline.

As the shear layers separate from square cylinder, the fluid flow is subjected to momentum loss in the wake region. Therefore, the time averaged streamwise velocity

profile exhibits a rapid drop in the wake region of the cylinders. However, outside the wake it returns to the free stream value, which is apparent from the figure. As the flow structure develops downstream, the wake widens as fluid entrained into the wake from the edges of cylinder periodically. Another sign of such entrainment process can be perceived from time averaged transverse velocity profile. At very near the wake region exhibit high fluid entrainment towards the centerline. However, such process is dissipated significantly beyond the distance of 3D in the downstream wake region.

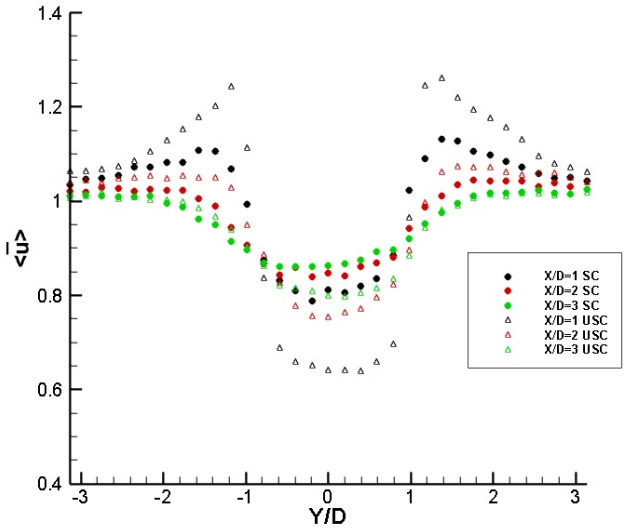

Figure 4.16. Comparison of time averaged streamwise velocities for SC and USC

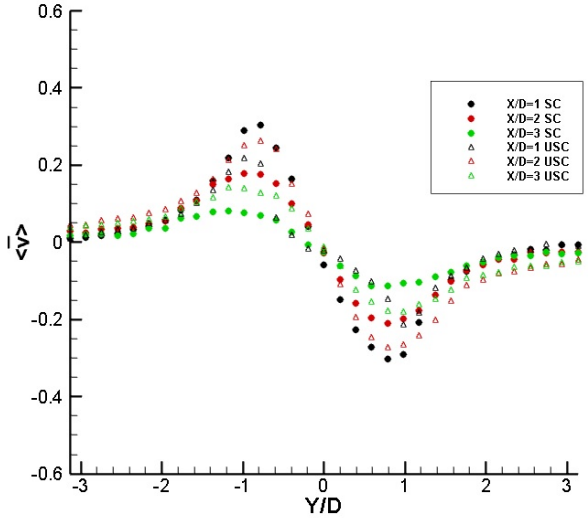

Figure 4.17. Comparison of time averaged transverse velocities for SC and USC

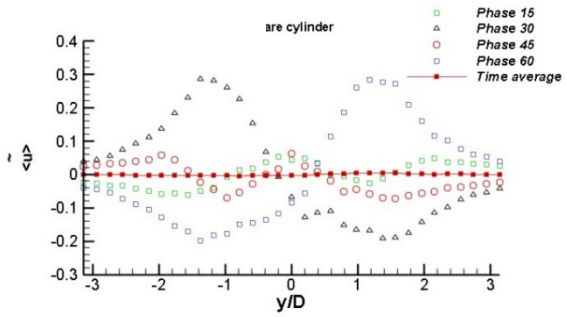

(a)

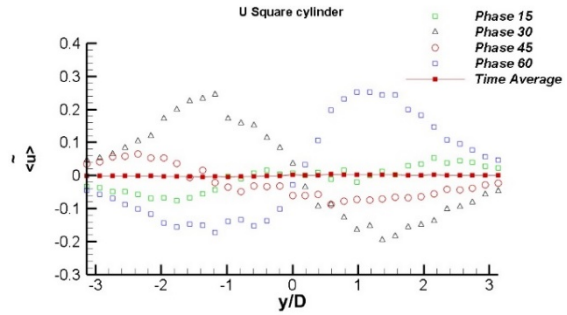

(b)

Figure 4.18. Phase averaged coherent streamwise velocity components profile measured at x/D=3.0 at various phases for (a) Square cylinder, (b) U shape cylinder

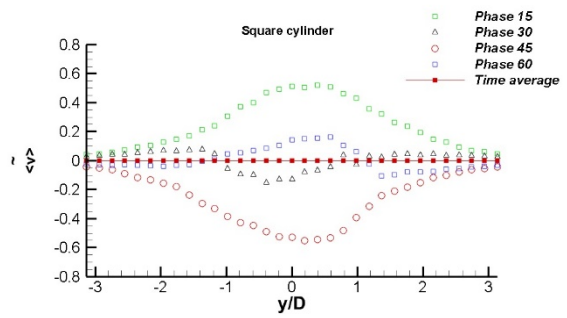

(a)

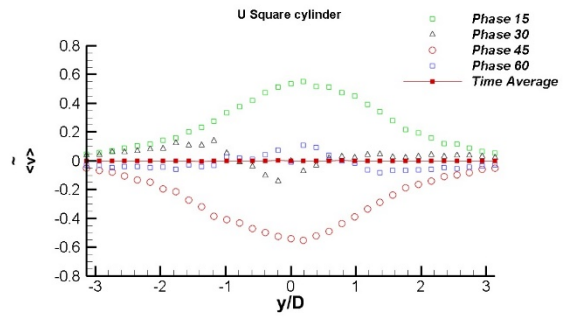

(b)

Figure 4.19. Phase averaged coherent transverse velocity component profile measured at x/D = 3.0 at various phases for (a) Square cylinder, (b) U shape cylinder

Clearly, dividing a cycle into insufficient number of phases resulted in discrete variation for phase averaging rather than a continuous variation of the properties. In this research, 60 phases during one cycle have been employed. Figures 4.18 and 4.19 illustrate the phase averaged variations of coherent streamwise and transverse velocity components measured at x/D = 3.0 at four different phases, respectively. The obtained time mean phase averaged coherent properties over one cycle implies zero values within accuracy of ±1 %. Figures 4.18 and 4.19 demonstrated such observation for both SC and USC cases.

4.7 Experimental Uncertainty

The measurement errors by CTA hotwire systems were under influence of calibration equipment, positioning (the alignment of the probe in the experimental set-up), linearization (curve fitting), electrical noise and turbulence intensity of free stream. However, the commercial CTA's have low drift and low noise with negligible effects on uncertainty of measurement. A dedicated calibrator has been employed for the calibration process and therefore the uncertainty due the calibrator would be in order of MSE (Mean Square Error) of the calibrated probes that were in the range of 0.02 – 0.05%. On the other hand, CTA velocity measurement accuracy depends on the turbulence intensity level of the flow. Error in high turbulence intensity (around 35%) wake region for X wire measurements has been reported by Tutu and Chevray (1975) up to 28%. In this work regions with similar level of turbulence intensity and also regions with turbulence intensity 15% or lower have been observed.

Therefore, the error in result such as figure 4.10 might match to a value as reported by Tutu and Chevray (1975) for high turbulence intensity hot wire measurements. However, for u component measurement in high turbulence intensity wake region such

as figure 4.2 and figure 4.3, the error is compatible with accuracy of the calibration which is less than 2% in this work.

Chapter 5

COMPARISON OF FLOW STRUCTURES IN THE WAKE REGION OF A TRIANGULAR CYLINDER AND AN L SHAPE CYLINDER

5.1 Introduction

In this chapter, two different geometries have been selected in order to test and confirm the obtained conclusion regarding the square and U shape cylinder. For this purpose, a triangular cylinder (TC) has been modified to an L shape cylinder (LSC) and the wake regions downstream of both cylinders have been compared in terms of flow structures and other aerodynamic characteristics. Hence, coherent and incoherent flow structures of wake region have been presented in detail for a triangular cylinder and an L shape cylinder to demonstrate the possible dissimilarities of flow structures.

The experiment was conducted at free stream velocity U_∞=11.2 ± 2% m/s with measured turbulence intensity of 0.6% at this speed. An L shape cylinder and triangular cylinder with a cross section of 25 mm x 25 mm were investigated in this study. Note that the thickness of the L shape cylinder profile is 2 mm. With the end plates employed, the aspect ratio (AR) of the cylinders were 14 and the corresponding blockage ratio of cylinders were 7%.

The experimental setup and schematic of the triangular and L shape cylinders has been illustrated in figures 5.1 (a) and 4.1 (b), respectively. The corresponding Reynolds

number in the domain of investigation between 1.0 D to 6.0 D in the wake region of the cylinders (1.0 ≤x/D≤ 6.0) was Re=18,100 (Re=ρUD/μ based on the cylinder width D) resulted in turbulent vortex shedding behind the both cylinders.

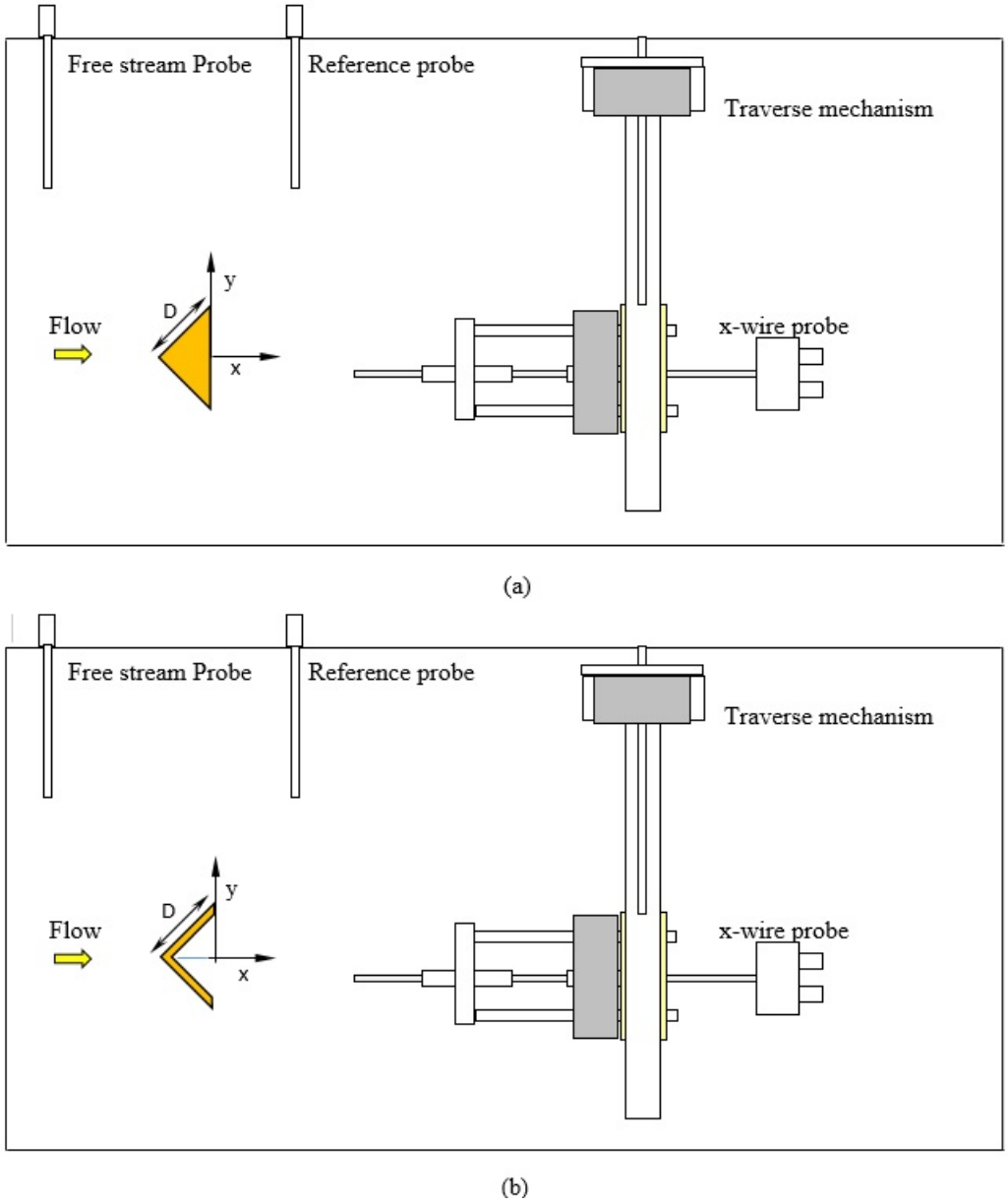

Figure 5.1. Experimental setup and coordinates (Top view) (a) Triangular cylinder (b) L shape cylinder

5.2 Spectral Analysis

In order to identify the vortex shedding frequency and quantitative comparison between triangular and L shape cylinder, Fast Fourier Transform (FFT) has been implemented on the acquired velocity data. Therefore, the dominant shedding frequency (f) can be observed as a single peak corresponding to the Strouhal number in the wake of cylinders. The instantaneous velocity acquired at various x/D locations and transverse directions have been used for frequency spectra determination. The dominant shedding frequency of the L shape cylinder has been found as $f = 48.8\ Hz$ corresponding to the Strouhal number of s_t =0.109 while the dominant shedding frequency of the triangular cylinder has been found as $f = 53.7\ Hz$ corresponding to the Strouhal number s_t =0.119.

5.3 Phase Averaged Flow Structure

The objective of this study is to investigate the formation of vortex shedding phenomenon in the wake region behind triangular and L shape cylinders. For that reason, the development of vortex street in the wake region behind both cylinders, have been demonstrated in figures 5.2 to 5.5.

Figures 5.2 and 5.3 illustrate the phase averaged streamwise velocity components acquired at various x/D locations in the downstream wake region of the TC and LSC, respectively. From these figures, it is apparent that the flow structures behind the LSC have been affected by the employed modification. It can be observed from the figures that the wake region downstream of the LSC exhibit a delay in wake recovery in comparison to the TC. In other words, the dominant status of the vortex shedding phenomena occurs at a higher x/D ratio for the LSC in comparison to the TC case.

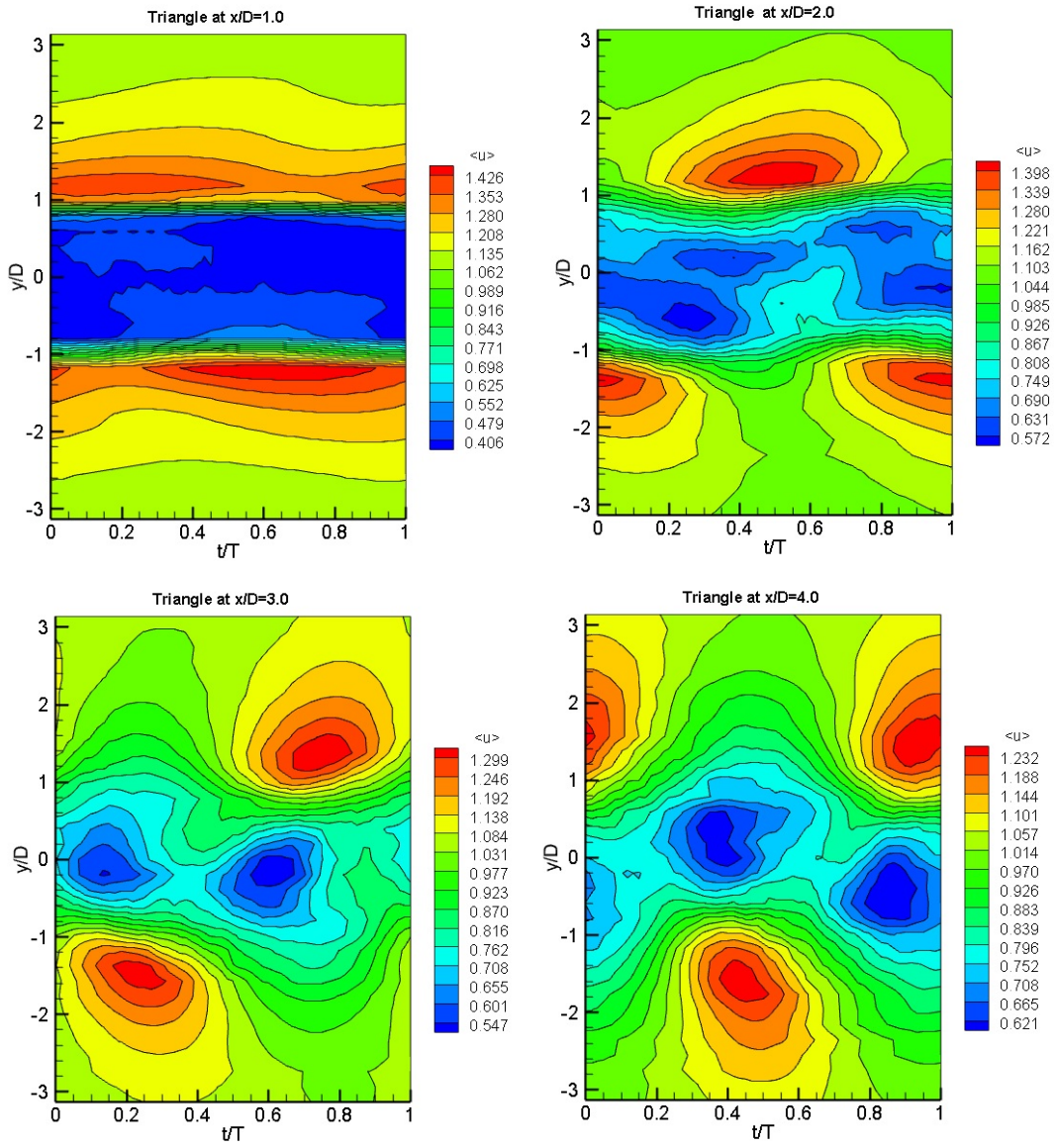

Figure 5.2. Streamwise velocity measured at various x/D locations in downstream wake of the triangular cylinder

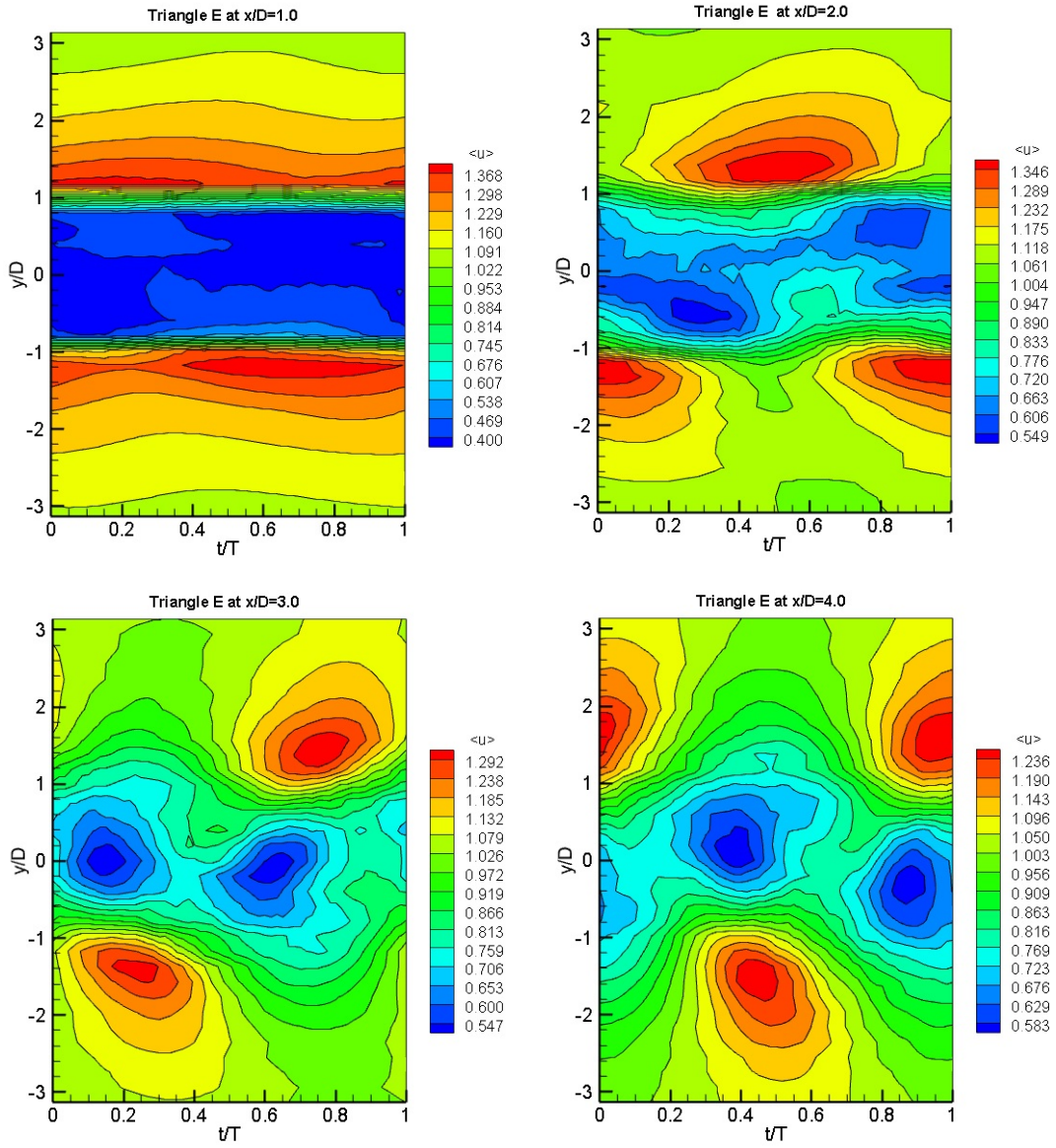

Figure 5.3. Streamwise velocity measured at various x/D locations in downstream wake of the L shape cylinder

Figures 5.4 and 5.5 demonstrate the phase averaged transverse velocity components acquired at various x/D locations in the downstream wake region of the TC and LSC, respectively. From these figures, it is also apparent that the flow structures behind the LSC have been affected by the employed modification. It can be observed from figures that the wake region behind the LSC exhibit a delay in wake recovery in comparison to the TC. In other words, the dominant status of the vortex shedding phenomena occur at a higher x/D location for the LSC in comparison to the TC.

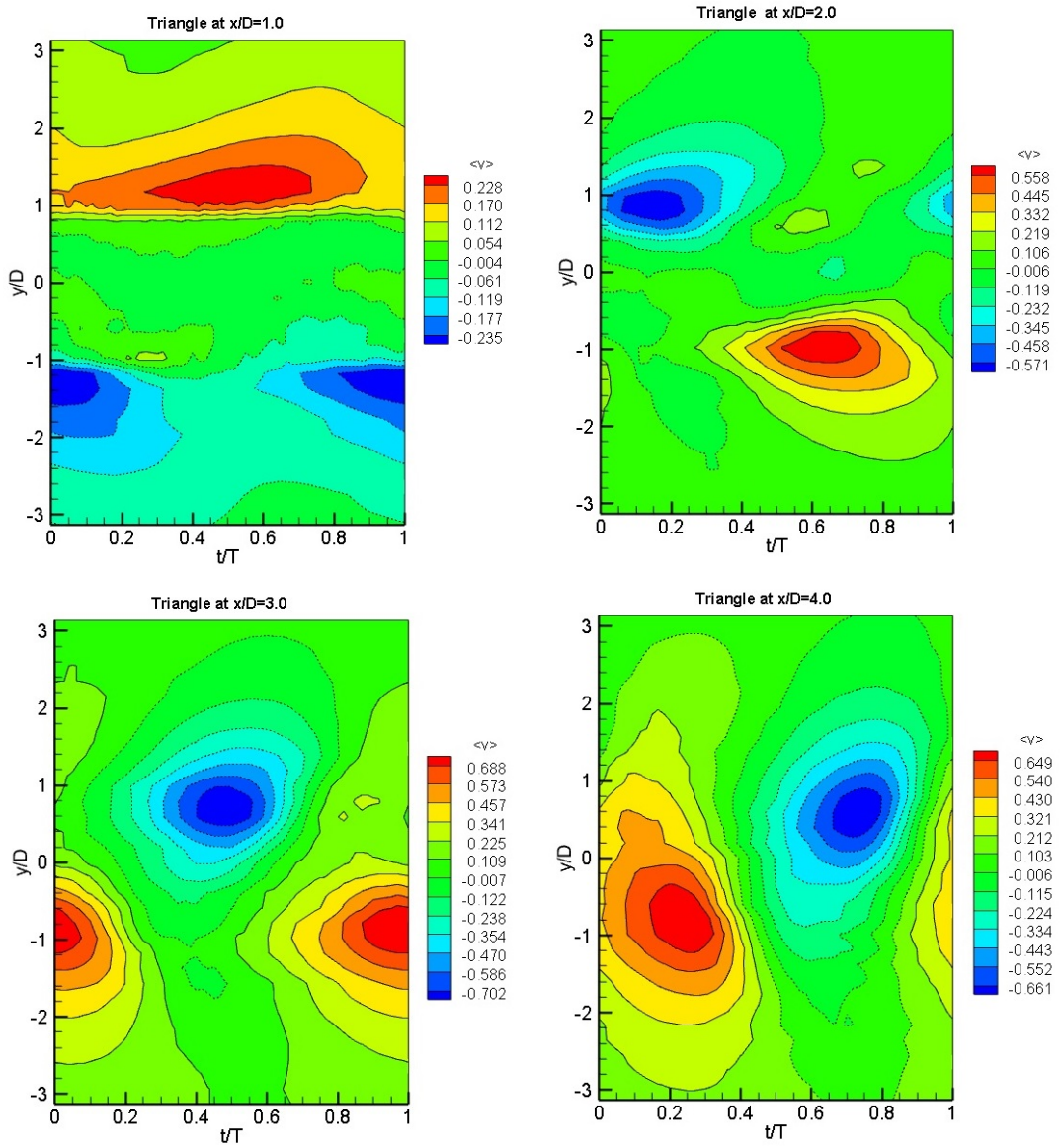

Figure 5.4. Transverse velocity measured at various x/D locations in downstream wake of the triangular cylinder

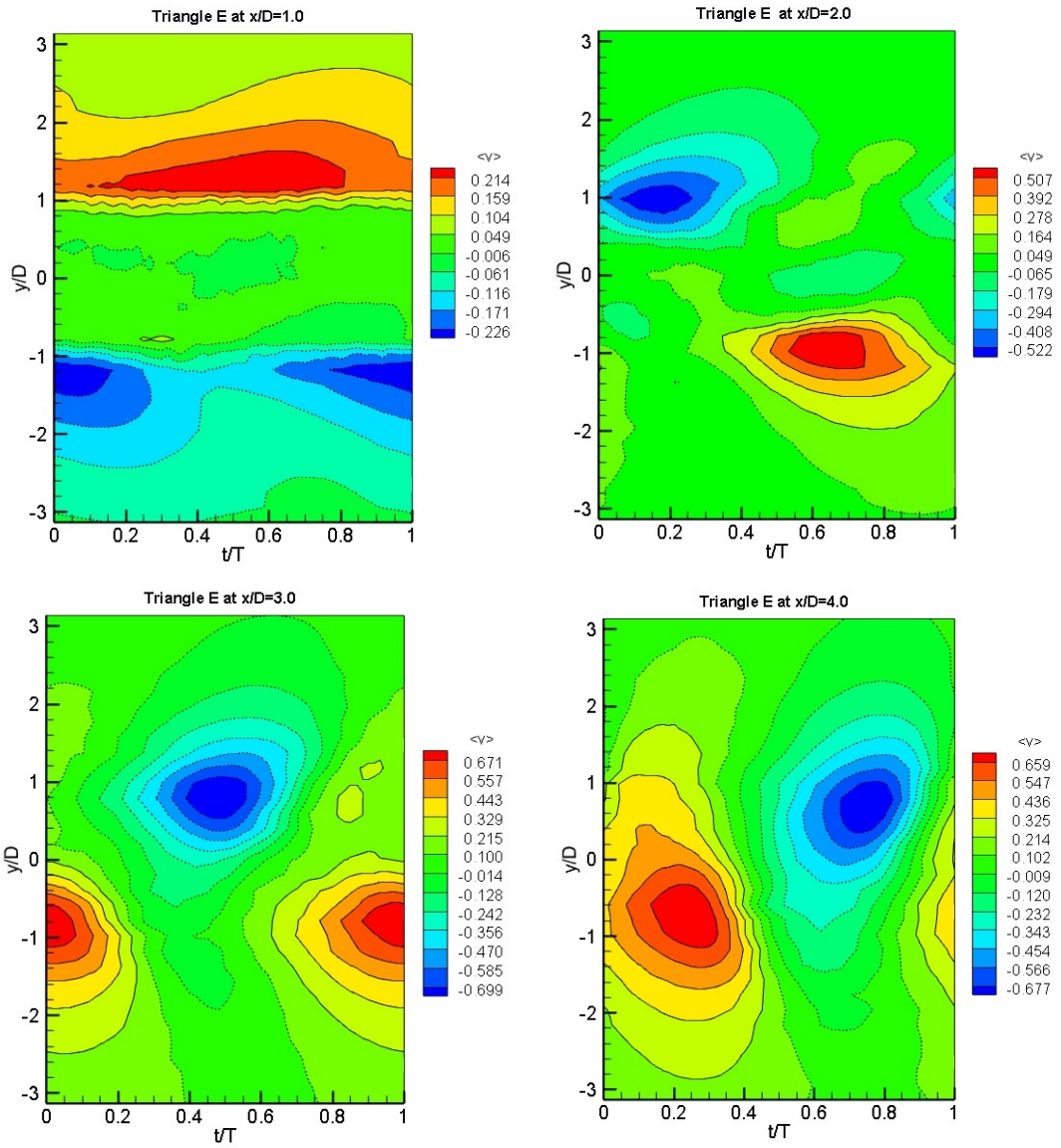

Figure 5.5. Transverse velocity measured at various x/D locations in downstream wake of the L shape cylinder

5.4 Coherent Flow Structure

The variation of phased averaged coherent velocities $\langle\tilde{u}\rangle$ and $\langle\tilde{v}\rangle$ are illustrated in figures 5.6-5.9. Figures 5.6 and 5.7 illustrate the phase averaged coherent streamwise velocity components acquired at various x/D locations in the downstream wake region of the TC and the LSC case, respectively. From these figures, it is apparent that the flow structures behind the LSC have been affected by the employed modification. It can be concluded from the figure that LSC modification resulted in an alteration of

coherent structure in the wake region very close to the cylinder base (i.e. x/D=1.0) and a narrower coherent structure has been observed. However, further downstream in the wake region, the effect of the LSC diminishes and flow exhibit similar structure to the LC case. Development of the coherent structures is clearly apparent as the vortices being convected further downstream in the wake region.

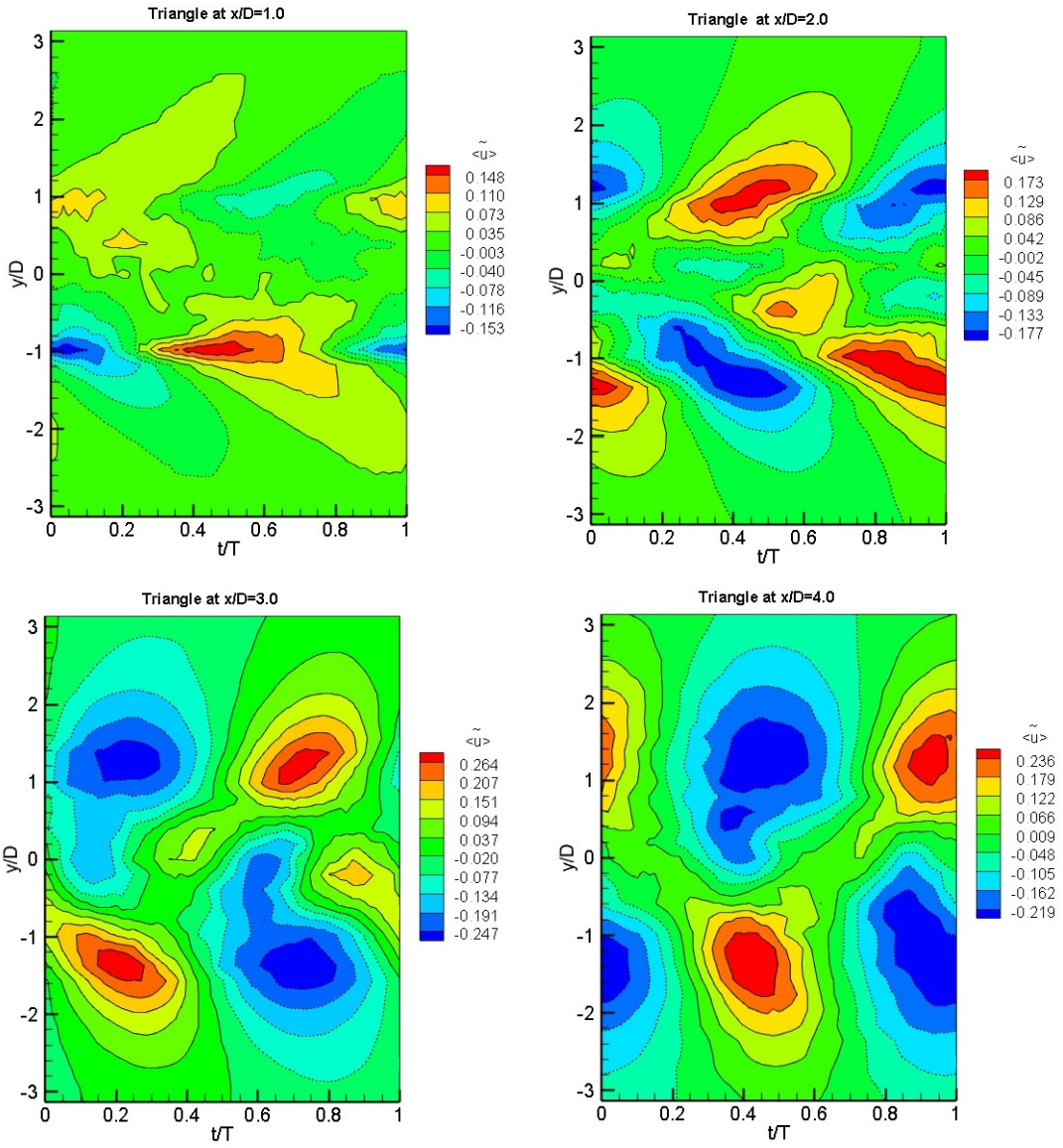

Figure 5.6. Coherent streamwise velocity measured downstream of the triangular cylinder

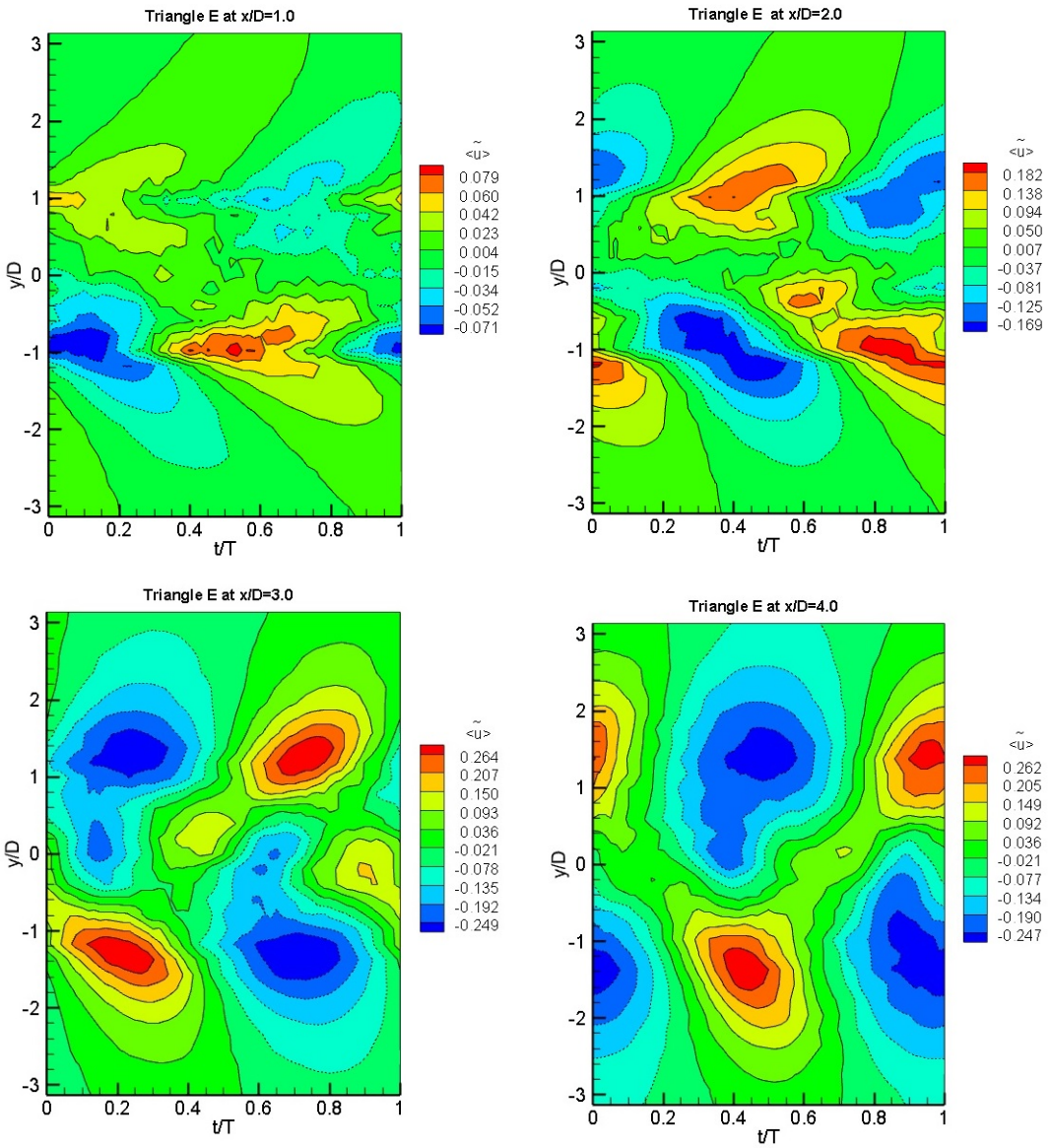

Figure 5.7. Coherent streamwise velocity measured downstream of the L shape cylinder

Figures 5.8 and 5.9 show the phase averaged coherent transverse velocity components acquired at various x/D locations in the downstream wake region of the TC and LSC, respectively. From comparison between the $\langle u \rangle$ peak value and $\langle \tilde{u} \rangle$ peak value, on average, it was observed that the coherent structure peak is around 16% of the phase averaged values for both cases of the LSC and the TC. On the other hand, for the case of transverse velocity, on average, the coherent structure peak is around 63 % and 60

% of the TC and LSC phase averaged values, respectively which was caused by a significant lateral momentum during the vortex shedding process.

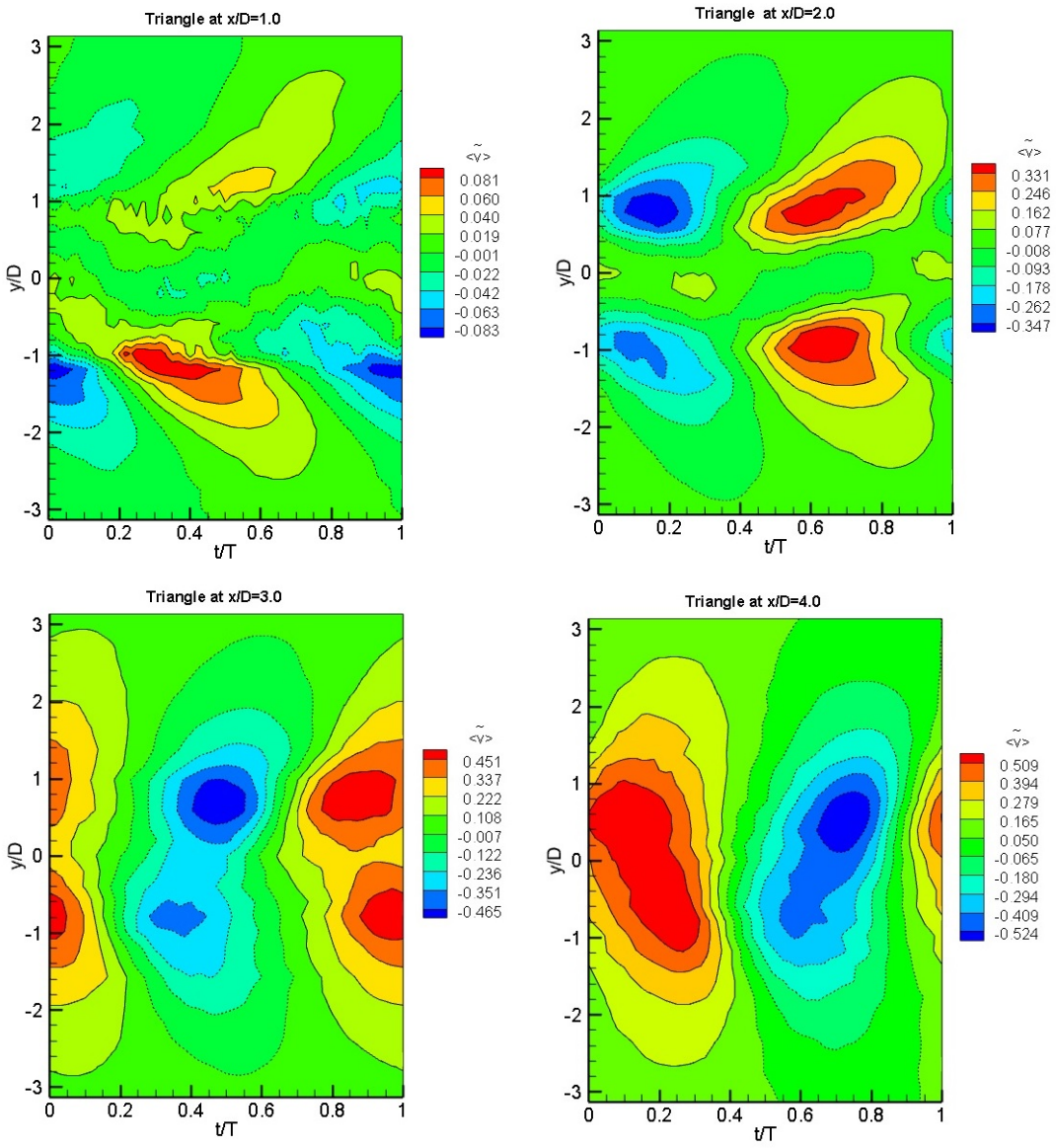

Figure 5.8. Coherent transverse velocity measured downstream of the triangular cylinder

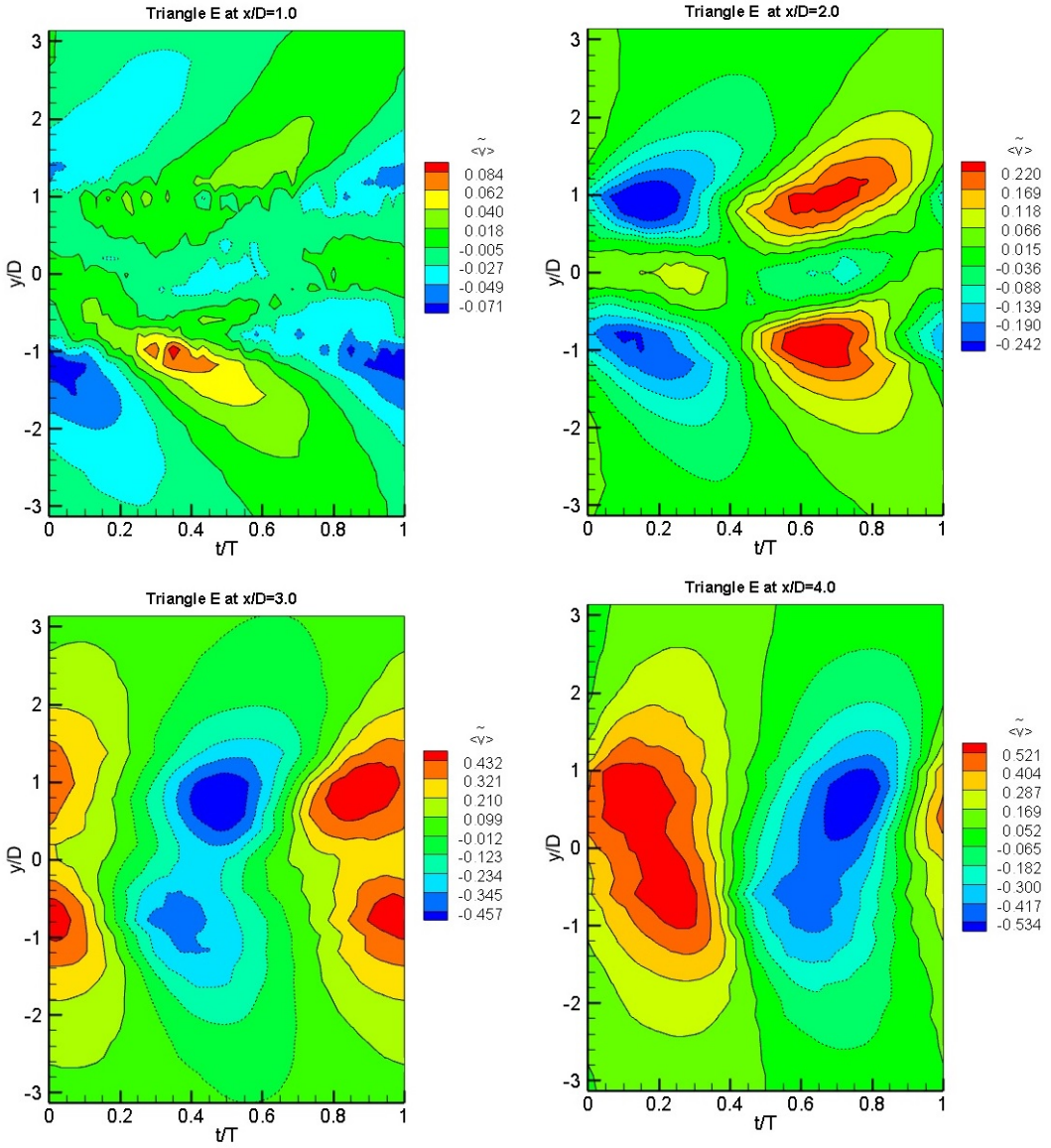

Figure 5.9. Coherent transverse velocity measured downstream of the L shape cylinder

As discussed previously, triple decomposition would provide a better illustration of vortex shedding phenomenon. Therefore, to investigate the development of coherent structure of shedding phenomenon, coherent Turbulent Kinetic Energy (TKE) production in the wake region behind triangular and L shape cylinders have been presented in figures 5.10 and 5.11, respectively.

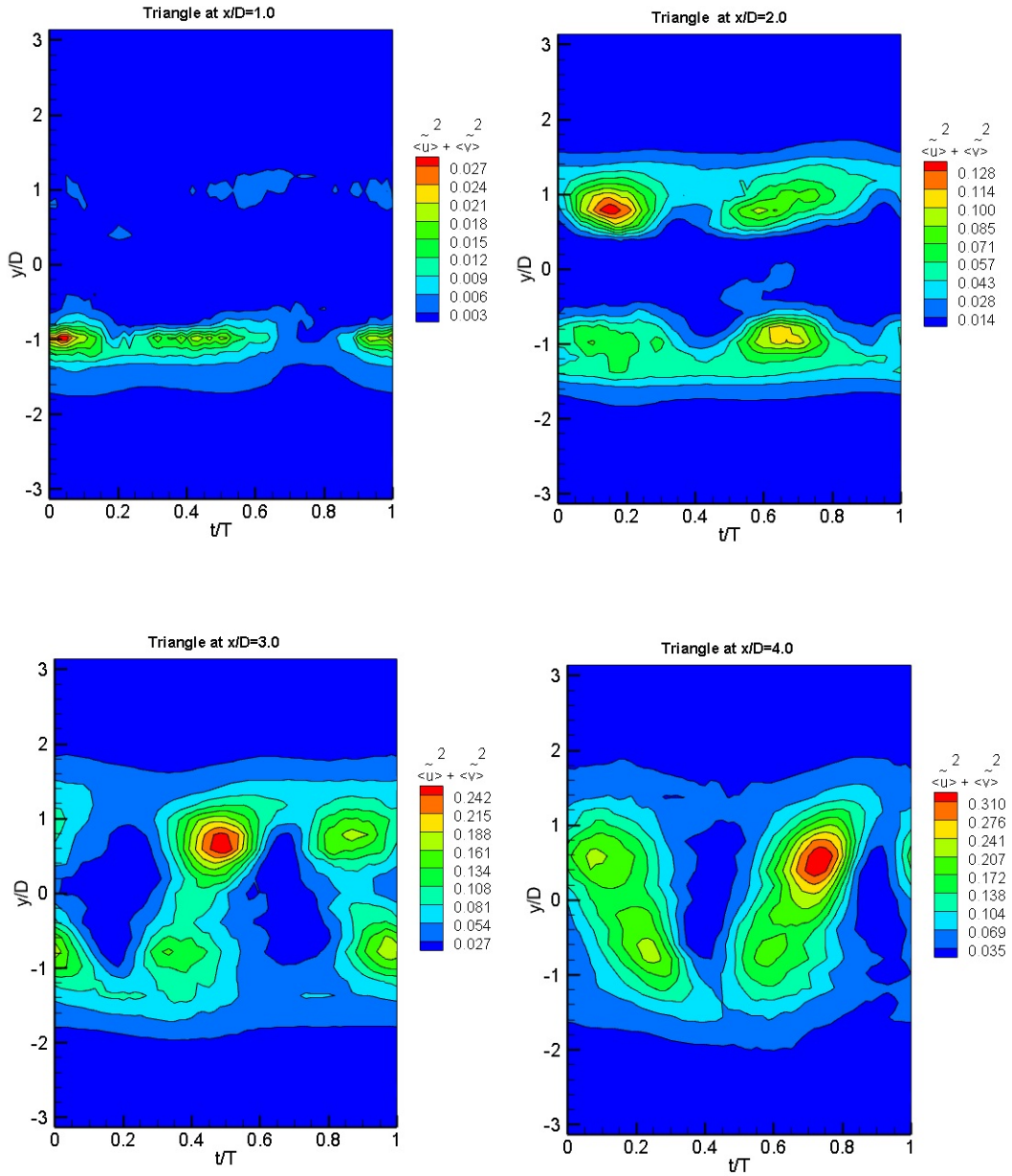

Figure 5.10. Coherent Turbulent Kinetic Energy production in the wake region of the triangular cylinder

Figures 5.10 and 5.11 demonstrate the coherent turbulent kinetic energy production acquired at various x/D locations in the downstream wake regions of TC and LSC, respectively. A comparison between the LSC and the TC shows a similar development of TKE in the wake region. At near wake (i.e. x/D=1.0), coherent turbulent kinetic energy peaks are observed along the edges. As the probe moves downstream in the wake region namely x/D= 3.0, these peaks are developed toward the centreline.

However, from a comparison between LSC and TC it can be concluded that the L modification causes a delay in the development of such flow structure.

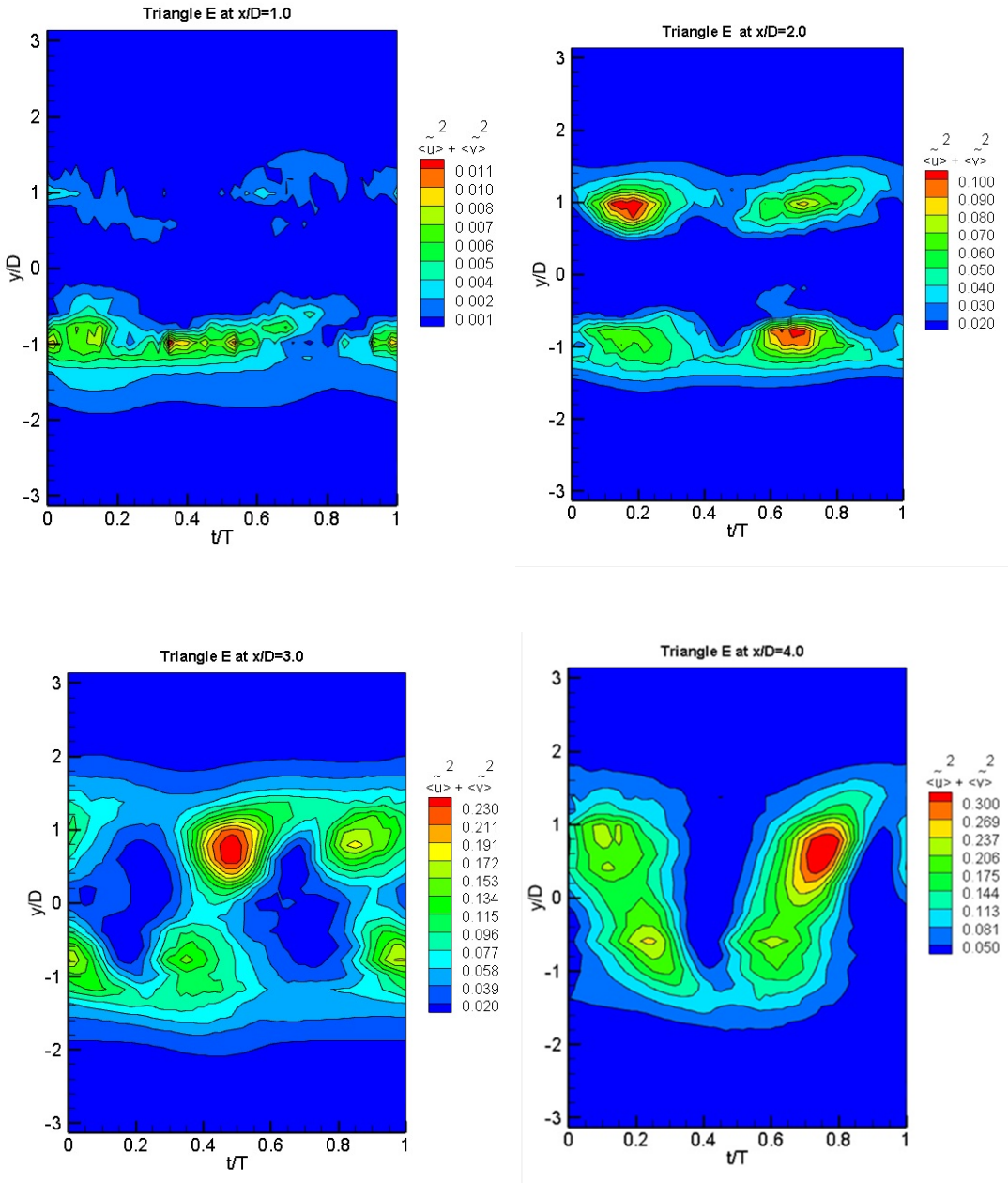

Figure 5.11. Coherent Turbulent Kinetic Energy production in the wake region of the L shape cylinder

It can be concluded from the figures that at wake region close to the base, the wake behind TC exhibit higher coherent TKE peak. On the contrary, further downstream the wake region, LSC demonstrate higher peak level for coherent TKE. In other words,

the LSC delays the development of alternate vortices at the near base. Hence, the wake region demonstrates lower coherent TKE as apparent in figures. However, further downstream in the wake region behind the LSC case, flow possess higher coherent TKE which implies that entrainment of fluid into LSC gap eventually causes development of stronger vortices.

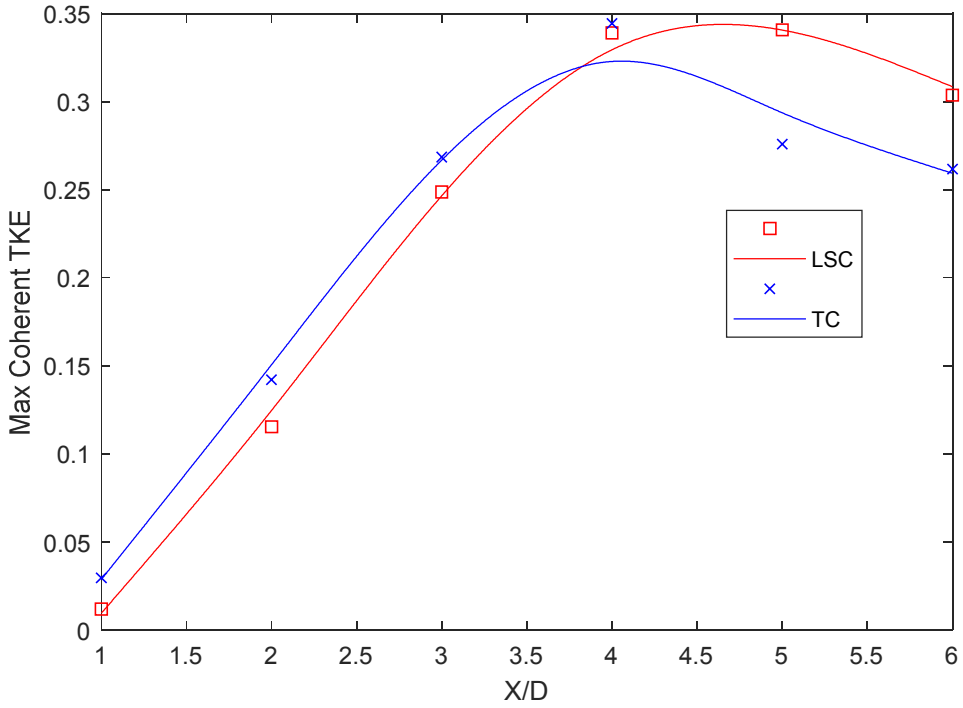

Figure 5.12. Maximum coherent TKE vs x/D location for LSC and TC

Figure 5.12 shows the detected peak value of TC and LSC coherent TKE for various x/D locations, respectively. It is seen from figure 5.12 that the coherent TKE peak of the LSC is lower than the coherent TKE peak of the TC in the near wake region. The detected reductions in the LSC coherent TKE peak at x/D=1, x/D=2, x/D=3, and x/D=4 are about 59 %, 19 %, 7 %, and 2 %, respectively. The situation is different in the far wake region at x/D=5, x/D=6. The coherent TKE peak of LSC is higher than the coherent TKE peak of TC in the far wake region at x/D=5, x/D=6. The detected

increases in the LSC coherent TKE peak at x/D=5 and x/D=6 are about 24 %, and 16 % respectively. It is apparent from the figure that the maximum coherent TKE peak of the LSC occurs at a larger x/D ratio which can be concluded as an indication of a location delay in the wake region in comparison to the TC case.

The similarity between the detected flow behavior observed in figure 5.12 and figure 4.12 in Chapter 4 is a clear confirmation about the effect of the hollow space as a geometry modification on the flow structures.

Chapter 6

INTERACTING WAKES OF TWO INCLINED FLAT PLATES IN TANDEM ARRANGEMENT

6.1 Introduction

In this chapter, vortex shedding phenomenon behind two inclined flat plates in tandem arrangement have been studied experimentally. The effects of gap ratio (g/D) between the plates together with angle of attack (α) on the wake flow structure, incoherent and coherent properties have been investigated.

Different set of experiments have been conducted for gap ratios od 0.5 and 1.0 between plates. In addition, various angles of attack (70-90 degree) have been studied to reveal the effects of inclination on the wake region in terms of shedding frequency and the Strouhal number variation.

The measurements have been carried out at constant free stream velocity of U_∞=11.8 ± 2% m/s, and corresponding Reynolds number 2.3×10^4 (Re=ρUD/μ based on the flat plate width) with measured free stream turbulence intensity 0.7% at this speed. Two flat plates with cross sectional measurement of 30 mm width by 6 mm thickness made of plexiglass with corresponding blockage ratio between 5 - 6% (for angles of attack between 70 and 90 degrees) were used for the experiments. All the measurements were acquired at the midpoint of the wind tunnel in the z-direction where the flow can be considered as two-dimensional flow.

Figure 6.1 illustrates the schematic of the two flat plates in tandem arrangement, experimental set up and the coordinates. The angle of attack for both plates varies between 70 and 90 degrees and the gap between the two plates g/D varies in the range of 0.5 and 1.0 for this experiments, as illustrated in the figure.

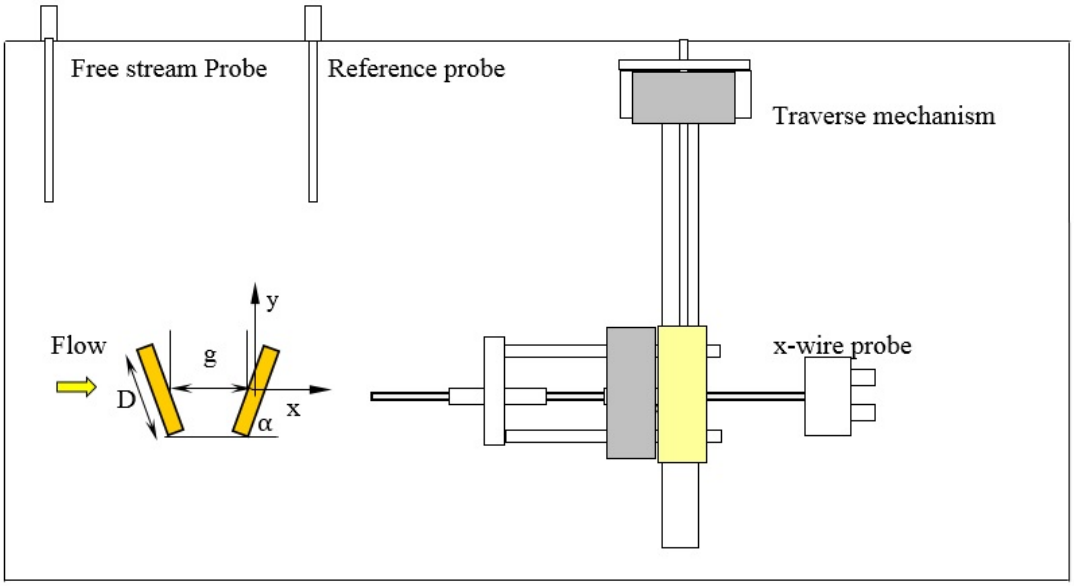

Figure 6.1. Experimental setup and coordinates

The velocity field have been acquired for various x/D locations between 1.0D and 5.0D ($1.0 \leq x/D \leq 5.0$) downstream the aft plate in the wake region, and to obtain the most distinguishable peak for Fast Fourier Transform analysis, the probe traversed in transverse direction between $y/D = \pm 2.61$.

6.2 Spectral Analysis

In order to determine the dominant vortex shedding frequency in the domain of interest Fast Fourier transformation (FFT) has been implemented on the acquired velocity component. As a result, the most powerful spectral peak corresponded to the dominant vortex shedding frequency.

Table 6.1. The vortex shedding frequency for various g/D and the angle of attack

	$\boldsymbol{\alpha}$		
g/D	70	80	90
0.5	47.3	43.5	41.4
1.0	48.8	44.7	42.6

Table 6.2. The Strouhal number (s_t) for various g/D and the angle of attack

	$\boldsymbol{\alpha}$		
g/D	70	80	90
0.5	0.120	0.110	0.105
1.0	0.124	0.113	0.108

Table 6.3. The modified Strouhal number (s_t') for various g/D and the angle of attack

	$\boldsymbol{\alpha}$		
g/D	70	80	90
0.5	0.112	0.108	0.105
1.0	0.116	0.111	0.108

Table 6.1 presents the dominant vortex shedding frequency for various g/D and the angle of attack $\boldsymbol{\alpha}$. It is seen that for a given g/D, the dominant vortex shedding frequency decreases as the angle of attack increases. Moreover, it can be observed that for a given angle of attack $\boldsymbol{\alpha}$, the dominant vortex shedding frequency increases as the gap ratio g/D increases.

Table 6.2 demonstrates the Strouhal number ($s_t = fD/U_\infty$) for various g/D and the angle of attack $\boldsymbol{\alpha}$. From the table, it can be concluded that Strouhal number decreases as the angle of attack increases. Also, it is observed that for a given angle of attack $\boldsymbol{\alpha}$, the Strouhal number increases as the gap ratio g/D increases.

In addition, it is also interesting to investigate the Strouhal number of vortex shedding scaled with projected width, D'=D sinα, of the plate normal to flow stream. Thus, the modified Strouhal number ($s_t' = fD'/U_\infty$) can be computed as: $s_t' = f\text{D sin}\alpha/U_\infty$. Table 6.3 presents the modified Strouhal number for various g/D and the angle of attack $\boldsymbol{\alpha}$. From the table, it is seen that the modified Strouhal number decreases as the angle of attack increases. Also, it is observed that for a given angle of attack $\boldsymbol{\alpha}$, the modified Strouhal number increases as the gap ratio g/D increases.

6.3 Phase Averaged Flow Structure

One of the objective of this study is to investigate the formation of vortex street in the wake region of two tandem inclined flat plates. Development of flow structure and vortex shedding in the wake region behind two inclined plates have been illustrated in figures 6.2-6.7. The vortex shedding phenomenon and the periodic flow patterns for both streamwise and transverse velocity components are completely evident in these figures.

One feature of the streamwise velocity contours is that two low level zones exist along the centerline downstream of the aft plate. These two low level zone drifted 1/2 period from each other. Therefore, such observation implies that the downstream wake behind the aft plate encounters a shedding frequency twice the reference frequency of vortex shedding in streamwise direction. This observation also has been confirmed by implementing FFT analysis on acquired streamwise data behind the aft plate. Such phenomenon would be as a result of interaction of two shear layers initiated from the edges of the plates. However, the wake regions beyond the edges were encountering normal shedding frequency. Another interesting feature of streamwise contour is that in addition to two low level zones close to the centerline, two peaks exist at the same normalized time (t/T) at the edges of the wake. These alternating peaks correspond to the vortices shed from initiated shear layers of the edges of plates.

The comparison of the streamwise and transverse velocity contours demonstrated that although the peaks of streamwise velocity were formed close to the center line, maximum positive and negative magnitude in the case of transverse velocity existed and developed beyond the edges of the plates in the wake region. Remarkably, it was

also observed that the peaks in streamwise velocity coincide with changes in transverse velocity direction, which is the evident of formation of Karman Vortex Street. Therefore, as the streamwise velocity reaches its peak, the transverse velocity changes the direction and ¼ period later reaches its peak towards the centerline. As a result after a vortex is shed, a significant momentum transfer towards the opposite shear layer is observable.

Another significant observation is the development of streamwise and transverse velocity towards downstream in the wake region. As it can be seen from the figures, as the probe move downstream the vortex shedding phenomenon is more apparent from streamwise velocity component and it exhibit more waviness structure. On the other hand, the transverse velocity develops toward the centerline and at x/D=4.0 it become approximately as wide as the wake region.

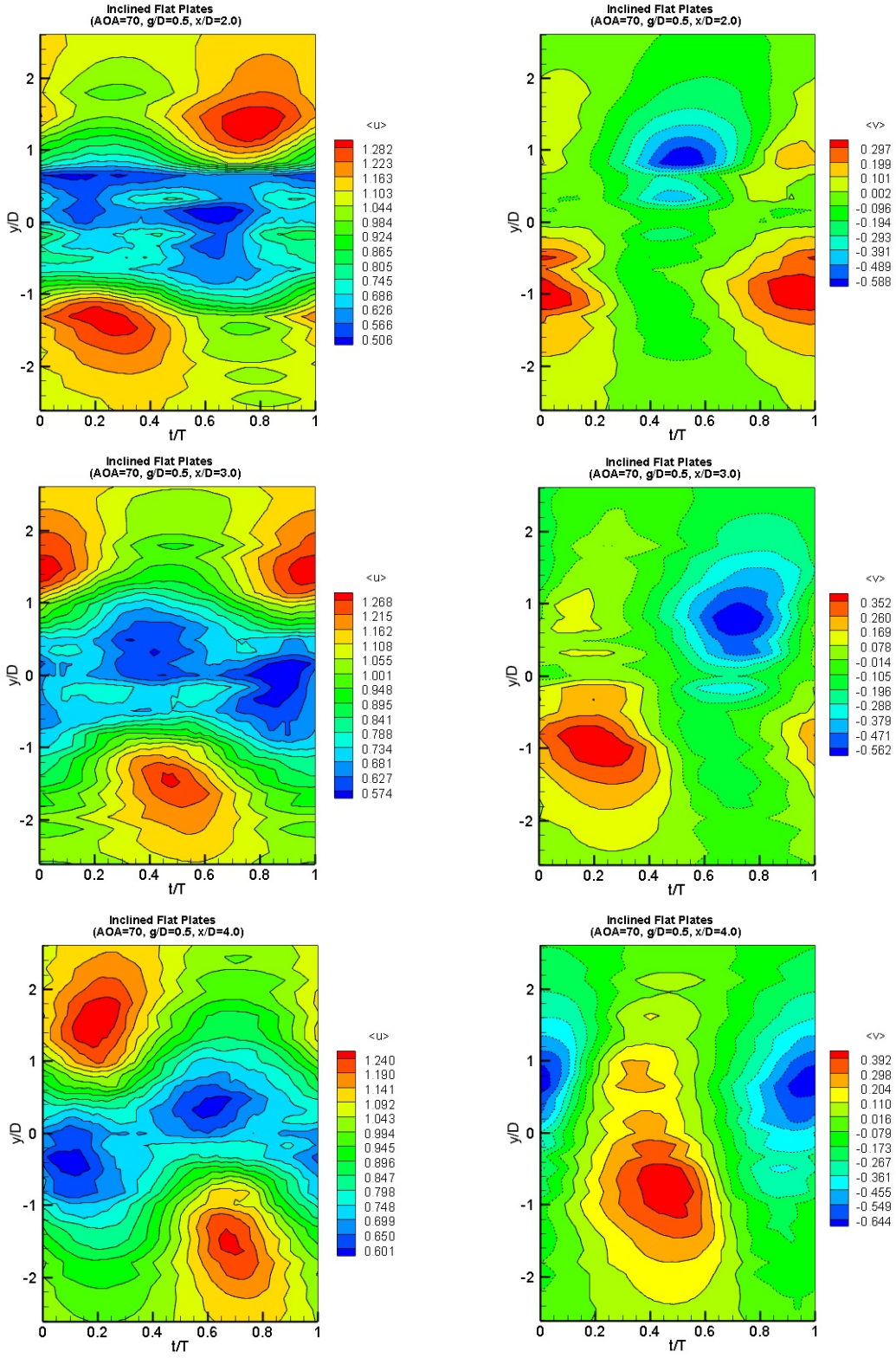

Figure 6.2. Streamwise and transverse velocity measured at various x/D locations downstream of two tandem inclined flat plates at g/D=0.5, α=70

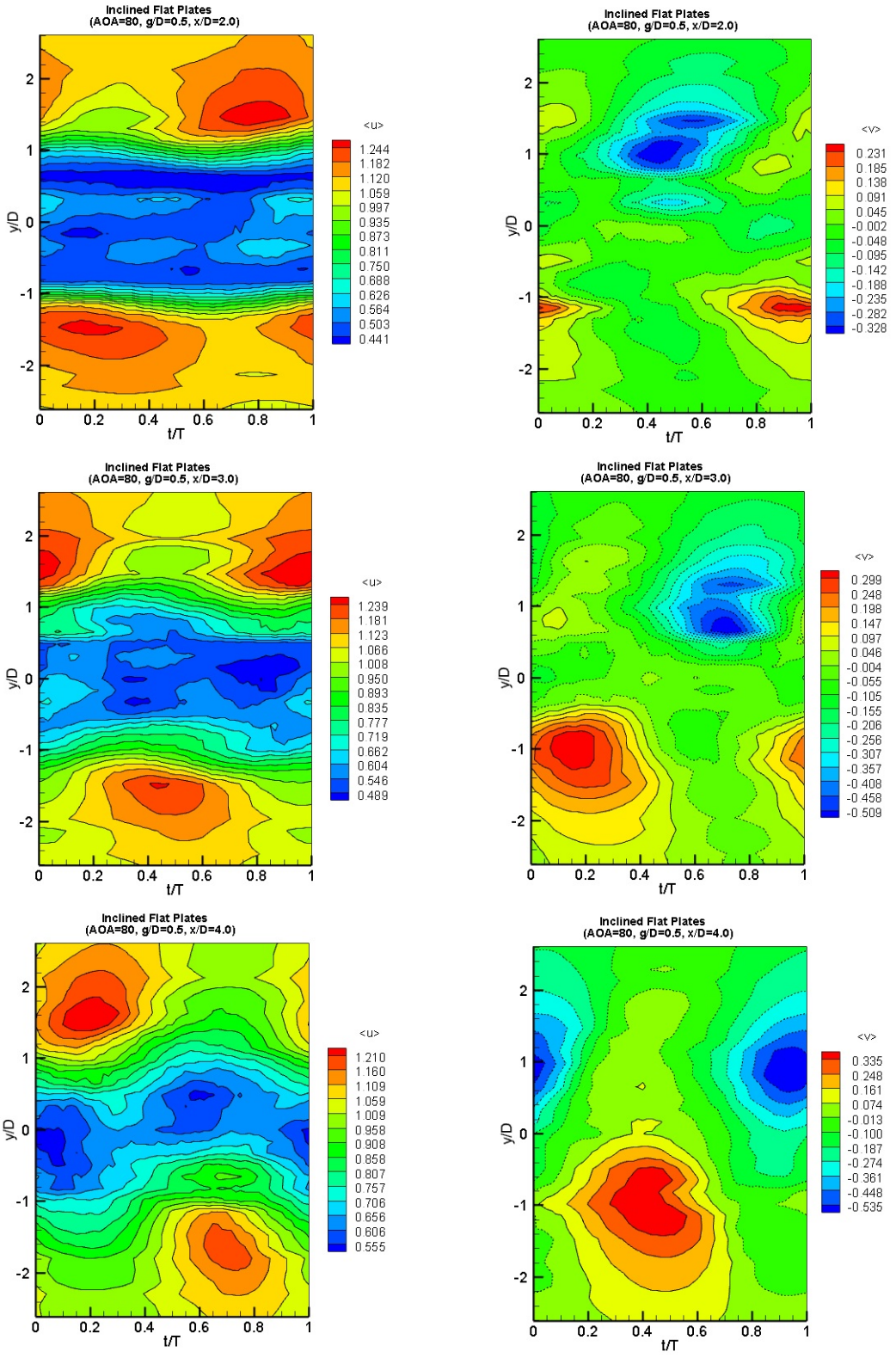

Figure 6.3. Streamwise and transverse velocity measured at various x/D locations downstream of two tandem inclined flat plates at g/D=0.5, α=80

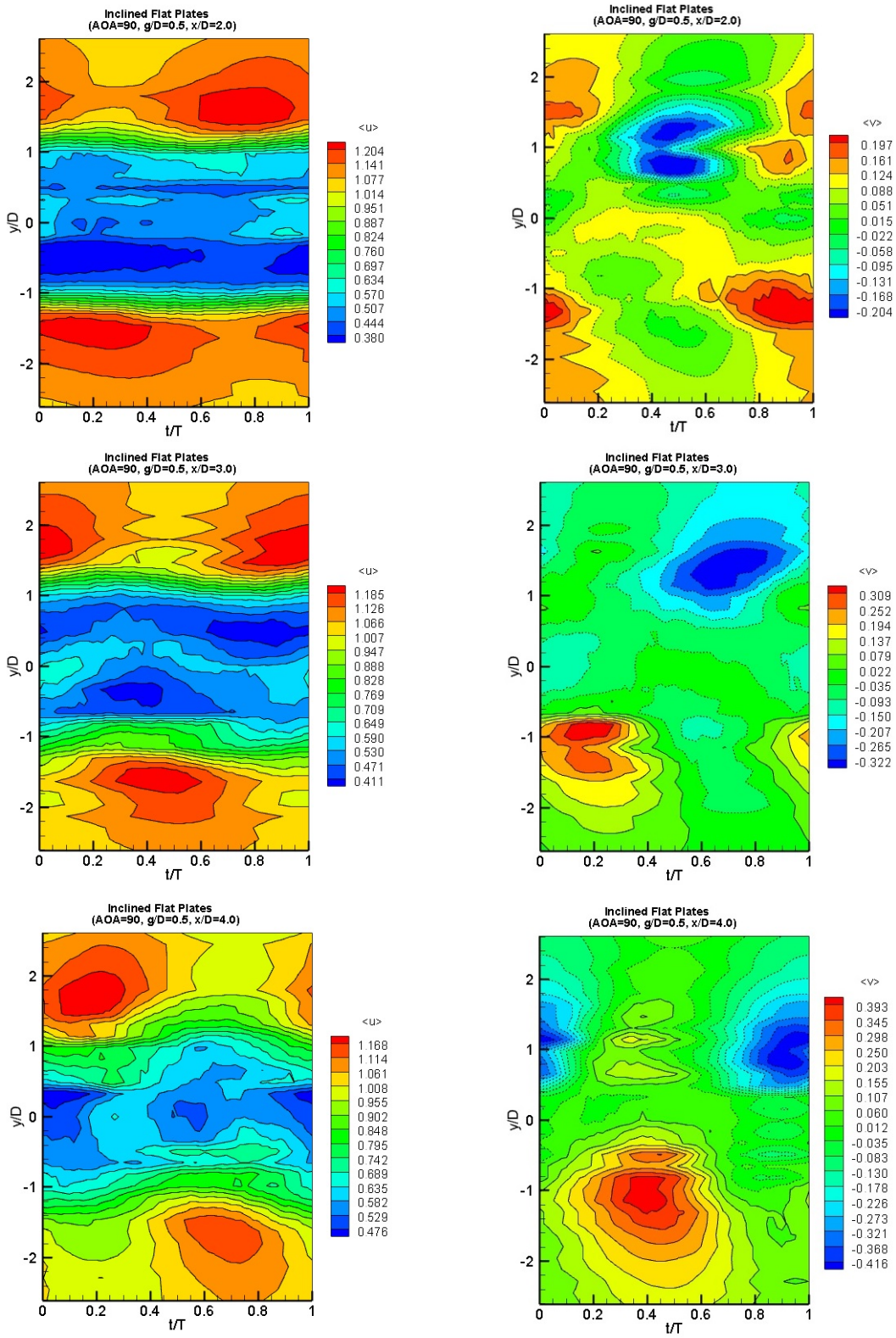

Figure 6.4. Streamwise and transverse velocity measured at various x/D locations downstream of two tandem inclined flat plates at g/D=0.5, α=90

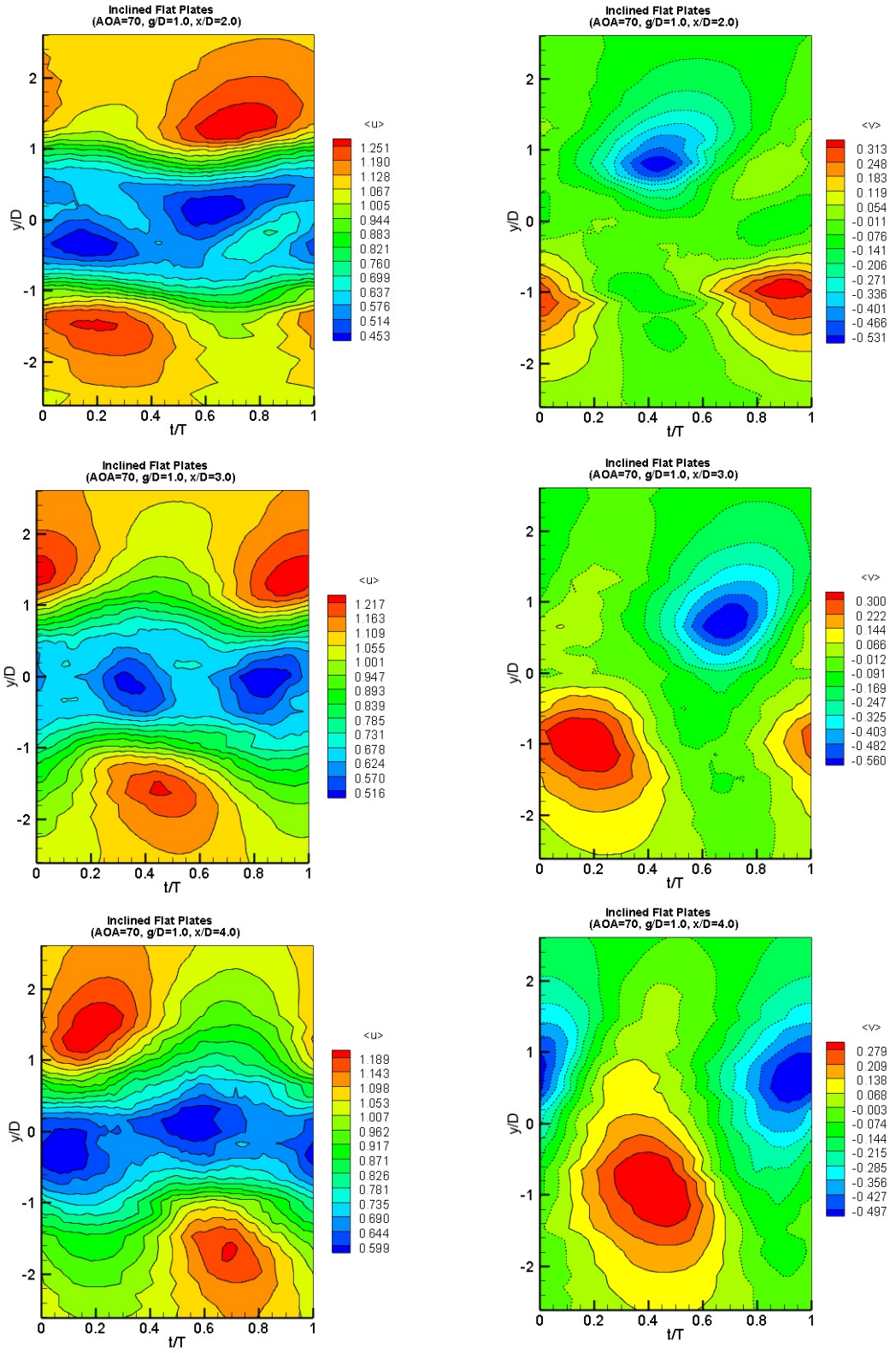

Figure 6.5. Streamwise and transverse velocity measured at various x/D locations downstream of two tandem inclined flat plates at g/D=1.0, α=70

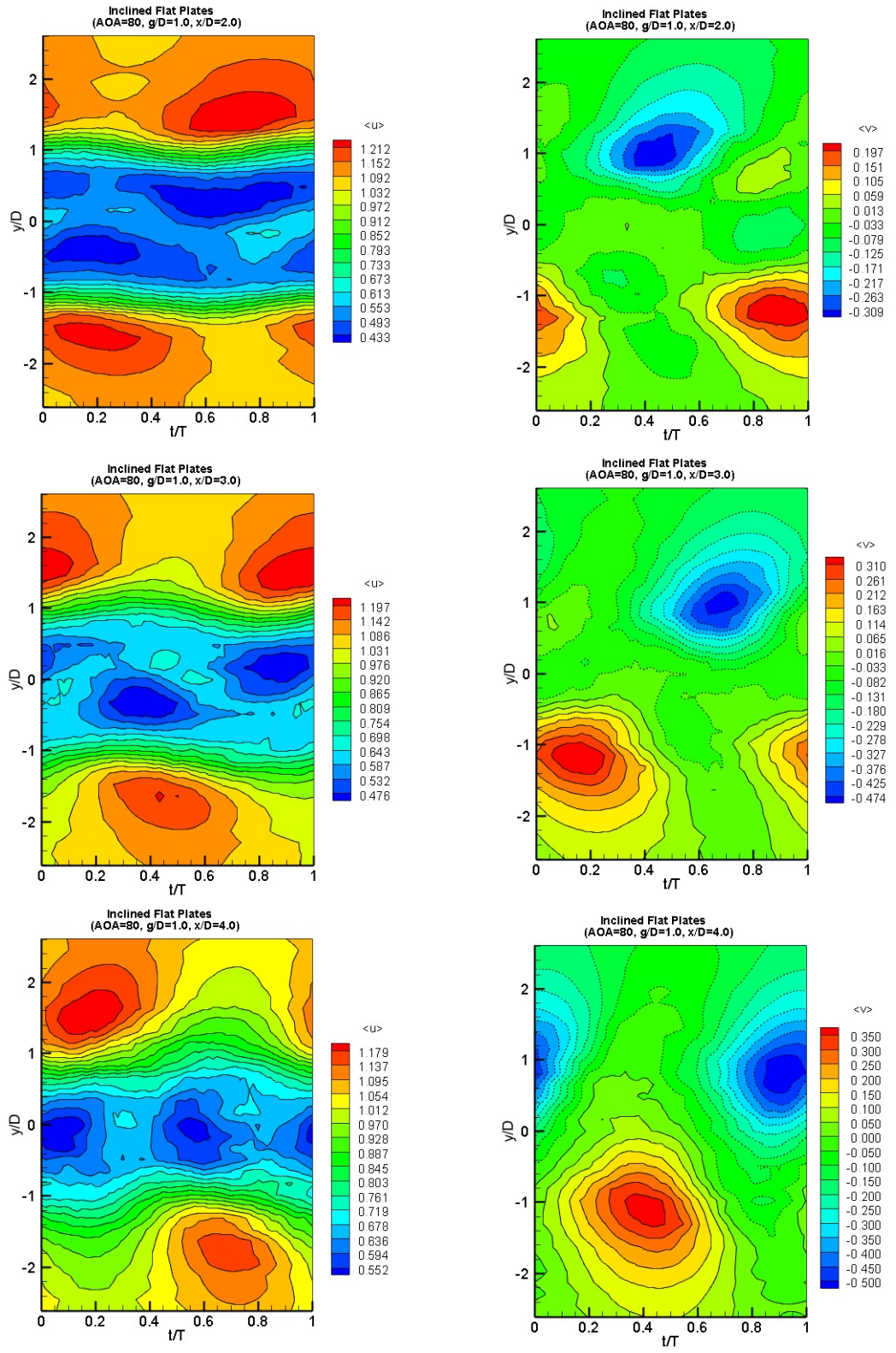

Figure 6.6. Streamwise and transverse velocity measured at various x/D locations downstream of two tandem inclined flat plates at g/D=1.0, α=80

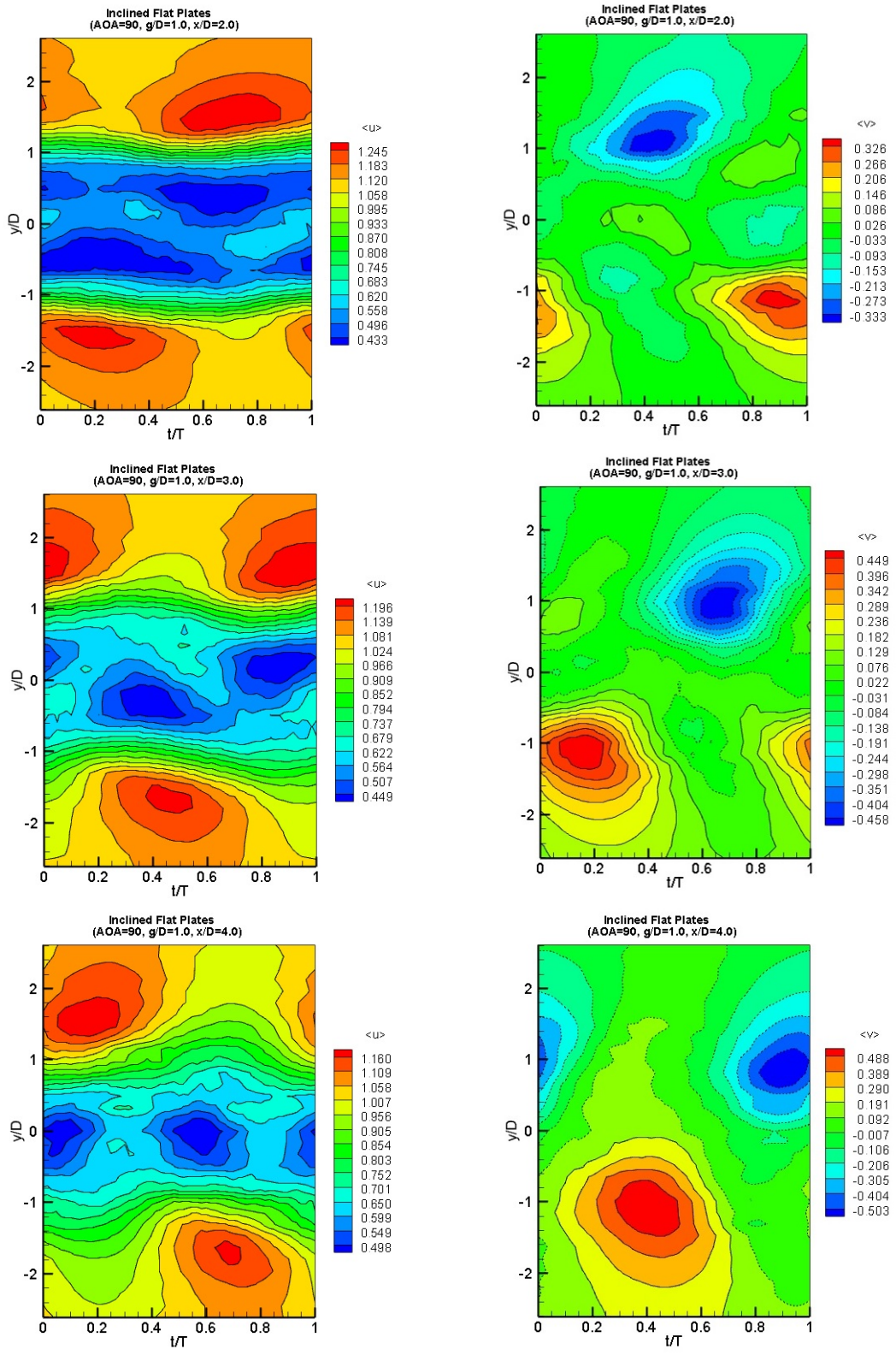

Figure 6.7. Streamwise and transverse velocity measured at various x/D locations downstream of two tandem inclined flat plates at g/D=1.0, α=90

6.4 Coherent Flow Structure

As a primary purpose of this study, the Vortex shedding phenomenon has been studied by employing the triple decomposition technique rather than the classical Reynolds decomposition to distinguish the incoherent turbulent flow fluctuation from coherent vortex shedding structure for a better understanding of this phenomenon. Therefore, in this section extracted coherent vortex shed structure from incoherent turbulent fluctuations have been presented in figures 6.8-6.13. As it can be seen from the coherent streamwise and coherent transverse velocity contours, vortex shedding phenomenon is more clear and apparent than corresponding phase averaged contours. From those figures, the existence of the peak of coherent structure along the edges behind the aft plate are clearly observable. Although the coherent transverse velocity exhibit similar pattern, however as the probe moves downstream the wake the coherent structure transverse direction develops and become as wide as the wake region.

It is observed that for the cases of tandem plates at g/D=0.5 and g/D=1.0, the coherent structure peaks decrease as the angle of attack raised from 70 to 90 degrees. Moreover, it is seen that for the cases of tandem plates at the angle of attack of 70 and 80 degrees, the coherent structure peaks decrease as the gap between the plates increases while for the case of the angle of attack of 90 degree, the coherent structure peaks increase as the gap between the plates increases.

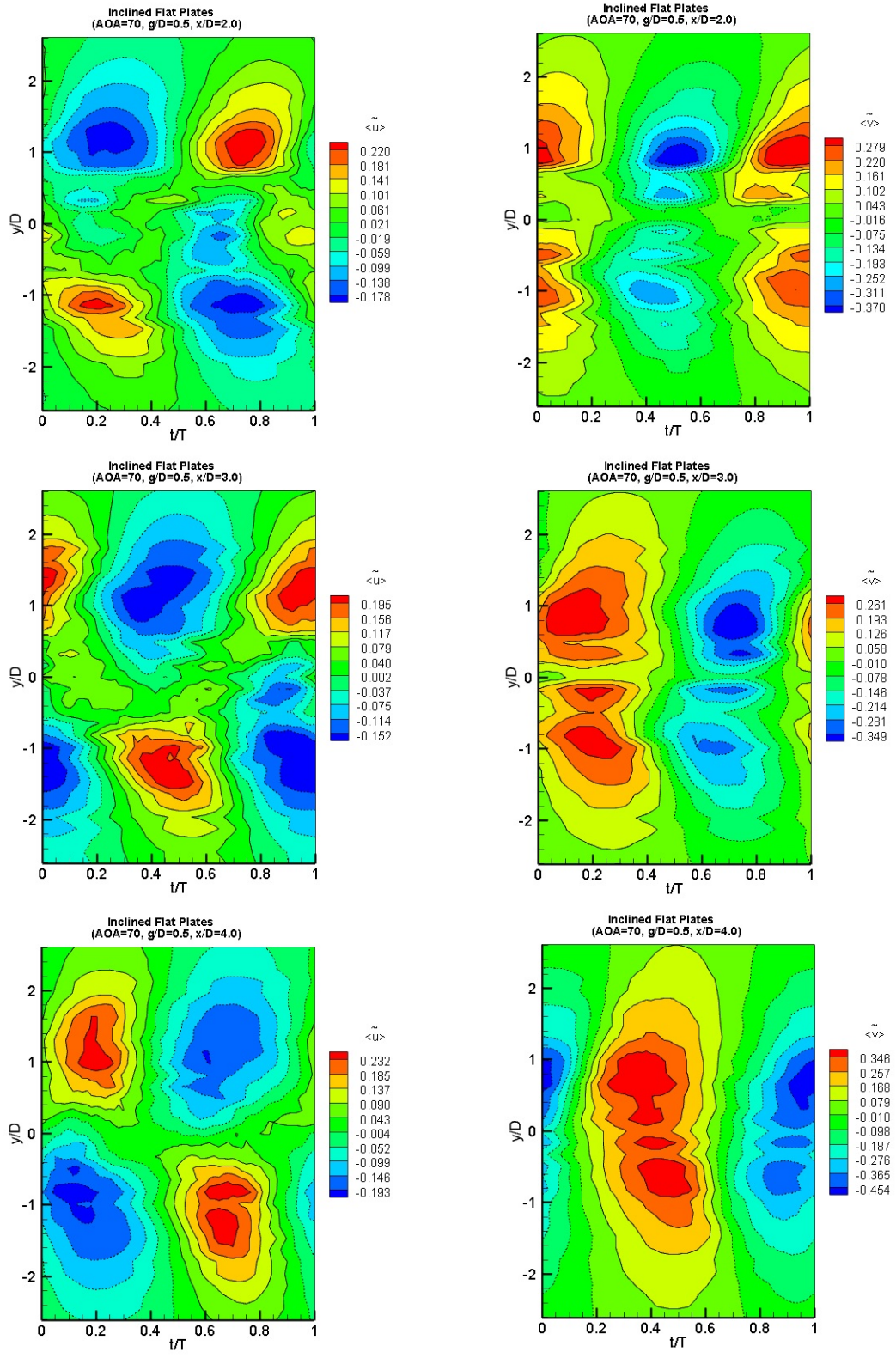

Figure 6.8. Coherent streamwise and coherent transverse velocity measured at various x/D locations downstream of two tandem inclined flat plates at g/D=0.5, α=70

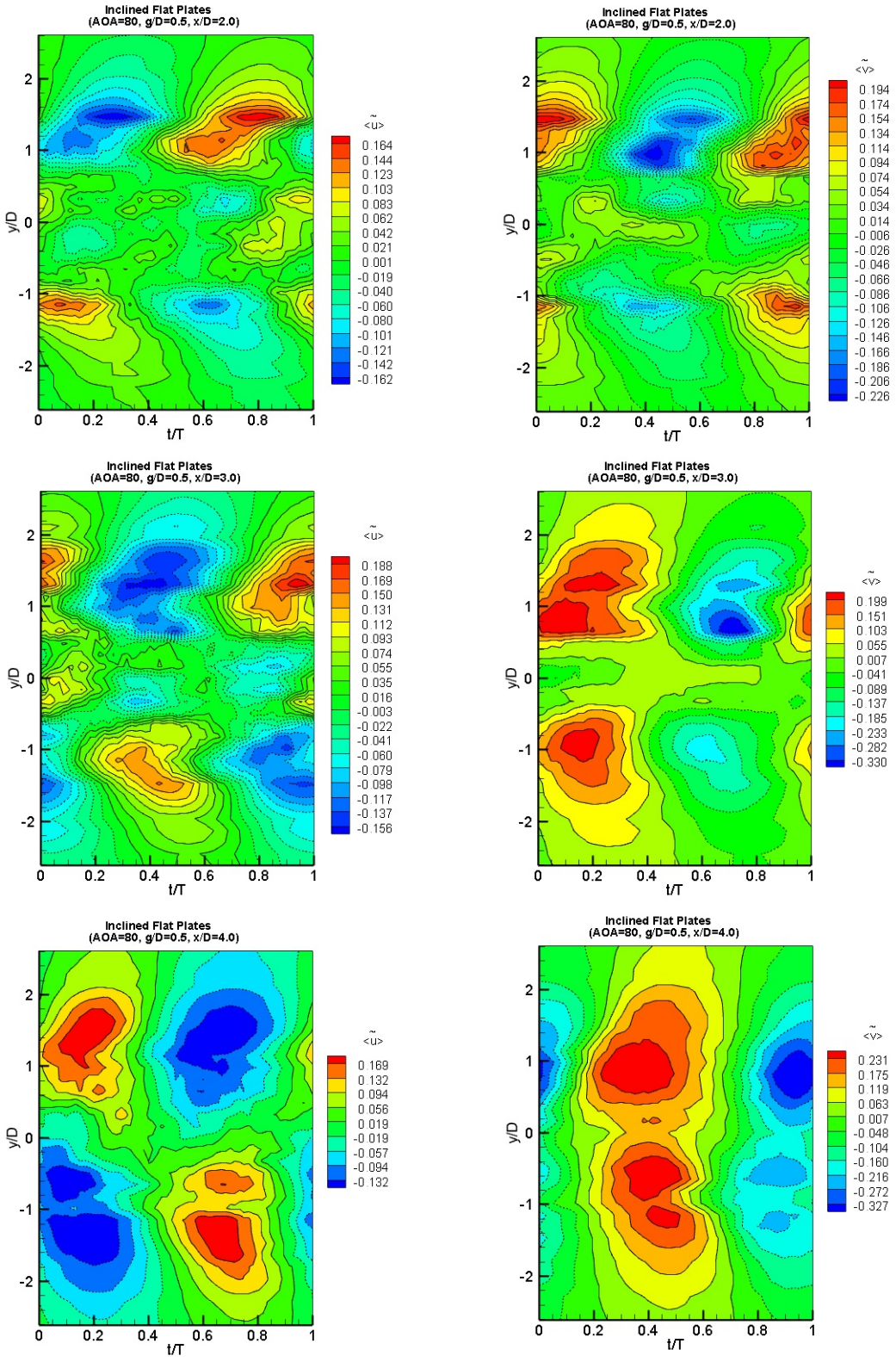

Figure 6.9. Coherent streamwise and coherent transverse velocity measured at various x/D locations downstream of two tandem inclined flat plates at g/D=0.5, α=80

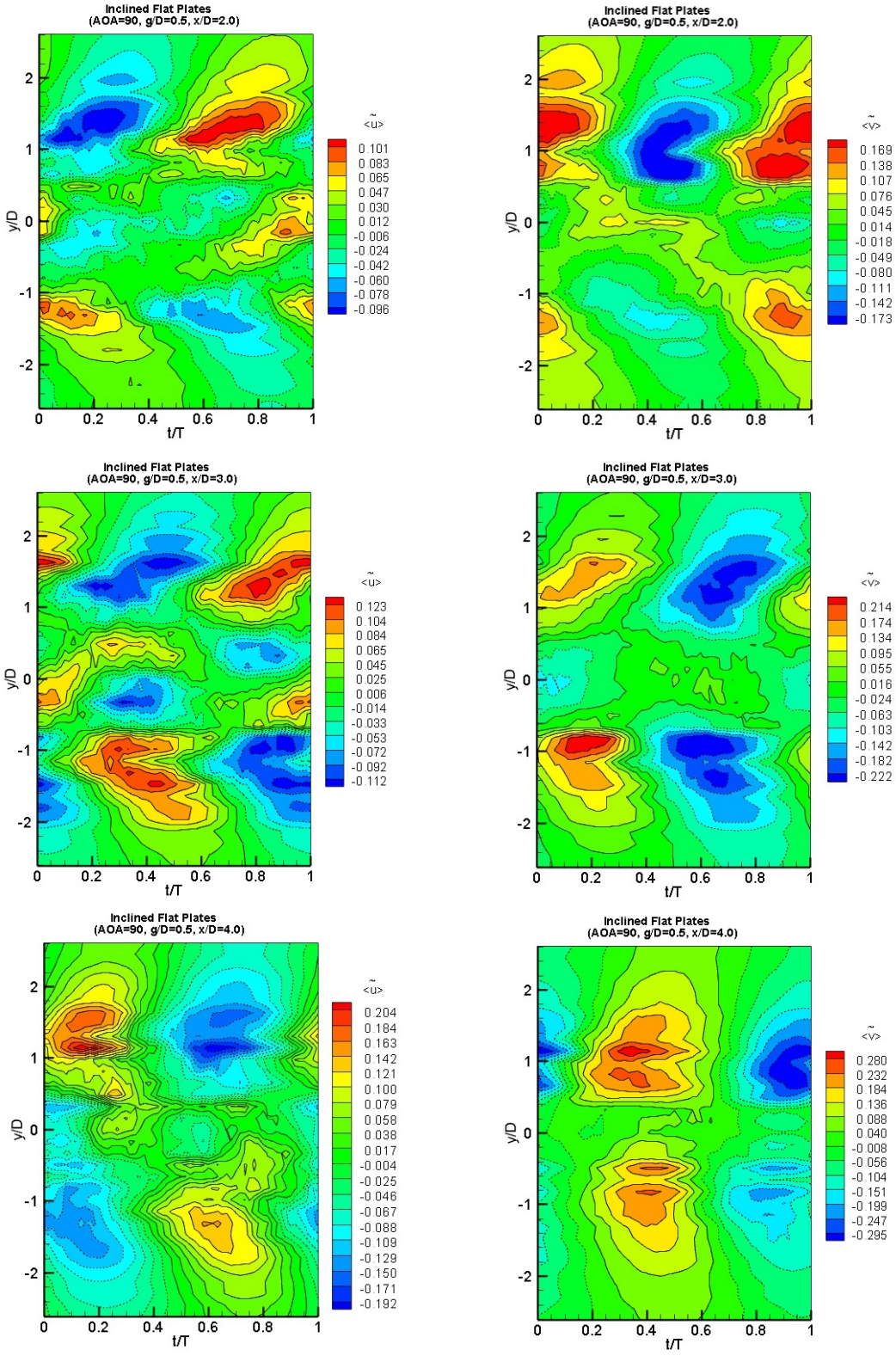

Figure 6.10. Coherent streamwise and coherent transverse velocity measured at various x/D locations downstream of two tandem inclined flat plates at g/D=0.5, α=90

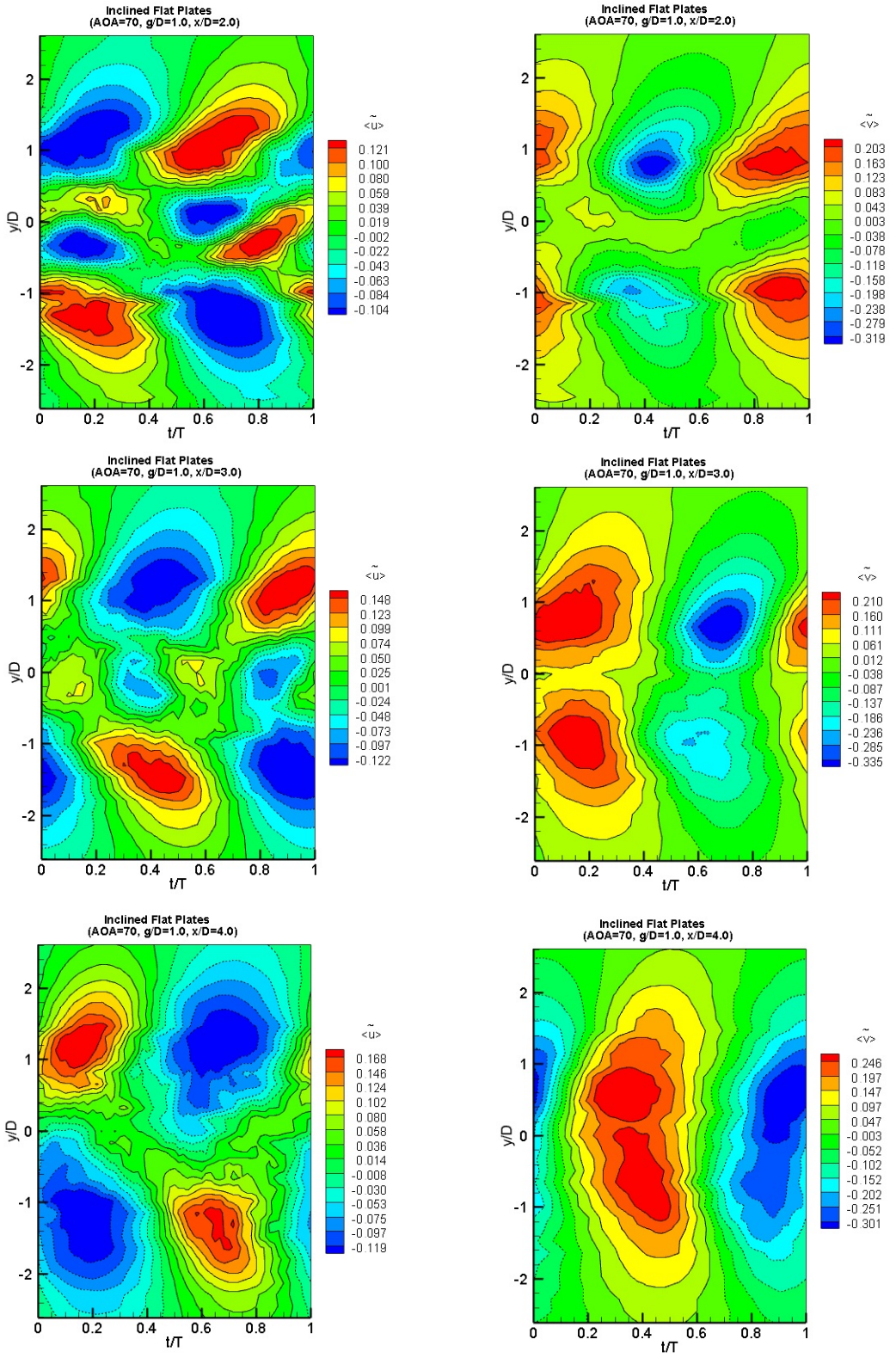

Figure 6.11. Coherent streamwise and coherent transverse velocity measured at various x/D locations downstream of two tandem inclined flat plates at g/D=1.0, α=70

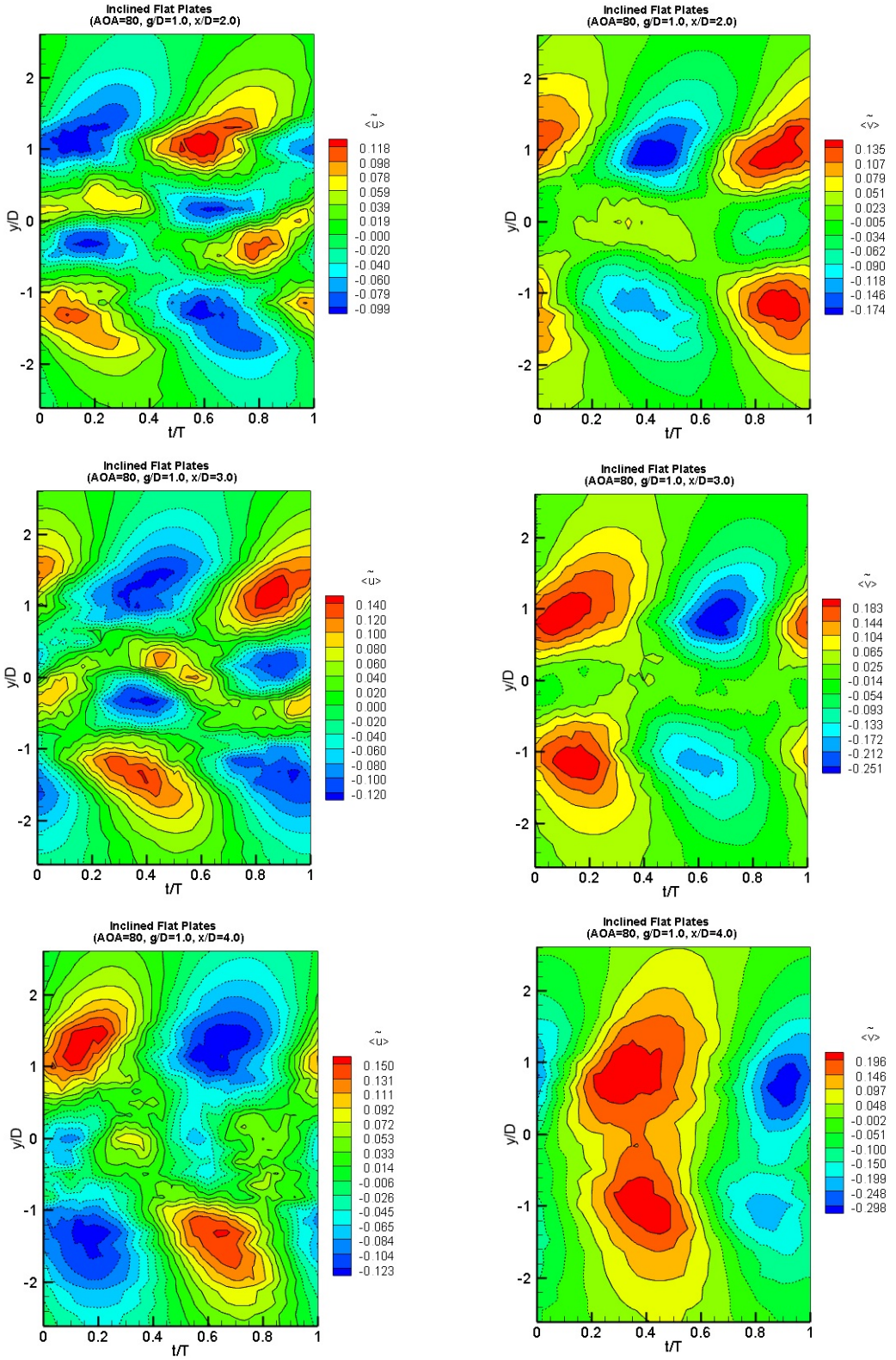

Figure 6.12. Coherent streamwise and coherent transverse velocity measured at various x/D locations downstream of two tandem inclined flat plates at g/D=1.0, α=80

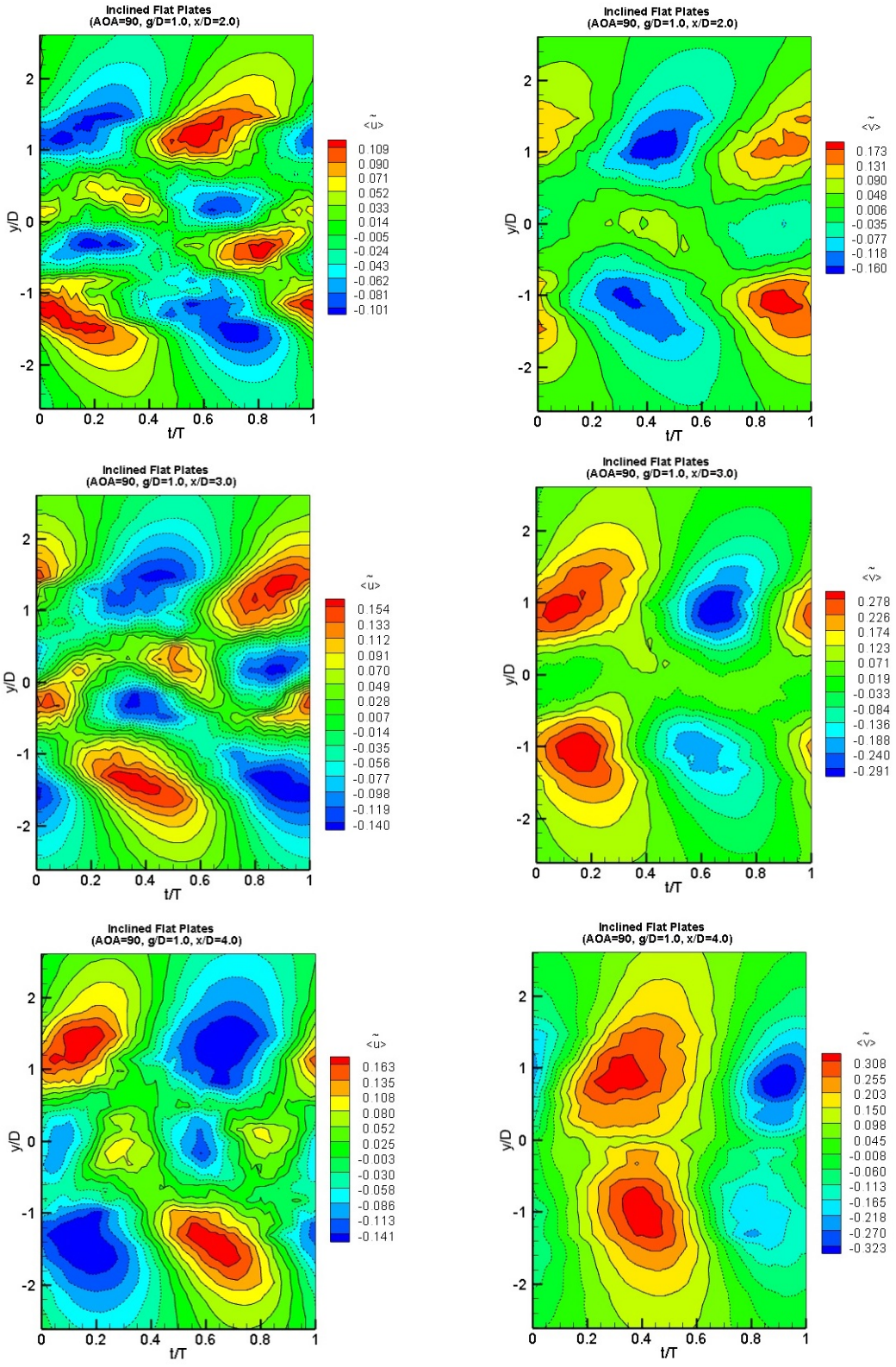

Figure 6.13. Coherent streamwise and coherent transverse velocity measured at various x/D locations downstream of two tandem inclined flat plates at g/D=1.0, α=90

6.5 Turbulent Kinetic Energy

As discussed triple decomposition distinguishes between coherent structure or vortex shedding phenomenon and incoherent structure of turbulent fluctuations. Therefore, it is possible to concentrate on the periodic shedding phenomenon. Coherent turbulent kinetic energy production at three different normalized streamwise coordinate in the wake region of two tandem inclined plates have been illustrated in figures 6.14-6.16. Development of the coherent turbulent kinetic energy is clearly recognizable from those figures. It can be seen that in the wake region close to the downstream plate there is no apparent features of periodic flow. However farther in the downstream wake, the periodic features of flow develops and become more observable. As probe moves downstream in the wake from x/D= 2.0 to 4.0, the coherent TKE production peaks increases gradually for all cases. However, comparison between g/D=0.5 and 1.0, reveals that the coherent TKE peak production decreases as the gap ratio g/D increases for all measured x/D locations in the wake region in cases of angles of attack of 70 and 80 degrees. As the gap ratio increases more fluid particle entrain into gap region during the shedding process. Therefore, such reduction in coherent TKE production peak is observed.

The situation is vice versa in case of the angle of attack of 90 degree. In other words, the coherent TKE peak production increases as the gap ratio g/D increases. Moreover, it can be observed that the coherent TKE peak production decreases as the angle of attack raised from 70 to 90 degrees for both gap ratios of g/D=0.5 and 1.

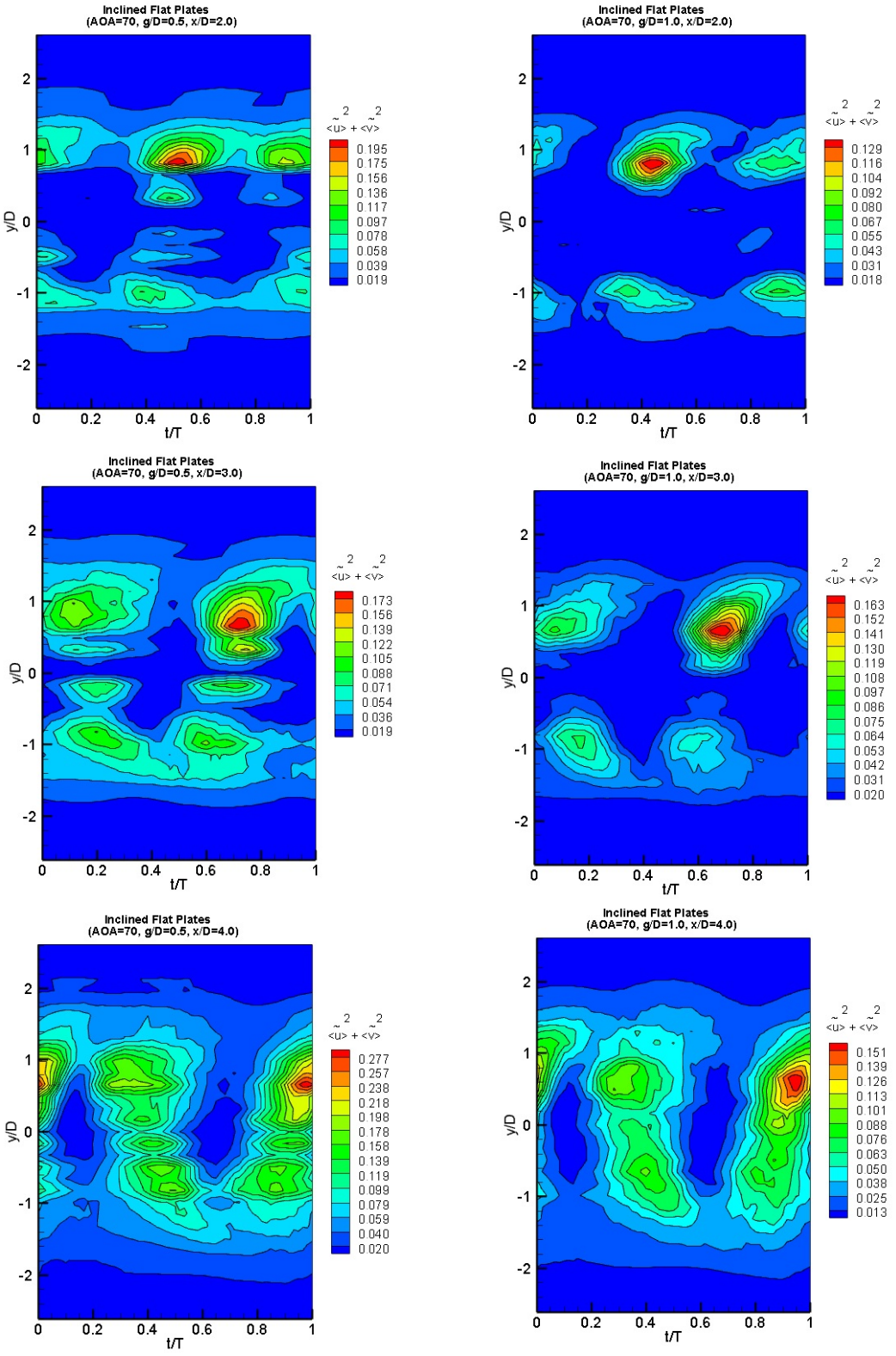

Figure 6.14. Coherent Turbulent Kinetic Energy production measured at various x/D locations in the wake region of two tandem inclined flat plates at α=70

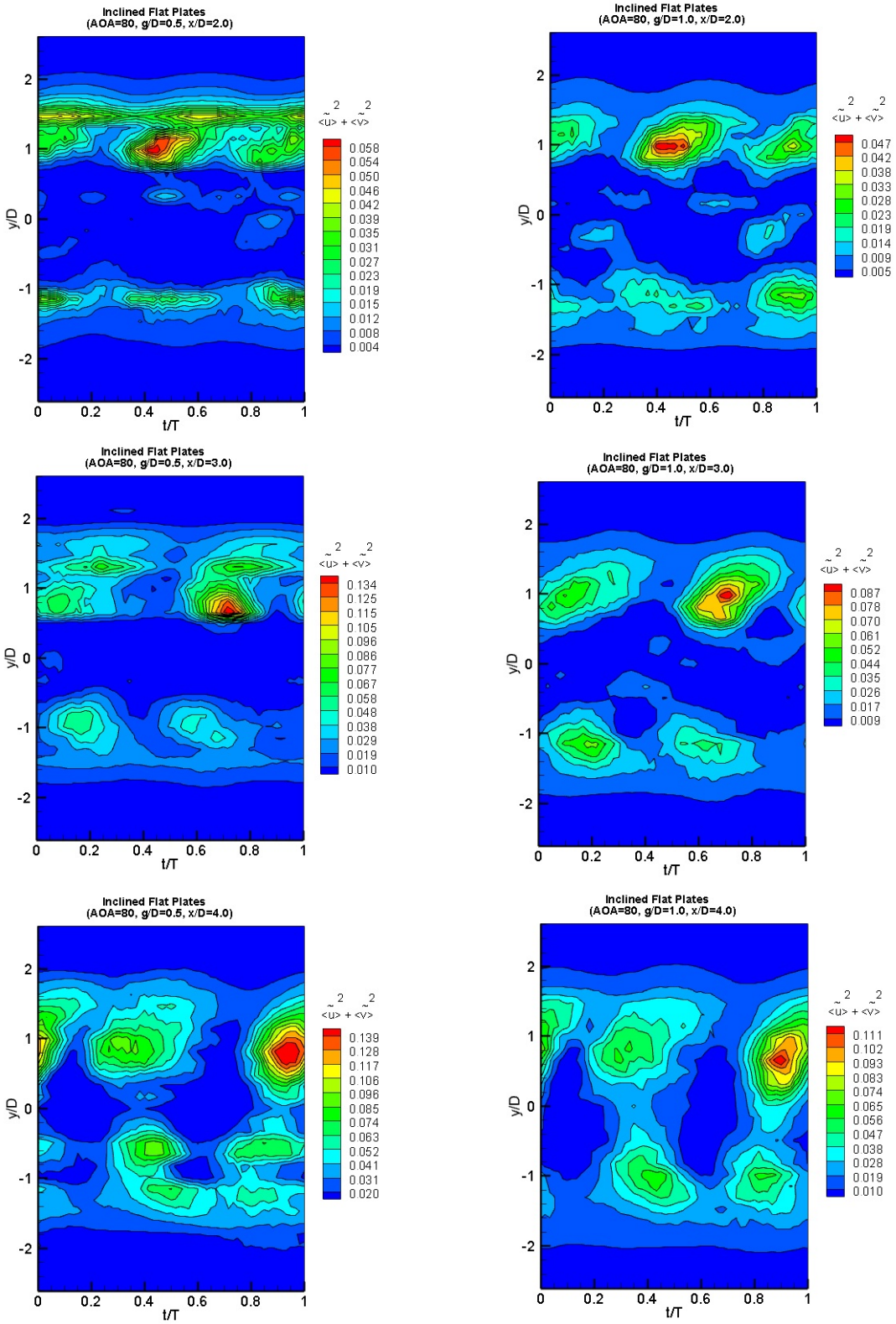

Figure 6.15. Coherent Turbulent Kinetic Energy production measured at various x/D locations in the wake region of two tandem inclined flat plates at α=80

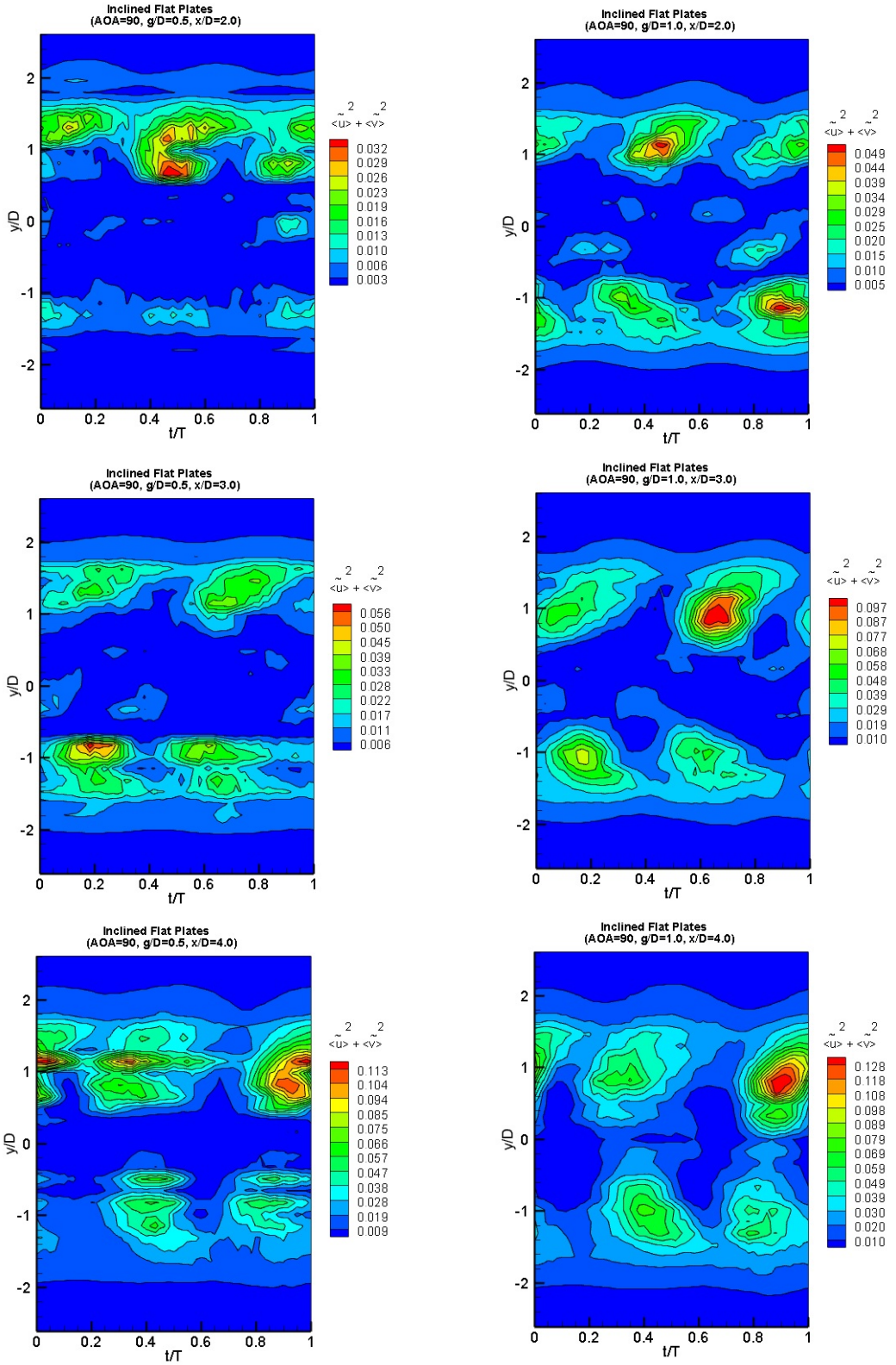

Figure 6.16. Coherent Turbulent Kinetic Energy production measured at various x/D locations in the wake region of two tandem inclined flat plates at α=90

6.6 Time Averaged Properties

Quantifying development and decay of different properties in the downstream wake region are of great importance. Thus for a quantitative comparison between different tandem plates arrangement, time averaged streamwise and transverse velocity for various x/D locations downstream of the aft plate have been presented. Time averaged streamwise and transverse velocity profiles are depicted in figures 6.17 and 6.18.

It can be seen from the figures that while streamwise velocity profile shows symmetry along the centerline, transverse velocity profile shows anti-symmetric variation. Moreover, the time averaged transverse velocity exhibits max positive and negative peaks approximately along the edges. These peaks can be an indication of rolled vortices from the edges of the plates. It can be seen that as the angle of attack increases these peaks occur at higher y/D.

It was also observed that while the time averaged streamwise velocity profiles recovers as the probe moves further downstream in the wake region, the time mean transverse velocity decays significantly. As the shear layers separated from the plates, the fluid flow subjected to momentum loss in the wake region. Therefore, the time averaged streamwise velocity profile exhibit a drop in the wake region behind the plate. However, outside the wake it return to free stream value which is apparent from the figure. As the flow develops toward the downstream, the wake widen as the fluid entrained into the wake from the edges of plates periodically. Another sign of such entrainment process can be spotted from time averaged transverse velocity profile. At near the wake region exhibit high fluid entrainment toward the centerline. However, such process dissipated significantly beyond 4D in the downstream wake.

Geometries such as normal plate exhibit a symmetrical periodical train of vortices being shed alternately from the edges of the bodies in the wake region. Although these vortices rolled up in opposite direction, but they contain similar strength. As a result, the time mean flow over symmetrical bluff bodies exhibit zero mean lift and symmetric pattern along the wake centerline. On the contrary, flow over asymmetrical geometry such as inclined flat plate exhibit asymmetrical flow structure and as a result none-zero mean lift generated on the flat plate. As it can be seen from the transverse velocity profile, the wake region behind the trailing edge exhibit higher momentum transfer towards the centerline than the leading edge. In addition, the time averaged transverse velocity along the wake centerline is also nonzero due to asymmetric nature of the inclined plates.

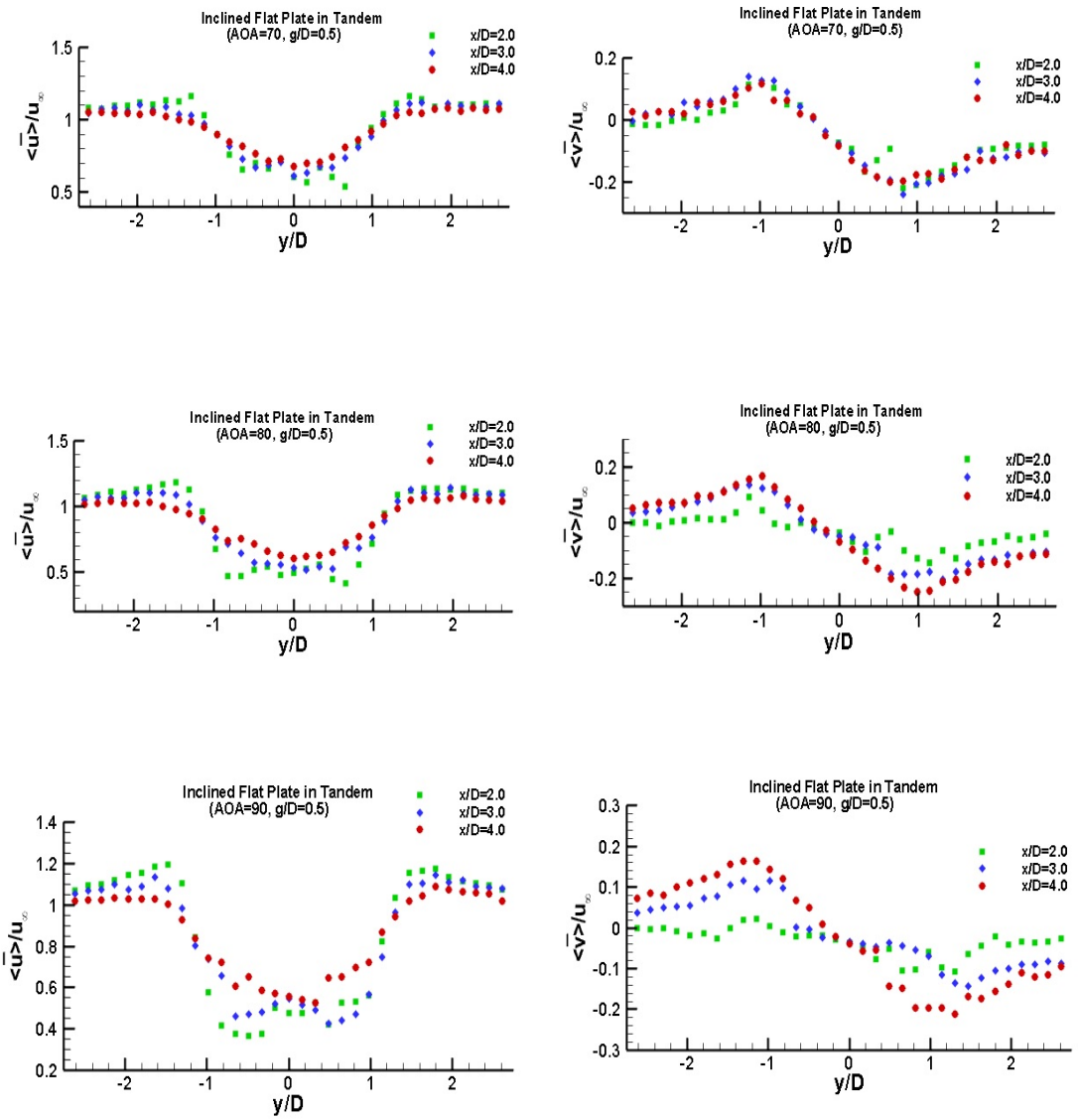

Figure 6.17. Comparison of variation of time averaged streamwise and traverse velocity measured at various x/D locations in the wake region of two tandem inclined flat plates for g/D=0.5

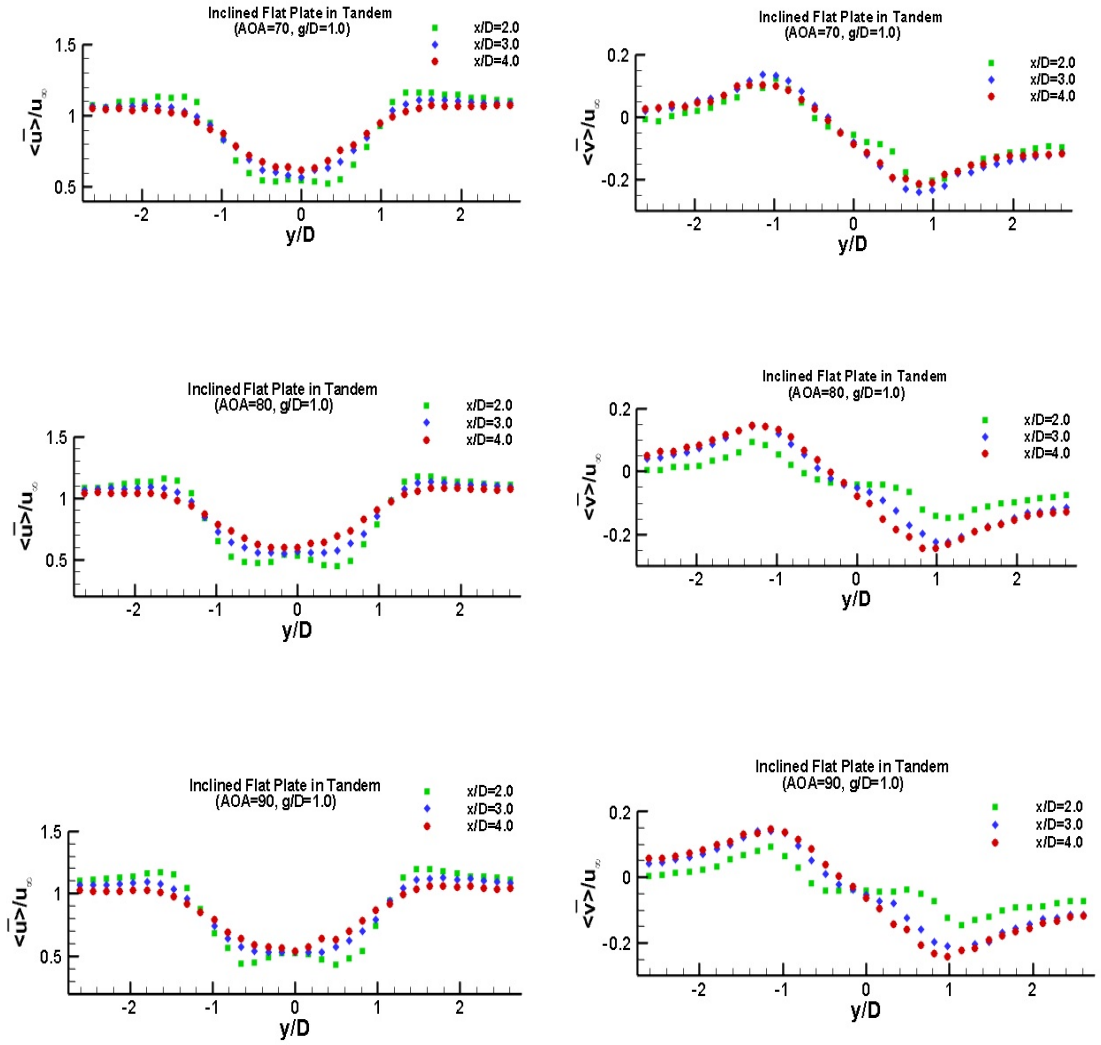

Figure 6.18. Comparison of variation of time averaged streamwise and traverse velocity measured at various x/D locations in the wake region of two tandem inclined flat plates for g/D=1.0

Chapter 7

CONCLUSION

7.1 Final Remarks

In this study, vortex shedding in the wake region of single and dual bluff bodies have been investigated experimentally in detail. Firstly, the effects of entrainment of fluid through the hollow space in square and triangular cylinders have been studied in terms of velocity components, turbulent kinetic energy and similarities and dissimilarities in coherent and incoherent flow structures have been addressed to shed some light on the vortex shedding phenomenon. Finally, interacting wakes of two inclined flat plates in tandem arrangement have been studied to probe the effects of gap ratio and angle of attack of the plates on the flow structures. Based on the experimental observation, the following conclusions were drawn:

U shape cylinder

1- For both square cylinder (SC) and U shape cylinder (USC), the dominant shedding frequency and the Strouhal number have been found as $f = 48.8\ Hz$ and s_t =0.109, respectively.

2- The wake region behind the USC exhibits a delay in wake recovery in comparison to the SC. In other words, the dominant status of the vortex shedding phenomenon occurs at a higher x/D ratio for USC in comparison to the SC.

3- On average, the coherent streamwise velocity peak is around 20% of the phase

averaged peak values for both cases of USC and SC.

4- On average, the coherent transverse velocity peak is around 77 % and 70 % of the SC and USC phase averaged peak values, respectively.
5- The coherent TKE peak of USC is about 25 % lower than the coherent TKE peak of the SC in the near wake region while on average it is about 15 % higher in the far wake region.
6- The maximum coherent TKE peak of USC occurs at a larger x/D ratio which can be concluded as an indication of a location delay in the wake region in comparison to the SC case.

L shape cylinder

1- The dominant shedding frequency and the Strouhal number of the L shape cylinder (LSC) have been found as $f = 48.8\,Hz$ and s_t =0.109, respectively.
2- The dominant shedding frequency and the Strouhal number of the triangular cylinder (TC) have been found as $f = 53.7\,Hz$ and s_t =0.119, respectively.
3- The wake region behind the LSC exhibits a delay in wake recovery in comparison to the TC. In other words, the dominant status of the vortex shedding phenomena occur at a higher x/D for LSC in comparison to the TC.
4- On average, the coherent streamwise velocity peak is around 16% of the phase averaged peak values for both cases of LSC and TC.
5- On average, the coherent transverse velocity peak is around 63 % and 60 % of the TC and LSC phase averaged peak values, respectively.
6- The coherent TKE peak of LSC is about 22 % lower than the coherent TKE peak of the TC in the near wake region while on average it is about 20 % higher in the far wake region.

7- The maximum coherent TKE peak of LSC occurs at a larger x/D ratio which can be concluded as an indication of a location delay in the wake region in comparison to the TC case.

Inclined flat plates in tandem arrangement

1- For a given gap ratio g/D, the Strouhal number decreases as the angle of attack increases.
2- For a given gap ratio g/D, the coherent TKE peak production decreases as the angle of attack increases.
3- For a given angle of attack α, the Strouhal number increases as the gap ratio g/D increases.
4- In cases of the angle of attack of 70 and 80 degrees, the coherent TKE peak production decreases as the gap ratio g/D increases.
5- In case of the angle of attack of 90 degrees, the coherent TKE peak production increases as the gap ratio g/D increases.

7.2 Suggestions for Future Studies

Further study on the aerodynamic force of the various investigated configurations is suggested. Such a study is critical for bluff bodies in tandem arrangement where the gap between them acts as a key factor. Bluff bodies in close proximity act similar to a "single body" and hence vortices cannot roll up inside the gap between the bodies, and the initiated shear layers from upstream body bypass this dead flow region and form vortices behind the downstream body. Whereas, for larger gap between the bodies, vortices also roll up inside the gap and the vortex shedding phenomenon occurs independently from each body. As a result, the drag force is entirely influenced by such a phenomenon and it requires great attention.

Moreover, the PIV measuring technique can be employed for further studies of the tandem inclined plates. The PIV has the capability of global flow field velocity measurement while hot wire anemometer (HWA) only provides point-wise measurements. Therefore, the gap region between the two plates can be also investigated to provide better insight into these problems.

REFERENCES

Afgan, I., Benhamadouche, S., Han, X., Sagaut, P., & Laurence, D. (2013). Flow over a flat plate with uniform inlet and incident coherent gusts. *Journal of Fluid Mechanics, 720*, 457-485.

Agarwal, R., & Dhiman, A. (2014). Flow and heat transfer phenomena across two confined tandem heated triangular bluff bodies. *Numerical Heat Transfer, Part A: Applications, 66*(9), 1020-1047.

Agarwal, R., & Dhiman, A. (2015). Confined flow and heat transfer phenomena of non-Newtonian shear-thinning fluids across a pair of tandem triangular bluff bodies. *Numerical Heat Transfer, Part A: Applications, 68*(2), 174-204.

Auteri, F., Belan, M., Cassinelli, C., & Gibertini, G. (2009). Interacting Wakes of Two Normal Flat PlatesAn investigation based on phase averaging of LDA signals. *Journal of Visualization, 12*(4), 307-321.

Auteri, F., Belan, M., Gibertini, G., & Grassi, D. (2008). Normal flat plates in tandem: An experimental investigation. *Journal of Wind Engineering and Industrial Aerodynamics, 96*(6), 872-879.

Balachandar, R., Chu, V. H., & Zhang, J. (1997). Experimental study of turbulent concentration flow field in the wake of a bluff body. *Journal of Fluids Engineering, 119*(2), 263-270.

Bearman, P. (1971). An investigation of the forces on flat plates normal to a turbulent flow. *Journal of Fluid Mechanics, 46*(1), 177-198.

Bearman, P., & Trueman, D. (1972). Investigation of flow around rectangular cylinders. *Aeronautical Quarterly, 23*(AUG).

Bradshaw, Peter. (1996). *An Introduction to Turbulence and Its Measurement*: Pergamon Press.

Bradshaw, Peter. (2013). *An Introduction to Turbulence and Its Measurement: Thermodynamics and Fluid Mechanics Series*: Elsevier.

Brunn, H. H. (1995). Hot-wire anemometry: principles and signal analysis: Oxford University Press Inc.

Bruun, H. H. (1996). Hot-wire anemometry: principles and signal analysis: IOP Publishing.

Cantwell, Brian, & Coles, Donald. (1983). An experimental study of entrainment and transport in the turbulent near wake of a circular cylinder. *Journal of fluid mechanics, 136*, 321-374.

Carassale, L., Freda, A., & Marrè-Brunenghi, M. (2014). Experimental investigation on the aerodynamic behavior of square cylinders with rounded corners. *Journal of Fluids and Structures, 44*, 195-204.

Chen, J. M., & Fang, Y. C. (1996). Strouhal numbers of inclined flat plates. *Journal of Wind Engineering and Industrial Aerodynamics, 61*(2), 99-112.

Chen, J. M., & Liu, C. H. (1999). Vortex shedding and surface pressures on a square cylinder at incidence to a uniform air stream. *International Journal of Heat and Fluid Flow, 20*(6), 592-597.

Dennis, S., Qiang, W., Coutanceau, M., & Launay, J. L. (1993). Viscous flow normal to a flat plate at moderate Reynolds numbers. *Journal of Fluid Mechanics, 248*, 605-635.

Hacışevki, H., & Teimourian, A. (2015). Comparison of flow structures in the wake region of two similar normal flat plates in tandem and a square cylinder. *Experimental Thermal and Fluid Science, 69*, 169-177.

Hacışevki, H., & Teimourian, A. (2016). Interacting wakes of a narrow and a wide flat plate in tandem arrangement. *Fluid Dynamics Research, 48*(1), 015505.

Huang, R., & Lin, B. (2011). Effects of flow patterns on aerodynamic forces of a square cylinder at incidence. *Journal of Mechanics, 27*(3), 347-355.

Huang, R., Lin, B., & Yen, S. (2010). Time-averaged topological flow patterns and their influence on vortex shedding of a square cylinder in crossflow at incidence. *Journal of Fluids and Structures, 26*(3), 406-429.

Hussain, AKM. (1986). Coherent structures and turbulence. *Journal of Fluid Mechanics, 173*, 303-356.

Igarashi, T. (1984). Characteristics of the flow around a square prism. *Bulletin of JSME, 27*(231), 1858-1865.

Ingham, D., Tang, T., & Morton, B. (1990). Steady two-dimensional flow through a row of normal flat plates. *Journal of Fluid Mechanics, 210*, 281-302.

Iungo, G. V., & Buresti, G. (2009). Experimental investigation on the aerodynamic loads and wake flow features of low aspect-ratio triangular prisms at different wind directions. *Journal of Fluids and Structures, 25*(7), 1119-1135.

Jorgensen, FE. (1971). Directional sensitivity of wire and fiber-film probes. *DISA information, 11*(3), 1-7.

Kiya, M., & Matsumura, M. (1988). Incoherent turbulence structure in the near wake of a normal plate. *Journal of Fluid Mechanics, 190*, 343-356.

Knauss, D. T., John, J., & Marks, C. (1976). The vortex frequencies of bluff cylinders at low Reynolds numbers. *Journal of Hydronautics, 10*(4), 121-126.

Kurtulus, D., Scarano, F., & David, L. (2007). Unsteady aerodynamic forces estimation on a square cylinder by TR-PIV. *Experiments in Fluids, 42*(2), 185-196.

Lam, K. (1996). Phase-locked eduction of vortex shedding in flow past an inclined flat plate. *Physics of Fluids (1994-present), 8*(5), 1159-1168.

Lam, K., & Leung, M. (2005). Asymmetric vortex shedding flow past an inclined flat plate at high incidence. *European Journal of Mechanics-B/Fluids, 24*(1), 33-48.

Lam, K., & Wei, C. (2010). Numerical simulation of vortex shedding from an inclined flat plate. *Engineering Applications of Computational Fluid Mechanics, 4*(4), 569-579.

Lyn, D., Einav, S., Rodi, W., & Park, J.-H. (1995). A laser-Doppler velocimetry study of ensemble-averaged characteristics of the turbulent near wake of a square cylinder. *Journal of Fluid Mechanics, 304*, 285-319.

Maiti, D. K., & Bhatt, R. (2014). Vortex shedding suppression and aerodynamic characteristics of square cylinder due to offsetting of rectangular cylinders towards a plane. *Ocean Engineering, 82*, 91-104.

Mazharoğlu, Ç., & Hacışevki, H. (1999). Coherent and incoherent flow structures behind a normal flat plate. *Experimental Thermal and Fluid Science, 19*(3), 160-167.

McClean, J., & Sumner, D. (2014). An experimental investigation of aspect ratio and incidence angle effects for the flow around surface-mounted finite-height square prisms. *Journal of Fluids Engineering, 136*(8), 081206.

Miran, S., & Sohn, C. H. (2015). Numerical study of the rounded corners effect on flow past a square cylinder. *International Journal of Numerical Methods for Heat & Fluid Flow, 25*(4), 686-702.

Miran, S., & Sohn, C. H. (2016). Influence of incidence angle on the aerodynamic characteristics of square cylinders with rounded corners: A numerical investigation. *International Journal of Numerical Methods for Heat & Fluid Flow, 26*(1), 269-283.

Najjar, F. M., & Vanka, S. (1995). Simulations of the unsteady separated flow past a normal flat plate. *International journal for numerical methods in fluids, 21*(7), 525-547.

Nakamura, Y. (1996). Vortex shedding from bluff bodies and a universal Strouhal number. *Journal of Fluids and Structures, 10*(2), 159-171.

Nakamura, Y., Ohya, Y., & Tsuruta, H. (1991). Experiments on vortex shedding from flat plates with square leading and trailing edges. *Journal of Fluid Mechanics, 222*, 437-447.

Narasimhamurthy, V. D., & Andersson, H. I. (2009). Numerical simulation of the turbulent wake behind a normal flat plate. *International Journal of Heat and Fluid Flow, 30*(6), 1037-1043.

Oudheusden, B. W. V., Scarano, F., Hinsberg, N. P. V.., Watt, D. W. (2005). Phase-resolved characterization of vortex shedding in the near wake of a square section cylinder at incidence, *Experiments in Fluids 39* (1), 86-98.

Okajima, A. (1982). Strouhal numbers of rectangular cylinders. *Journal of Fluid Mechanics, 123*, 379-398.

Ozgoren, M. (2006). Flow structure in the downstream of square and circular cylinders. *Flow Measurement and Instrumentation, 17*(4), 225-235.

Ozgoren, M., Pinar, E., Sahin, B., & Akilli, H. (2011). Comparison of flow structures in the downstream region of a cylinder and sphere. *International Journal of Heat and Fluid Flow, 32*(6), 1138-1146.

Perry, AE, & Steiner, TR. (1987). Large-scale vortex structures in turbulent wakes behind bluff bodies. Part 1. Vortex formation processes. *Journal of fluid mechanics, 174*, 233-270.

Provansal, M., Schouveiler, L., & Leweke, T. (2004). From the double vortex street behind a cylinder to the wake of a sphere. *European Journal of Mechanics-B/Fluids, 23*(1), 65-80.

Raisee, M., Jafari, A., Babaei, H., & Iacovides, H. (2010). Two-dimensional prediction of time dependent, turbulent flow around a square cylinder confined in a channel. *International journal for numerical methods in fluids, 62*(11), 1232-1263.

Reynolds, WC, & Hussain, AKMF. (1972). The mechanics of an organized wave in turbulent shear flow. Part 3. Theoretical models and comparisons with experiments. *Journal of Fluid Mechanics, 54*(02), 263-288.

Saha, A., Muralidhar, K., & Biswas, G. (2000). Experimental study of flow past a square cylinder at high Reynolds numbers. *Experiments in Fluids, 29*(6), 553-563.

Saha, A. K. (2007). Far-wake characteristics of two-dimensional flow past a normal flat plate. *Physics of Fluids (1994-present), 19*(12), 128110.

Saha, A. K. (2013). Unsteady flow past a finite square cylinder mounted on a wall at low Reynolds number. *Computers & Fluids, 88*, 599-615.

Saha, A. K., & Shrivastava, A. (2015). Suppression of vortex shedding around a square cylinder using blowing. *Sadhana, 40*(3), 769-785.

Sakamoto, H., & Arie, M. (1983). Vortex shedding from a rectangular prism and a circular cylinder placed vertically in a turbulent boundary layer. *Journal of Fluid Mechanics, 126*, 147-165.

Sarioglu, M. (2017). Control of flow around a square cylinder at incidence by using a splitter plate. *Flow Measurement and Instrumentation, 53*, 221-229.

Sarioglu, M., & Yavuz, T. (2000). Vortex shedding from circular and rectangular cylinders placed horizontally in a turbulent flow. *Turkish Journal of*

Engineering & Environmental Sciences/Turk Muhendislik ve Cevre Bilimleri Dergisi, 24(4), 217-228.

Sheard, G. J. (2011). Wake stability features behind a square cylinder: focus on small incidence angles. *Journal of Fluids and Structures, 27*(5-6), 734-742.

Sohankar, A., Esfeh, M. K., Pourjafari, H., Alam, M. M., & Wang, L. (2018). Feature of the flow over a finite length square cylinder on a wall at various incidence angles. *Wind and Structures*, *26* (5), 317-329.

Sohankar, A., & Najafi, M. (2018). Control of vortex shedding, forces and heat transfer from a square cylinder at incidence by suction and blowing. *International Journal of Thermal Sciences, 129*, 266-279.

Srigrarom, S., & Koh, A. (2008). Flow field of self-excited rotationally oscillating equilateral triangular cylinder. *Journal of Fluids and Structures, 24*(5), 750-755.

Steiner, TR, & Perry, AE. (1987). Large-scale vortex structures in turbulent wakes behind bluff bodies. Part 2. Far-wake structures. *Journal of Fluid Mechanics, 174*, 271-298.

Sung, H. J., Kim, Y. N., & Hyun, J. M. (1994). Discrete vortex simulation of pulsating flow behind a normal plate. *Journal of Fluids Engineering, 116*(4), 862-869.

Tamura, T., & Miyagi, T. (1999). The effect of turbulence on aerodynamic forces on a square cylinder with various corner shapes. *Journal of Wind Engineering and Industrial Aerodynamics, 83*(1), 135-145.

Tamura, T., Miyagi, T., & Kitagishi, T. (1998). Numerical prediction of unsteady pressures on a square cylinder with various corner shapes. *Journal of Wind Engineering and Industrial Aerodynamics, 74*, 531-542.

Teimourian, A., Hacisevki, H., Bahrami, A. (2017). Experimental study on flow past two inclined flat plates in tandem arrangement. *Journal of Wind Engineering and Industrial Aerodynamics, 169*, 1-11.

Tu, J., Zhou, D., Bao, Y., Han, Z., & Li, R. (2014). Flow characteristics and flow-induced forces of a stationary and rotating triangular cylinder with different incidence angles at low Reynolds numbers. *Journal of Fluids and Structures, 45*, 107-123.

Tutu, NK, & Chevray, R. (1975). Cross-wire anemometry in high intensity turbulence. Journal of Fluid Mechanics, 71(04), 785-800.

Van Oudheusden, B., Scarano, F., Van Hinsberg, N., & Watt, D. (2005). Phase-resolved characterization of vortex shedding in the near wake of a square-section cylinder at incidence. *Experiments in Fluids, 39*(1), 86-98.

Wang, S., Zhu, L., Zhang, X., & He, G. (2011). Flow past two freely rotatable triangular cylinders in tandem arrangement. *Journal of Fluids Engineering, 133*(8), 081202.

Wang, Y. C., & Wu, W. Q. (2004). Numerical simulation of flow around square cylinder using RNG k-ε turbulence model. *Journal of Hydrodynamics. Ser. A, 19*, 916-920.

Yagmur, S., Dogan, S., Aksoy, M. H., Goktepeli, I., & Ozgoren, M. (2017). Comparison of flow characteristics around an equilateral triangular cylinder via PIV and Large Eddy Simulation methods. *Flow Measurement and Instrumentation, 55*, 23-36.

Yang, D., Pettersen, B., Andersson, H. I., & Narasimhamurthy, V. D. (2012). Vortex shedding in flow past an inclined flat plate at high incidencea). *Physics of Fluids (1994-present), 24*(8), 084103.

Yen, S. C., & Yang, C. W. (2011). Flow patterns and vortex shedding behavior behind a square cylinder. *Journal of Wind Engineering and Industrial Aerodynamics, 99*(8), 868-878.

Yoon, D. H., Yang, K. S., & Choi, C. B. (2010a). Flow past a square cylinder with an angle of incidence. *Physics of Fluids (1994-present), 22*(4), 043603.

Yoon, D. H., Yang, K. S., & Choi, C. B. (2010b). Flow past a square cylinder with an angle of incidence. *Physics of Fluids, 22*(4), 043603.

APPENDIX

Convertor1 Program

```
c
**********************************************************************
*
c       CONVERTING ACQUIRED VELOCITY DATA TO MATLAB MATRIX
FORMAT
c
**********************************************************************
*
        character ic1,ic2,ic3,ic4,ic5,ic6
       character*24 file1
       character*27 file2
       print *,'     Program to prepare m file for Matlab '
       print *,' '
       print *,'       Exp No  =?'
       read *,iexp
       call number(iexp,ic5,ic6)
       print *,'       ix= ? '
       read *,ix
       print *,'  Enter first grid no   iymin= ?'
       read *,iymin
       print *,'  Enter last grid no  iymax= ?'
       read *,iymax
       print *,'Enter number of ensembles ?'
       read *,iens
       imax=10240
       print *,'Number of data samples is selected as =',imax
       call number(ix,ic1,ic2)
      do ir=iymin,iens*iymax
      print *,' '
      print *,'ir  =  ',ir
      call number(ir,ic3,ic4)
```

```
   file1='c:\flowpt\data\'//ic5//ic6//'x'//ic1//ic2//'.w'//ic3//ic4
   file2='c:\matlab\filter\e'//ic5//ic6//'x'//ic1//ic2//ic3//ic4//'.
  +m'
   open(1,file=file1)
   open(2,file=file2)

   do i=1,imax
   read(1,*)t,u,v,ur
   if(i.eq.1)then
   write(2,21)t,ur
   end if
   if(i.gt.1.and.i.lt.imax)then
   write(2,22)t,ur
   end if
   if(i.eq.imax)then
   write(2,23)t,ur
   end if
   end do
   end do
21 format('a=[',f7.5,1x,f7.3,';')
22 format(f7.5,1x,f7.3,';')
23 format(f7.5,1x,f7.3,'];')
   stop
   end
   subroutine number(input,io1,io2)
   character io1,io2

     if(input.lt.10)then
     io1=48
     io2=input+48
```

```
else if(input.ge.10.and.input.lt.20)then
io1=49
io2=input+38
else if(input.ge.20.and.input.lt.30)then
io1=50
io2=input+28
else if(input.ge.30.and.input.lt.40)then
io1=51
io2=input+18
 else if(input.ge.40.and.input.lt.50)then
io1=52
io2=input+8
else if(input.ge.50.and.input.lt.60)then
io1=53
io2=input-2
else if(input.ge.60.and.input.lt.70)then
io1=54
io2=input-12
 else if(input.ge.70.and.input.lt.80)then
io1=55
io2=input-22
 else if(input.ge.80.and.input.lt.90)then
io1=56
io2=input-32
else if(input.ge.90.and.input.lt.100)then
io1=57
io2=input-42
end if

return
end
```

Convertor2 Program

```
c
**********************************************************************
*
c     BLENDING FILTERED AND UNFILTERED VELOCITY DATA FOR
FURTHER                c     ANALYSIS
c
**********************************************************************
*


      parameter (ii=10240)
      dimension t1(ii),t2(ii),u(ii),v(ii),uref(ii),ufilt(ii),ur(ii)
      character ic1,ic2,ic3,ic4,ic5,ic6
      character*29 file2
      character*24 file3
      character*32 file1

      print *,' Data Amalgamation for Ensemble Phase Averaging '
      print *,' '
      print *,'      Exp No  =?'
      read *,iexp
      call number(iexp,ic5,ic6)

      print *,'      ix= ?'
      read *,ix

      print *,'  Enter first grid no   iymin ?'
      read *,iymin
      print *,'  Enter last grid no   iymax  ?'
      read *,iymax
      print *,'Enter number of ensembles ?'
      read *,iens
```

```
  call number(ix,ic1,ic2)

  print *,'Enter no of removed cycles  scycle=?'
  read *,scycle
  print *,'Enter U infinity (m/s)?'
  read *,uinf
  imax=ii-1
  print *,' '
  print *,' Number of data samples is selected as =',imax

  do ir=iymin,iens*iymax
 print *,' '
 print *,'   ir=  ',ir
 print *,' '

 call number(ir,ic3,ic4)
 file1='c:\f32\ensprgs\data\e'//ic5//ic6//'x'//ic1//ic2//ic3//ic4//
+'.dat'

   file2='c:\matlab\filter\e'//ic5//ic6//'x'//ic1//ic2//ic3//ic4//
+'.flt'
  file3='c:\flowpt\data\'//ic5//ic6//'x'//ic1//ic2//'.w'//ic3//ic4
 open(1,file=file1)
 open(2,file=file2)
 open(3,file=file3)
 do i=1,imax+1
 if(i.eq.1)then
 read(2,*)ddelay1,ddelay2,freq
 else
 read(2,*)t2(i),uref(i),ufilt(i)
 read(3,*)t1(i-1),u(i-1),v(i-1),ur(i-1)
```

```
  end if
  end do




  write(1,11)scycle,uinf,freq,ddelay1,ddelay2
  do i=2,imax+1
  write(1,10)t1(i-1),uref(i),ufilt(i),u(i-1),v(i-1)
  end do
  close(2)
  end do
10 format(f7.4,1x,f7.3,1x,f7.3,1x,f7.3,1x,f7.3)
11 format(f4.1,1x,f5.2,1x,f6.2,1x,f8.5,1x,f8.5)
  stop
  end


  subroutine number(input,io1,io2)
  character io1,io2

   if(input.lt.10)then
   io1=48
   io2=input+48
   else if(input.ge.10.and.input.lt.20)then
   io1=49
   io2=input+38
   else if(input.ge.20.and.input.lt.30)then
   io1=50
   io2=input+28
```

```
else if(input.ge.30.and.input.lt.40)then
io1=51
io2=input+18
 else if(input.ge.40.and.input.lt.50)then
io1=52
io2=input+8
else if(input.ge.50.and.input.lt.60)then
io1=53
io2=input-2
else if(input.ge.60.and.input.lt.70)then
io1=54
io2=input-12
 else if(input.ge.70.and.input.lt.80)then
io1=55
io2=input-22
 else if(input.ge.80.and.input.lt.90)then
io1=56
io2=input-32
else if(input.ge.90.and.input.lt.100)then
io1=57
io2=input-42
end if

return
end
```

Ensemble Program

```
c
**********************************************************************
*
c       CALCULATION OF ENSEMBLE-PHASE AVERAGED STATISTICAL
PROPERTIES
c                              AND DERIVATIVE OF STRESSES
c
**********************************************************************
*


      character ic1,ic2,ic3,ic4,ic5,ic6
      character*30 file4,file6
      character*31 file2,file3,file5,file7
      character*32 file1
      character*25 file8,file9
      parameter (ii=10239,jj=1000,nr=99,nn=61,kk=18,ll=10)
      dimension uph(kk,nr,nn),vph(kk,nr,nn),uphav(kk,nr,nn),t(ii),
     +  cohstr(kk,nr,nn),vphav(kk,nr,nn),ucoh(kk,nr,nn),vcoh(kk,nr,nn),
     +  udas(kk,nr,nn),vdas(kk,nr,nn),udassq(kk,nr,nn),vdassq(kk,nr,nn),
     +  stress(kk,nr,nn),sumudas(kk,nr,nn),sumvdas(kk,nr,nn),ufilt(ii),
     +  sumusq(kk,nr,nn),sumvsq(kk,nr,nn),sumstres(kk,nr,nn),u(ii),
     +  avudas(kk,nr,nn),avvdas(kk,nr,nn),avusq(kk,nr,nn),per(jj),
     +  avvsq(kk,nr,nn),avstress(kk,nr,nn),sumuph(kk,nr,nn),uref(ii),
     +  sumvph(kk,nr,nn),tref(jj),tfilt(jj),delay(jj),avucoh(kk,nr),
     +  avvcoh(kk,nr),avsqu(kk,nr),avsqv(kk,nr),avcostrs(kk,nr),v(ii),
     +  udasav(kk,nr),vdasav(kk,nr),avusqr(kk,nr),avvsqr(kk,nr),
     +  avstres(kk,nr),uuphav(kk,nr,nn),vvphav(kk,nr,nn),vort(kk,nr,ll),
     +  avuphav(kk,nr),avvphav(kk,nr),uav(kk,nr),vav(kk,nr)


      print *,' '
      print *,'     CALCULATION OF COHERENT and INCOHERENT
PROPERTIES'
```

```
print *,' '
print *,'       Exp No  =?'
read *,iexp
call number(iexp,ic5,ic6)
print *,'  Enter number of ensembles ?'
read *,iens

print *,'  Enter first grid no for analysis    iymin= ? '
read *,iymin
print *,'  Enter last grid no  for analysis    iymax= ?'
read *,iymax
print *,'  Enter first grid no for analysis    ixmin= ?'
read *,ixmin
print *,'  Enter last grid no for analysis     ixmax= ?'
read *,ixmax
print *,' '
print *,'  DOMAIN maximum y-grid iymaxx ?'
read *,iymaxx
print *,'  DOMAIN maximum x-grid ixmaxx ?'
read *,ixmaxx
print *,' '
print *,'Enter starting X/d for the domain xstart (e.g 4.0 )'
read *,xstart
print *,' '
xlength=160
ylength=137.2
dwidth=25.
print *,'Domain is',xlength,' X ',ylength,'Y '
print *,' '
print *,' '
print *,' '
```

```
if(iens.eq.1)then
irstrt=iymin*iens
else
irstrt=(iymin*iens)-(iens-1)
end if
dx=xlength/((ixmaxx-1)*1000)
dy=ylength/((iymaxx-1)*1000)

do ix=ixmin,ixmax
inftot=0
uinftot=0.
 do ir=irstrt,iens*iymax
sumudas(ix,ir,1)=0.
sumvdas(ix,ir,1)=0.
sumusq(ix,ir,1)=0.
sumvsq(ix,ir,1)=0.
sumstres(ix,ir,1)=0.
ucohtot=0.
vcohtot=0.
totusq=0.
totvsq=0.
totcostr=0.
suphav=0.
svphav=0.
udastot=0.
vdastot=0.
usqrtot=0.
vsqrtot=0.
stresstot=0.
sumref=0.
```

```
      sumfilt=0.
      sumdelay=0.
      n=0.
      ut=0.
      vt=0.
      jcount=0
      call number(ix,ic1,ic2)
      call number(ir,ic3,ic4)
     file1='c:\f32\ensprgs\data\e'//ic5//ic6//'x'//ic1//ic2//ic3//ic4/
    +/'.dat'
     open(1,file=file1)
     read(1,*) scycle,uinf,freq,ddelay1,ddelay2


      halfper=0.5/freq
      uinftot=uinftot+uinf
      inftot=inftot+1
        do i=1,ii
        read(1,*)t(i),uref(i),ufilt(i),u(i),v(i)
        u(i)=u(i)/uinf
        v(i)=v(i)/uinf

c
**********************************************************************
**
c       start averaging after (scycle=2-5) cycles
c
**********************************************************************
**


         if(t(i).gt.(scycle*2*halfper))then
```

```
        sumref=uref(i)+sumref
        sumfilt=ufilt(i)+sumfilt
        n=n+1
        if(n.eq.1)istart0=i
        end if
        end do
      avuref=sumref/(ii-istart0)
      avufilt=sumfilt/(ii-istart0)
        do i=1,ii
        uref(i)=uref(i)-avuref
        ufilt(i)=ufilt(i)-avufilt
        end do

c
**********************************************************************
*
c      Determination of phase delay
c
**********************************************************************
*

      n1=1
        do i=istart0,ii-1
        if(uref(i).lt.0.and.uref(i+1).gt.0.or.
     +   uref(i).gt.0.and.uref(i+1).lt.0)then
        tref(n1)=((uref(i)*(t(i)-t(i+1)))/(uref(i+1)-uref(i)))+t(i)
        n1max=n1
        n1=n1+1
        end if
        end do

      n2=1
```

```
      do i=istart0,ii-1
      if(ufilt(i).lt.0.and.ufilt(i+1).gt.0.or.
     +   ufilt(i).gt.0.and.ufilt(i+1).lt.0)then
      tfilt(n2)=((ufilt(i)*(t(i)-t(i+1)))/(ufilt(i+1)-ufilt(i)))+
     +   t(i)
      if(n2.le.2.and.ufilt(i).lt.0.and.ufilt(i+1).gt.0.)then
      if(n2.eq.1)jcount=1
      if(n2.eq.2)jcount=2
      istart=i
      end if
      n2max=n2
      n2=n2+1
      iend=i+1
      end if
      end do

     n=1
      do n1=2,n1max
       do n2=2,n2max
       dif1=abs(((tfilt(n2)-tref(n1))-ddelay2)/ddelay2)
       dif2=abs(((tfilt(n2)-tfilt(n2-1))/halfper)-1)
       dif3=abs(((tref(n1)-tref(n1-1))/halfper)-1)
       if(dif2.lt.0.25.and.dif3.lt.0.25.and.dif1.lt.0.25)then
       delay(n)=tfilt(n2)-tref(n1)
c        if(delay(n).gt.0.)then
       sumdelay=sumdelay+delay(n)
       n=n+1
c        end if
       end if
       end do
      end do
```

```
      if(n.gt.1)then
      avdelay2=sumdelay/(n-1)
      else
      avdelay2=ddelay2
      end if
      if(n.eq.1)then
      print *,'*WARNING*(phase delay loop never used)'
      print *,'CHECK INPUT DELAY OR DATA'
      end if
      if(n.gt.1.and.n.lt.30)then
      print *,' '
      print *,'WARNING* phase delay loop was used only',n,' times '
      end if



c
**********************************************************************
*
c      Determination of periods
c
**********************************************************************
*


      if(jcount.eq.1)then
      if(mod(n2max,2).gt.0)then
      ncycle=(n2max-1)/2
      else
      ncycle=(n2max-2)/2
      end if
      end if
      if(jcount.eq.2)then
      if(mod(n2max,2).gt.0)then
```

```
  ncycle=((n2max-1)/2)-1
  else
  ncycle=(n2max/2)-1
  end if
  end if
  do j=1,ncycle
  if(jcount.eq.1)then
    per(j)=tfilt(2*j+1)-tfilt(2*j-1)
  else if(jcount.eq.2)then
     if(j.eq.1)then
     per(1)=tfilt(4)-tfilt(2)
     else
     per(j)=tfilt(2*j+2)-tfilt(2*j)
     end if
   else
   print *,'jcount ne 1 or 2 '
   end if
  end do

  icount=icount+1
  if(iens.eq.1)iy=ir
  if(iens.gt.1.and.icount.le.iens)then
  iy=(ir+(iens-1))/iens
  end if
  if(icount.eq.iens)icount=0
 print *,' '
 print *,'       ix         iy         ir          n     avd
+elay2         ncycle '
 print *,ix,iy,ir,n,avdelay2,ncycle
```

```
c
**********************************************************************
*
c       Calculation of u average and v average
c
**********************************************************************
*



c     temporarily set ddelay1=0.0002
        do i=1,ii
        ddelay1=0.
        t(i)=t(i)+ddelay1+avdelay2
        end do
        do i=istart,iend
        ut=ut+u(i)
        vt=vt+v(i)
        end do
       uav(ix,ir)=ut/(iend-istart)
       vav(ix,ir)=vt/(iend-istart)


c
**********************************************************************
*
c       Phase averaging and coherent properties at selected phase points
c
**********************************************************************
*


       itmax=61
        do it=1,itmax
        uphh=0.
        vphh=0.
```

```
ncount=0
 do j=1,ncycle
 if(jcount.eq.1)then
 time=(((it-1)*1.)/(itmax-1))*per(j)+tfilt((2*j)-1)
 else
 time=(((it-1)*1.)/(itmax-1))*per(j)+tfilt(2*j)
 end if

  do i=istart-10,iend
  if(t(i).lt.time.and.t(i+1).gt.time)then
  ncount=ncount+1
  uph(ix,ir,it)=(u(i)+u(i+1))/2
  vph(ix,ir,it)=(v(i)+v(i+1))/2
  sumuph(ix,ir,it)=uph(ix,ir,it)+uphh
  sumvph(ix,ir,it)=vph(ix,ir,it)+vphh
  uphh=sumuph(ix,ir,it)
  vphh=sumvph(ix,ir,it)
  end if
  end do
 end do
 uphav(ix,ir,it)=sumuph(ix,ir,it)/ncount
 vphav(ix,ir,it)=sumvph(ix,ir,it)/ncount
 ucoh(ix,ir,it)=uphav(ix,ir,it)-uav(ix,ir)
 vcoh(ix,ir,it)=vphav(ix,ir,it)-vav(ix,ir)
 uuphav(ix,ir,it)=uinf*uphav(ix,ir,it)
 vvphav(ix,ir,it)=uinf*vphav(ix,ir,it)
 cohstr(ix,ir,it)=ucoh(ix,ir,it)*vcoh(ix,ir,it)
 ucohtot=ucoh(ix,ir,it)+ucohtot
 vcohtot=vcoh(ix,ir,it)+vcohtot
 totusq=ucoh(ix,ir,it)**2+totusq
 totvsq=vcoh(ix,ir,it)**2+totvsq
```

```
          totcostr=cohstr(ix,ir,it)+totcostr
          suphav=uphav(ix,ir,it)+suphav
          svphav=vphav(ix,ir,it)+svphav
         end do

c
**********************************************************************
*
c       Averaged coherent properties
c
**********************************************************************
*
        avuphav(ix,ir)=suphav/itmax
        avvphav(ix,ir)=svphav/itmax
        avucoh(ix,ir)=ucohtot/itmax
        avvcoh(ix,ir)=vcohtot/itmax
        avsqu(ix,ir)=totusq/itmax
        avsqv(ix,ir)=totvsq/itmax
        avcostrs(ix,ir)=totcostr/itmax

c
**********************************************************************
*
c       Incoherent statistical properties
c
**********************************************************************
*

         do it=1,itmax
         ncount=0
          do j=1,ncycle
          if(jcount.eq.1)then
          time=(((it-1)*1.)/(itmax-1))*per(j)+tfilt((2*j)-1)
```

```
          else
          time=(((it-1)*1.)/(itmax-1))*per(j)+tfilt(2*j)
          end if
           do i=istart-10,iend
           if(t(i).lt.time.and.t(i+1).gt.time)then
           ncount=ncount+1
           udas(ix,ir,it)=(u(i)+u(i+1))/2-uphav(ix,ir,it)
           vdas(ix,ir,it)=(v(i)+v(i+1))/2-vphav(ix,ir,it)
           udassq(ix,ir,it)=udas(ix,ir,it)**2
           vdassq(ix,ir,it)=vdas(ix,ir,it)**2
           stress(ix,ir,it)=udas(ix,ir,it)*vdas(ix,ir,it)
           end if
           end do
          sumudas(ix,ir,it)=sumudas(ix,ir,it)+udas(ix,ir,it)
          sumvdas(ix,ir,it)=sumvdas(ix,ir,it)+vdas(ix,ir,it)
          sumusq(ix,ir,it)=sumusq(ix,ir,it)+udassq(ix,ir,it)
          sumvsq(ix,ir,it)=sumvsq(ix,ir,it)+vdassq(ix,ir,it)
          sumstres(ix,ir,it)=sumstres(ix,ir,it)+stress(ix,ir,it)
          end do


c
**********************************************************************
c         average over total periods
c
**********************************************************************


         avudas(ix,ir,it)=sumudas(ix,ir,it)/ncount
         avvdas(ix,ir,it)=sumvdas(ix,ir,it)/ncount
         avusq(ix,ir,it)=sumusq(ix,ir,it)/ncount
         avvsq(ix,ir,it)=sumvsq(ix,ir,it)/ncount
         avstress(ix,ir,it)=sumstres(ix,ir,it)/ncount
```

```
        end do



c
**********************************************************************
c       average over one cycle
c
**********************************************************************


        do it=1,itmax
        udastot=avudas(ix,ir,it)+udastot
        vdastot=avvdas(ix,ir,it)+vdastot
        usqrtot=avusq(ix,ir,it)+usqrtot
        vsqrtot=avvsq(ix,ir,it)+vsqrtot
        stresstot=avstress(ix,ir,it)+stresstot
        end do
        udasav(ix,ir)=udastot/itmax
        vdasav(ix,ir)=vdastot/itmax
        avusqr(ix,ir)=usqrtot/itmax
        avvsqr(ix,ir)=vsqrtot/itmax
        avstres(ix,ir)=stresstot/itmax
        end do
        close(1)
       uinfav=uinftot/inftot
       print *,'uinfav=',uinfav
       end do


c
**********************************************************************
****
c      Ensemble Averaging
```

```
c
**********************************************************************
****


      do ix=ixmin,ixmax
      do iy=iymin,iymax
      if(iens.eq.1)then
      irstrt=iy*iens
      else
      irstrt=(iy*iens)-(iens-1)
      end if

      do it=1,itmax

      s1=0.
      s2=0.
      s3=0.
      s4=0.
      s5=0.
      s6=0.
      s7=0.
      s8=0.
      s9=0.
      s10=0.
      s11=0.
      s12=0.
      s13=0.
      s14=0.
      s15=0.
      s16=0.
```

```
s17=0.


 do ir=irstrt,iy*iens

 uphav(ix,iy,it)=uphav(ix,ir,it)/iens+s1
 s1=uphav(ix,iy,it)
 vphav(ix,iy,it)=vphav(ix,ir,it)/iens+s2
 s2=vphav(ix,iy,it)
 ucoh(ix,iy,it)=ucoh(ix,ir,it)/iens+s3
 s3=ucoh(ix,iy,it)
 vcoh(ix,iy,it)=vcoh(ix,ir,it)/iens+s4
 s4=vcoh(ix,iy,it)
 uuphav(ix,iy,it)=uuphav(ix,ir,it)/iens+s5
 s5=uuphav(ix,iy,it)
 vvphav(ix,iy,it)=vvphav(ix,ir,it)/iens+s6
 s6=vvphav(ix,iy,it)
 cohstr(ix,iy,it)=cohstr(ix,ir,it)/iens+s7
 s7=cohstr(ix,iy,it)
 udas(ix,iy,it)=udas(ix,ir,it)/iens+s8
 s8=udas(ix,iy,it)
 vdas(ix,iy,it)=vdas(ix,ir,it)/iens+s9
 s9=vdas(ix,iy,it)
 udassq(ix,iy,it)=udassq(ix,ir,it)/iens+s10
 s10=udassq(ix,iy,it)
 vdassq(ix,iy,it)=vdassq(ix,ir,it)/iens+s11
 s11=vdassq(ix,iy,it)
 stress(ix,iy,it)=stress(ix,ir,it)/iens+s12
 s12=stress(ix,iy,it)
 avudas(ix,iy,it)=avudas(ix,ir,it)/iens+s13
 s13=avudas(ix,iy,it)
```

```
  avvdas(ix,iy,it)=avvdas(ix,ir,it)/iens+s14
  s14=avvdas(ix,iy,it)
  avusq(ix,iy,it)=avusq(ix,ir,it)/iens+s15
  s15=avusq(ix,iy,it)
  avvsq(ix,iy,it)=avvsq(ix,ir,it)/iens+s16
  s16=avvsq(ix,iy,it)
  avstress(ix,iy,it)=avstress(ix,ir,it)/iens+s17
  s17=avstress(ix,iy,it)

  end do
end do
end do
end do


  do ix=ixmin,ixmax
  do iy=iymin,iymax

if(iens.eq.1)then
irstrt=iy*iens
else
irstrt=(iy*iens)-(iens-1)
end if

s18=0.
s19=0.
s20=0.
s21=0.
s22=0.
s23=0.
s24=0.
```

```
s25=0.
s26=0.
s27=0.
s28=0.
s29=0.
s30=0.
s31=0.
 do ir=irstrt,iy*iens

 avuphav(ix,iy)=avuphav(ix,ir)/iens+s18
 s18=avuphav(ix,iy)
 avvphav(ix,iy)=avvphav(ix,ir)/iens+s19
 s19=avvphav(ix,iy)
 avucoh(ix,iy)=avucoh(ix,ir)/iens+s20
 s20=avucoh(ix,iy)
 avvcoh(ix,iy)=avvcoh(ix,ir)/iens+s21
 s21=avvcoh(ix,iy)
 avsqu(ix,iy)=avsqu(ix,ir)/iens+s22
 s22=avsqu(ix,iy)
 avsqv(ix,iy)=avsqv(ix,ir)/iens+s23
 s23=avsqv(ix,iy)
 avcostrs(ix,iy)=avcostrs(ix,ir)/iens+s24
 s24=avcostrs(ix,iy)
 udasav(ix,iy)=udasav(ix,ir)/iens+s25
 s25=udasav(ix,iy)
 vdasav(ix,iy)=vdasav(ix,ir)/iens+s26
 s26=vdasav(ix,iy)
 avusqr(ix,iy)=avusqr(ix,ir)/iens+s27
 s27=avusqr(ix,iy)
 avvsqr(ix,iy)=avvsqr(ix,ir)/iens+s28
 s28=avvsqr(ix,iy)
```

```
          avstres(ix,iy)=avstres(ix,ir)/iens+s29
          s29=avstres(ix,iy)
          uav(ix,iy)=uav(ix,ir)/iens+s30
          s30=uav(ix,iy)
          vav(ix,iy)=vav(ix,ir)/iens+s31
          s31=vav(ix,iy)

c    print *,iy,ir,avstres(ix,ir),avsqu(ix,ir),avsqv(ix,ir),
c     +      avusqr(ix,ir)
          end do
          end do
          end do
c
**********************************************************************
c       Results
c
**********************************************************************

         do ix=ixmin,ixmax
         call number(ix,ic1,ic2)

        file2='c:\paper2\ensdata\cod'//ic5//ic6//'x'//ic1//ic2//'.dat'
        file3='c:\paper2\ensdata\avd'//ic5//ic6//'x'//ic1//ic2//'.dat'
        file4='c:\paper2\ensdata\3dd'//ic5//ic6//'x'//ic1//ic2//'.dat'
        file5='c:\paper2\ensdata\vec'//ic5//ic6//'x'//ic1//ic2//'.dat'
        file6='c:\paper2\ensdata\ave'//ic5//ic6//'x'//ic1//ic2//'.dat'
        file7='c:\paper2\ensdata\vor'//ic5//ic6//'x'//ic1//ic2//'.dat'
        file8='c:\gle\ensdata\'//ic5//ic6//'x'//ic1//ic2//'ad.dat'
        file9='c:\gle\ensdata\'//ic5//ic6//'x'//ic1//ic2//'bd.dat'
        open(2,file=file2)
        open(3,file=file3)
```

```
      open(4,file=file4)
      open(5,file=file5)
      open(6,file=file6)
      open(7,file=file7)
      open(8,file=file8)
      open(9,file=file9)
      write(2,20)ix
      write(2,21)
      write(2,22)ix,iymax,itmax
       do it=1,itmax
c       phase=(it*1./(itmax-1))-(0.5+(1./(itmax-1)))
       dd=0.005
       phase=(it-1)*1./(itmax-1)
       do iy=iymin,iymax
       y=(iy-((iymaxx+1)/2))*dy*1000./dwidth
       e1=avusq(ix,iy,it)+avvsq(ix,iy,it)
       e2=(ucoh(ix,iy,it)**2)+(vcoh(ix,iy,it)**2)
       e3=(ucoh(ix,iy,it)**2)
       e4=(vcoh(ix,iy,it)**2)
       e5=(cohstr(ix,iy+1,it)-cohstr(ix,iy,it))/dd
       e6=(avstress(ix,iy+1,it)-avstress(ix,iy,it))/dd
      write(2,*)phase,y,it,iy,uphav(ix,iy,it),vphav(ix,iy,it),
     +   ucoh(ix,iy,it),vcoh(ix,iy,it),cohstr(ix,iy,it),
     +   avusq(ix,iy,it),avvsq(ix,iy,it),avstress(ix,iy,it),
     +   e1,e2,e3,e4,e5,e6

      end do
      end do
      close(2)

      write(3,30)ix
```

```
      write(3,31)
      write(3,32)ix,iymax
      do iy=iymin,iymax
       y=(iy-((iymaxx+1)/2))*dy*1000./dwidth
       write(3,*)y,iy,avuphav(ix,iy),avvphav(ix,iy),avucoh(ix,iy),
     +   avvcoh(ix,iy),avsqu(ix,iy),avsqv(ix,iy),avcostrs(ix,iy),
     +   avusqr(ix,iy),avvsqr(ix,iy),avstres(ix,iy)

       write(8,80)y,avuphav(ix,iy),avvphav(ix,iy),avsqu(ix,iy),
     +    avsqv(ix,iy),uav(ix,iy)
       write(9,90)y,avcostrs(ix,iy),avusqr(ix,iy),avvsqr(ix,iy),
     +    avstres(ix,iy),vav(ix,iy)
      end do
      close(3)
      close(8)
      close(9)
      write(4,40)ix
      write(4,41)
      do it=1,itmax,2
c      phase=(it*1./(itmax-1))-(0.5+(1./(itmax-1)))
       phase=(it-1)*1./(itmax-1)
      write(4,42)ix,it,iymax
      do iy=iymin,iymax
       y=(iy-((iymaxx+1)/2))*dy*1000./dwidth
       e1=avusq(ix,iy,it)+avvsq(ix,iy,it)
       e2=(ucoh(ix,iy,it)**2)+(vcoh(ix,iy,it)**2)
       e3=(ucoh(ix,iy,it)**2)
       e4=(vcoh(ix,iy,it)**2)
       e5=(cohstr(ix,iy+1,it)-cohstr(ix,iy,it))/dd
       e6=(avstress(ix,iy+1,it)-avstress(ix,iy,it))/dd
      write(4,*)phase,y,it,iy,uphav(ix,iy,it),vphav(ix,iy,it),
```

```
     +    ucoh(ix,iy,it),
     +   vcoh(ix,iy,it),cohstr(ix,iy,it),avusq(ix,iy,it),
     +   avvsq(ix,iy,it),avstress(ix,iy,it),e1,e2,udas(ix,iy,it),
     +   vdas(ix,iy,it),e3,e4,e5,e6
         end do
         end do
         close(4)

         end do

         write(5,50)
         write(5,51)
         write(7,70)
         write(7,71)
         itt=0
         ncount=0
  100    ncount=ncount+1
         if(ncount.eq.1)then
         itt=1
         else if(ncount.eq.2)then
         itt=((itmax-1)/4)+1
         else if(ncount.eq.3)then
         itt=((itmax-1)/2)+1
         else if(ncount.eq.4)then
         itt=((itmax-1)*3/4)+1
         else
         itt=itmax
         end if

         if(ncount.gt.5)go to 101
         write(5,52)itt,iymax
```

```
      do ix=ixmin,ixmax
      do iy=iymin,iymax
       y=(iy-((iymaxx+1)/2))*dy*1000./dwidth
       x=(ix*dx*1000./dwidth)+xstart
       e1=avusq(ix,iy,itt)+avvsq(ix,iy,itt)
       e2=(ucoh(ix,iy,itt)**2)+(vcoh(ix,iy,itt)**2)
      write(5,*)x,y,ix,iy,uphav(ix,iy,itt),vphav(ix,iy,itt),
     +  ucoh(ix,iy,itt),vcoh(ix,iy,itt),cohstr(ix,iy,itt),
     +  avusq(ix,iy,itt),avvsq(ix,iy,itt),avstress(ix,iy,itt),e1,e2
      end do
      end do
      if(ixmax.lt.2.or.iymax.lt.2.or.ixmin.eq.ixmax.
     +  or.iymin.eq.iymax)go to 100

      write(7,72)itt,iymax-1,ixmax-1
      do i=ixmin,ixmax-1
      do j=iymin,iymax-1
       yy=((iy+0.5)-((iymaxx+1)/2))*dy*1000./dwidth
       xx=((ix+0.5)*dx*1000./dwidth)+xstart
      vort(i,j,itt)=((((((uuphav(i+1,j,itt)-uuphav(i,j,itt))/2)+
     +  uuphav(i,j,itt))-(((uuphav(i+1,j+1,itt)-uuphav(i,j+1,itt))/2)+
     +  uuphav(i,j+1,itt)))*dx)-(((((vvphav(i,j+1,itt)-vvphav(i,j,itt))
     +  /2)+vvphav(i,j,itt))+(((vvphav(i+1,j+1,itt)-vvphav(i+1,j,itt))/
     +  2)+vvphav(i+1,j,itt)))*dy))*(1./(2*dx*dy))*
     +  ((dwidth/1000)/uinfav)
      write(7,*)xx,yy,i,j,vort(i,j,itt)
      end do
      end do
101    close(5)
      close(7)
      write(6,60)
```

```
      write(6,61)
      do ix=ixmin,ixmax
      write(6,62)ix,iymax
      do iy=iymin,iymax
       y=(iy-((iymaxx+1)/2))*dy*1000./dwidth
      write(6,*)y,iy,avucoh(ix,iy),avvcoh(ix,iy),avsqu(ix,iy),
     +  avsqv(ix,iy),avcostrs(ix,iy),avusqr(ix,iy),
     +  avvsqr(ix,iy),avstres(ix,iy)
      end do
      end do
      close(6)

   20   format('TITLE = "Contour properties at X=',i2,' "')
   21   format('VARIABLES = "P", "Y" , "IT" , "IY" , "V1", "V2", "V3",
     +"V4", "V5", "V6", "V7", "V8" , "V20" , "V21" , "V22" , "V23" , "
     +V24" , "V25"')
   22   format('ZONE T="x(',i2,')',"',',1x,'I=',i2,', J=',i2,', F=POINT
     +')
   30   format('TITLE = "Averaged properties at X=',i2,' "')
   31   format('VARIABLES = "Y", "IY" , "V18", "V19", "V9", "V10", "V11
     +", "V12", "V13", "V14", "V15", "V16"')
   32   format('ZONE T="x(',i2,')',"',',1x,'I=',i2,', F=POINT')
   40   format('TITLE = "3-D properties at X=',i2,' "')
   41   format('VARIABLES = "P", "Y" , "IT" , "IY" , "V1", "V2", "V3",
     +"V4", "V5", "V6", "V7", "V8" , "V20" , "V21" ,"V22" , "V23" , "V24
     +" , "V25" , "V26"')
   42   format('ZONE T="x(',i2,'),t(',i2,')",',1x,'I=',i2,', F=POINT')
   50   format('TITLE = "Coherent & Incoherent Data in X-Y Domain"')
   51   format('VARIABLES = "X", "Y", "IX" , "IY" , "V1", "V2", "V3", "
     +V4", "V5", "V6", "V7", "V8" , "V20", "V21"')
   52   format('ZONE T="t(',i2,')',"',',1x,'I=',i2,', F=POINT')
```

```
60    format('TITLE = "Averaged properties in X-Y Domain"')
61    format('VARIABLES = "Y", "IY" , "V9", "V10", "V11", "V12", "V13
 +", "V14", "V15", "V16"')
62    format('ZONE T="x(',i2,')','"',',1x,'I=',i2,', F=POINT')
70    format('TITLE = "Vorticity Data in X-Y Domain"')
71    format('VARIABLES = "xx" , "yy" , "i", "j", "V17"')
72    format('ZONE T="t(',i2,')','"',',1x,'I=',i2,', J=',i2,', F=POINT
 +')
80    format(f5.2,1x,f9.6,1x,f9.6,1x,f9.6,1x,f9.6,1x,f9.6,1x,f7.4)
90    format(f5.2,1x,f9.6,1x,f9.6,1x,f9.6,1x,f9.6,1x,f9.6,1x,f7.4)
      if(iymin.ne.ixmin.or.iymax.ne.ixmax)then
      print *,' '
      print *,' '
      print *,'WARNING;Data for x-y plotting is not of same dimension
 +s'
     end if
     stop
     end

   subroutine number(input,io1,io2)
   character io1,io2

     if(input.lt.10)then
     io1=48
     io2=input+48
     else if(input.ge.10.and.input.lt.20)then
     io1=49
     io2=input+38
     else if(input.ge.20.and.input.lt.30)then
     io1=50
     io2=input+28
```

```
else if(input.ge.30.and.input.lt.40)then
io1=51
io2=input+18
 else if(input.ge.40.and.input.lt.50)then
io1=52
io2=input+8
else if(input.ge.50.and.input.lt.60)then
io1=53
io2=input-2
else if(input.ge.60.and.input.lt.70)then
io1=54
io2=input-12
 else if(input.ge.70.and.input.lt.80)then
io1=55
io2=input-22
 else if(input.ge.80.and.input.lt.90)then
io1=56
io2=input-32
else if(input.ge.90.and.input.lt.100)then
io1=57
io2=input-42
end if
     return
end
```